THE PROCEEDINGS OF
THE PHYSICAL SOCIETY

VOL. 58, PART 2 1 March 1946 No. 326

CRYSTAL STRUCTURE OF DOUBLE OXIDES OF THE PEROVSKITE TYPE

BY HELEN D. MEGAW,
Birkbeck College

MS. received 27 *September* 1945

ABSTRACT. The cell dimensions of a number of double oxides belonging to the perovskite type have been accurately determined from examination of high-angle lines on x-ray powder photographs. The structures found fall into groups, as follows :

(1) *Cubic* (*ideal perovskite type*). This includes $SrTiO_3$, $SrSnO_3$, $SrZrO_3$, $BaSnO_3$, $BaZrO_3$, $BaThO_3$; also $BaTiO_3$ above 120° c.

(2) *Tetragonal*. This includes the usual form of $BaTiO_3$ at room temperature, $PbTiO_3$, and $PbZrO_3$. The unit cell is derived from the cubic by simple extension or compression along one tetrad axis ; and, like the cubic, it contains the formula number of atoms.

(3) *Orthorhombic*. This includes $CaTiO_3$ (the mineral perovskite), $CaSnO_3$, $CaZrO_3$, and $CdTiO_3$ (fired above 1100° c.). The structure is derived from the cubic by a shear in the (010) plane and a slight extension or compression along the *b*-axis, giving a monoclinic pseudo-cell with *a* and *c* edges equal. The lattice is thus actually orthorhombic, and should be referred to new *a* and *c* axes lying at approximately 45° to the old in the same plane. There is an observed doubling of the cell edges, attributable to changes in some of the atomic parameters.

(4) *Rhombohedral*. $BaTiO_3$ can be prepared in this form, though the conditions are not yet fully established. The pseudo-cell is obtained by a very slight compression of the cubic cell along the cube diagonal ; the true cell is a multiple of this.

Steric considerations, based on Goldschmidt's ionic radii, are used to account for the occurrence of the different structure modifications.

§ 1. INTRODUCTION

THE mineral perovskite, $CaTiO_3$, has given its name to a very simple and important structure type, classified as E 21 in the *Strukturbericht*. This is cubic, with one formula-weight per unit cell. A large number of double oxides (as well as some iodates and double halides) are classified as belonging to this type. Early work on these, by Goldschmidt (1927) and his school, was directed to illustrating the two principles which are characteristic of multiple isodesmic structures, namely, the dependence of structure type on ionic radii and its relative independence of valency.

There was no emphasis in Goldschmidt's work on the detailed geometry of the individual structures. It was recognized that while some, such as $SrTiO_3$, were strictly cubic, others, such as perovskite itself, must from the crystallographic evidence be of lower symmetry, though the difference was not detectable by x-ray methods; while others again, such as $CaSnO_3$, showed departures from cubic symmetry in the geometry of the unit cell. Advances in x-ray technique in the intervening years now make possible more accurate determination of the cell dimensions and a more critical discrimination between the cubic and various " deformed " structures. Some work has already been done along these lines. Hoffman (1935) investigated a number of compounds, including some which had not been previously prepared, and classified them into " cubic " and " deformed " without attempting to describe the deformation in detail. Naray-Szabo (1943 a) made a complete investigation of the structure of perovskite, both single crystals and powder, and found the structure monoclinic; his results will be discussed in more detail later. He investigated a number of other related compounds (1943 b), distinguishing those which belonged to the same " new type " as perovskite from those which were strictly cubic, and showing their relationship to cubic ReO_3 and rhombohedral ScF_3. Recently the present author showed that $BaTiO_3$ possessed a tetragonal modification of the structure (Megaw, 1945). This was also found by Rooksby (1945), who gave a brief discussion of some of the other non-cubic structures.

It is clear that this group of compounds includes structures with a very varied symmetry, all based on small but completely different modifications of the same cubic elementary cell.

A comparison of the different variants, and an attempt to understand why one rather than another should occur in a given case, is likely to be useful in any further work on the nature of forces in ionic solids. The first step towards this is an accurate determination of the geometry of the unit cells of the different structures, which was the object of the present investigation.

§ 2. DESCRIPTION OF STRUCTURE

It seems convenient to define the term *perovskite type* to include all structures which retain a pseudo-cell derived from that of the ideal cubic structure E 21 by small distortions either of cell edge or of interaxial angle. The true cell may require a doubling of one or more edges of the psudo-cell, or a different choice of axes. When necessary, the cubic structure E 21 can be distinguished as the *ideal perovskite type*. Rooksby suggests that these structures should be called *pseudo-isomorphous*, but here the word *homotypic* is preferred, as it lays emphasis on the common crystal type, and does not carry the chemical implications involved in the use of the older word.

Compounds belonging to the perovskite type have in general the formula ABO_3, where the sum of the cation valencies is 6. (ReO_3 and WO_3 may be included as extreme cases in which one set of cation sites is completely unoccupied, and the sodium tungsten bronzes, Na_xWO_3, are an important example of a defect lattice with variable tungsten valency. Naray-Szabo classes all these as " sister-structures "). The present work deals only with the numerous group in which A is 2-valent, B 4-valent.

In the ideal type, the atomic parameters are as follows:

A	$\frac{1}{2}\frac{1}{2}\frac{1}{2}$
B	000
O	$\frac{1}{2}00$, $0\frac{1}{2}0$, $00\frac{1}{2}$

This gives a structure in which the B cations are surrounded by regular octahedra of oxygens, which are linked together by their corners to form a three-dimensional framework. The A cations occupy the large holes between the octahedra, where each is surrounded by 12 oxygens. The A-O and B-O electrostatic bond strengths (in Pauling's sense) are thus $\frac{2}{12}$ and $\frac{4}{6}$ or $\frac{1}{6}$ and $\frac{2}{3}$ respectively. There are no bond strengths equal to or greater than 1, and hence the structure may be classified as isodesmic (Evans, 1939). Chemically this implies that the compounds should be described as double oxides rather than as titanates, zirconates, etc., but the latter nomenclature is sometimes convenient and not seriously liable to mislead. Figure 1 (taken from Nara-Szabo's paper) shows the structure.

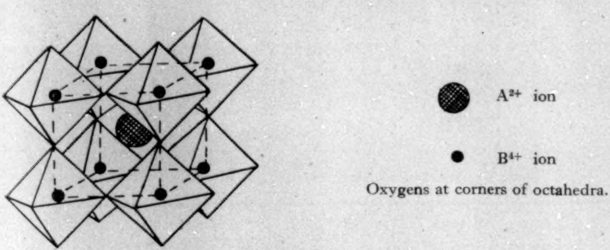

Figure 1. Ideal cubic perovskite structure.

In all the structures investigated, this topographical description remains true, though in many of them the framework loses its symmetrical construction. Two main types of deformation are possible, and may occur separately or together.

(1) The unit cell changes its shape, by altering either the relative lengths of the cell-edges or the axial angle.

(2) The atomic parameters of some or all of the atoms are slightly altered. Since in the ideal structure the atoms are in special positions, slight displacement in any direction involves a lowering of the symmetry, and in general also a doubling of at least one cell edge. Conversely, a doubled cell edge implies atomic parameters different from those of the ideal structure.

In the present work, no systematic attempt has been made to determine the atomic parameters, except in so far as the atoms are fixed in special positions by the symmetry of the unit cell, though some general conclusions have been drawn from the experimental data. The only detailed study of parameters is the work of Naray-Szabo on $CaTiO_3$, which is discussed later.

In table 1 is given a list of all the compounds $A^{2+}B^{4+}O_3$ of perovskite type for which information is available. Some of these are known to be dimorphous, and it seems probable that others may be. Thus, $CdTiO_3$ has the ilmenite structure when fired below 1050°, the perovskite structure when fired above this; $BaTiO_3$ is tetragonal at room temperature but changes reversibly to cubic at about 120°, and also shows the rhombohedral form described later. It is possible that the conflicting reports on $PbTiO_3$ are due to the occurrence of two different structures. This polymorphism should not be surprising in view of the frequency with which it occurs among minerals which have been thoroughly investigated, notably TiO_3 with its three forms, rutile, anatase and brookite.

Table 1. Classification of compounds of perovskite type

Cubic	Tetragonal	Orthorhombic or monoclinic	Rhombohedral	Non-cubic, type not known
$SrTiO_3$ (G, H, M)	$BaTiO_3$ Iα (M)	$CaTiO_3$ (B, N, M)	$BaTiO_3$ II (M)	$PbZrO_3$ (N, H)
$SrZrO_3$ (H, M)	$PbTiO_3$ (N, M, R)	$CaZrO_3$ (RES, M)		$PbSnO_3$ (N)
$SrSnO_3$ (H, M)	$PbZrO_3$ (M)	$PbTiO_3$ (CE)		$SrCeO_3$ (H)
$SrHfO_3$ (H)		$CdTiO_3$ (M)		$CdSnO_3$ (N)
$BaZrO_3$ (H, N, M)		$CaSnO_3$ (R, M)		
$BaSnO_3$ (N, M)		$CaCeO_3$ (N)		
$BaCeO_3$ (H)		$CdCeO_3$ (N)		
$BaPrO_3$ (H)		$PbCeO_3$ (N)		
$BaThO_3$ (H, M)				
$BaTiO_3$ Iβ (M)				

Letters in brackets indicate the authors whose classification is quoted:

G = Goldschmidt, 1927.
H = Hoffmann, 1935.
N = Naray-Szabo, 1943.
M = Megaw, 1946 (present work).
R = Rooksby, 1945.
B = Barth, 1925.
CE = Cole and Espenschied, 1937.
RES = Ruff, Ebert and Stephan, 1929.

§ 3. EXPERIMENTAL METHOD

All the substances investigated in the present work were prepared by firing together stoichiometric mixtures of the appropriate oxides or carbonates, at temperatures specified in each case. No special precautions were taken about quenching.

For the X-ray work, specimens were prepared either by rolling rods from a paste of the material mixed with powdered gum tragacanth, or by filling small celluloid tubes (Lonsdale and Smith, 1941). In general, powder photographs were taken with filtered Cu Kα radiation in a 19-cm. camera; for some of the cubic materials, a 9-cm. camera or unfiltered radiation was used. With a Philips sealed tube, run at 30 kv. and 20 ma., exposures in the 19-cm camera were from 6 to 15 hours. The photographs were measured with a glass scale, and the spacings calculated by the method of Bradley and Jay (1932). No special precautions were taken to allow for absorption, and the spacings derived from low-angle lines can therefore not be taken as accurate; but they were sufficiently good to index the high-angle lines, and these, using the $\cos^2\theta$ extrapolation, gave very exact values of the cell dimensions. For the cubic structure this extrapolation was straightforward; for the others, a method of successive approximations was used, as described below.

Estimates of the intensities were made visually.

§ 4. INTERPRETATION OF THE STRUCTURES

Photographs of typical substances are reproduced in figure 2. It will be seem from this that for most of the compounds the main lines (at least at the

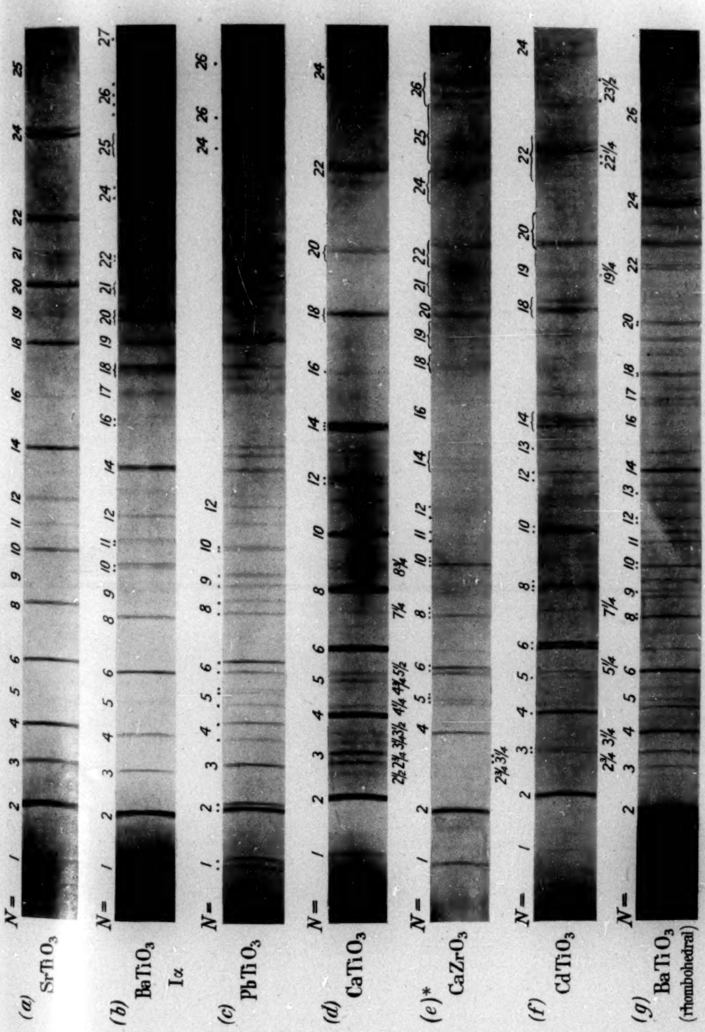
(a) SrTiO₃
(b) BaTiO₃ Iα
(c) PbTiO₃
(d) CaTiO₃
(e)* CaZrO₃
(f) CdTiO₃
(g) BaTiO₃ (rhombohedral)
N=

Figure 2.

Powder photographs taken in a 19-cm. camera with Cu $K\alpha$ radiation.

N values refer to pseudo-cell ; lines requiring doubled cell are indicated by fractional values of N.

* The dots between 5 and 10 are all slightly displaced to the right.

Table 2

N	Cubic indices	Tetragonal with $c/a>1$	Rhombohedral with $\alpha>90°$	Monoclinic with $a^*=b^*=c^*$
1	100	001, 100+010 Doublet with outer line stronger	100 Single line	100+001+010 Single line
2	110	101+011, 110 Doublet with inner line stronger	$1\bar{1}0$, 110 Symmetrical doublet	101, $110+011+1\bar{1}0+01\bar{1}$, $10\bar{1}$ Symmetrical triplet; middle line strongest
3	111	111 Single line	$11\bar{1}+1\bar{1}1+\bar{1}11$, 111 Doublet with inner line, stronger	$11\bar{1}$, 111 Symmetrical doublet
4	200	←	as 100	→
5	210	102+012, 201+021, 210+120 Three lines of equal intensity; outer pair a very close doublet	$2\bar{1}0$, 210 Symmetrical doublet	$20\bar{1}+10\bar{2}$, $210+012+120+021+2\bar{1}0+01\bar{2}+1\bar{2}0+02\bar{1}$, 201+102 Symmetrical triplet with middle line strongest
6	211	122, 211+121 Doublet with outer line stronger	$\bar{2}11$, $21\bar{1}$, $2\bar{1}1$, 211 Unsymmetrical triplet with middle line strongest, the inner pair being a very close doublet	$21\bar{1}+11\bar{2}$, $12\bar{1}$, 121, 211+112 Symmetrical set of four lines, consisting of two close pairs; outermost and innermost lines stronger than middle two

Note.—The descriptions of the line complexes refer to their appearance to visual examination only, and are not meant to be quantitatively exact.

low-angle end of the photograph) are simply related to the cubic pattern, a single line (or α-doublet) of the latter being replaced by a complex group.

The ***hkl*** indices of lines in any group are permutations of those characterizing the cubic line, which are known. A survey was made, for each kind of departure from cubic symmetry, of the possible permutations giving crystallographically distinct spacings in every group. From this the type of multiplet formation to be expected could be seen. Part of this survey is given in table 2. Comparison of the photographs with this table showed which type of structure was present; where the deformation was fairly large, the lowest-angle lines were used, but where it was smaller, sufficient resolution was only obtained at higher angles. Further refinement was achieved by the use of high-angle lines.

Some of the substances gave weaker lines intermediate in position between those that could be indexed from the small pseudo-cell as just described. These could be accounted for by doubling the cell-edges. To retain the pseudo-cubic description, all three cell-edges must be doubled ; whether this is in fact necessary, or whether the true cell may only need the doubling of one edge, can only be determined by an exact indexing of all the lines in question. This has not been carried out, owing to the lengthy calculations needed in some cases and the ambiguity which results from overlapping.

§ 5. GEOMETRY OF THE STRUCTURE AND EXACT EVALUATION OF CELL CONSTANTS

(i) *Cubic*

This structure is straightforward, and no discussion is needed.

(ii) *Tetragonal*

This structure is derived from the ideal cubic by a homogeneous extension or compression along one axis, which becomes the c-axis. In the substances investigated, there is no evidence of any doubling of the cell-edge; hence the atomic coordinates are as in the cubic structure. The general framework of linked octahedra round the smaller cations, with the larger cations in the holes, remains unaltered.

For a tetragonal structure, the spacings are given by:

$$d_{hkl}=\frac{1}{\sqrt{\left(\frac{h^2+k^2}{a^2}+\frac{l^2}{c^2}\right)}}=\frac{a}{\sqrt{\left(h^2+k^2+\frac{l^2}{r^2}\right)}}, \qquad \ldots\ldots(1)$$

where $c/a=r$. Approximate values of c and a may be found by single measurements of 004, 400, hence giving r.

Let $$h^2+k^2+\frac{l^2}{r^2}=N'=N+l^2\left(\frac{1}{r^2}-1\right).$$

($Cf.$ $h^2+k^2+l^2=N$ for a cubic crystal.)

Let $r=1+x$, where x is small.

Then $N'=N-2xl^2$.

Hence, where x^2 is negligible,

$$a = d_{hkl}\sqrt{N'_{hkl}} = d_{hkl}(\sqrt{N})\left(1-\frac{xl^2}{N}\right), \qquad \ldots\ldots(2)$$

or, more exactly,

$$a = d_{hkl}\sqrt{(N)}\sqrt{\left[1+\frac{l^2}{N}\left(\frac{1}{r^2}-1\right)\right]}. \qquad \ldots\ldots(2\,a)$$

Considering lines of high angle only, suitable for a Bradley-Jay extrapolation, $\sqrt{N'}$ can be calculated from the known r, and hence values of a found which are plotted against $\sin^2\theta$ in the usual way. An example is shown in figure 3 (a). If

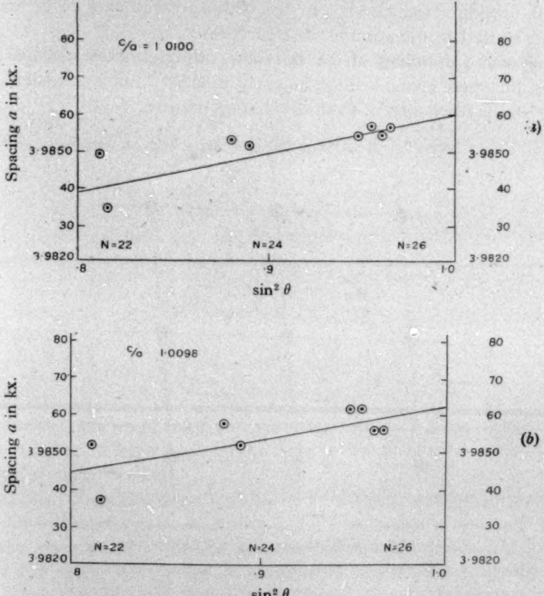

Figure 3. Extrapolation of a against $\sin^2\theta$ for $BaTiO_3$: (a) using value of c/a finally adopted; (b) using incorrect value of c/a. Reflections with $N=25$ are omitted as being less accurately measurable owing to their weakness.

r is accurate, all the points will be on the same straight line ; but if it is inaccurate, as in figure 3 (b), a line drawn through points corresponding to the complex with a given N will be inclined at an angle to the best line through all the points with different N's. The angle between these two lines is used to correct r, and a second approximation made, if necessary, to obtain the best value of a. The method is tedious for a single photograph, but can be systematized and shortened where many samples are being examined. In practice, while the above approximation (2) served for indexing the lines, the more exact expression (2 a) was used for calculating the cell dimensions.

(iii) *Monoclinic and orthorhombic structures*

All the substances in this group that have so far been investigated have a monoclinic pseudo-cell derived from the cubic cell by a simple shear, leaving the cell-edges *a* and *c* equal. Geometrically the lattice thus achieved has orthorhombic symmetry, and should be referred to new *a* and *c* axes, which are diagonals of the (010) face of the pseudo-cell, as shown in figure 4 (where the β-angle is exaggerated for clarity).

Some of the evidence on this point is considered later. It is, however, legitimate for purposes of calculation and comparison to retain the monoclinic pseudo-cell, leaving a transference to the orthorhombic axes to be made when required for a full determination of the structure.

There is also a doubling of the cell-edge, which implies change of atomic parameters, but these changes must be fairly small. This is considered in more detail later, in the discussion of the individual structures.

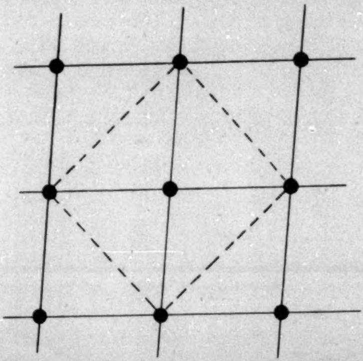

Figure 4. Projection of orthorhombic lattice on (010) plane, showing monoclinic pseudo-cells (full lines) and orthorhombic cell (dotted lines).

The angle β has been made markedly different from 90° to show up the geometrical relationship.

The structure remains homotypic with those previously described; the network of linked octahedra is retained, though these are no longer regular nor symmetrically placed.

To find the cell dimensions, a method of approximations was used. For a monoclinic crystal,

$$d_{hkl} = (h^2a^{*2} + k^2b^{*2} + l^2c^{*2} - 2\,hla^*c^* \cos\beta)^{-\frac{1}{2}}, \qquad \ldots\ldots(3)$$

where a^*, b^*, c^* are the reciprocal lattice dimensions:

$$a^* = 1/a \sin\beta, \quad b^* = 1/b, \quad c^* = 1/c \sin\beta. \qquad \ldots\ldots(4)$$

If $a^* = c^* = rb^*$ (in accordance with observation),

$$d_{hkl} = \frac{a \sin\beta}{\sqrt{\left(h^2 + \frac{k^2}{r^2} + l^2 - 2hl \cos\beta\right)}}.$$

Let
$$N'' = h^2 + \frac{k^2}{r^2} + l^2$$
$$= h^2 + k^2 + l^2 + k^2\left(\frac{1}{r^2} - 1\right)$$
$$= N + k^2\left(\frac{1}{r^2} - 1\right)$$

and let $r = 1 + y$, where y is small. ......(5)

Then
$$N'' = N - 2yk^2.$$
$$\therefore \quad d_{hkl} = \frac{a \sin\beta}{\sqrt{(N - 2yk^2 - 2hl\cos\beta)}}$$
$$= \frac{a \sin\beta}{\sqrt{N}} \cdot \frac{1}{\left(1 - \frac{k^2 y}{N} - \frac{hl}{N}\cos\beta\right)}. \qquad \text{......(6)}$$

Hence for two planes hkl, $hk\bar{l}$, with a mean spacing d, we have
$$\frac{d_{hkl} - d_{hk\bar{l}}}{d} = -\frac{2hl}{N}\cos\beta. \qquad \text{......(7)}$$

This can be used to calculate β. Again, comparing an $hk0$ line with the geometric mean of an $h0l$, $h0\bar{l}$ pair from the same complex, we have
$$d = (d_{h0l} \,.\, d_{h0\bar{l}})^{1/2} = \frac{a \sin\beta}{\sqrt{N}}.$$
$$\therefore \quad d_{hk0} = d\left(1 + \frac{k^2}{N}y\right). \qquad \text{......(8)}$$

This gives y.

With the best values of $\cos\beta$ and y so obtained, $a \sin\beta$ can be calculated from d_{hkl} for a number of high-angle lines, and the Bradley-Jay extrapolation carried out to get the correct values.

All the above work is done with main lines which can be indexed from the pseudo-cell, and in fact this indexing is used in tables 6 to 9. It remains to identify the extra lines. For this purpose the cell-dimensions are doubled, and spacings calculated from (6) for all possible values of hkl; comparison of these with the observed spacings serves to index the lines. In a good many cases the accuracy was not great enough to do this unambiguously, but it was sufficient to show that all lines could be indexed on the assumption of a doubled cell-edge.*

In practice it was found for all these structures that y was small compared with $\cos\beta$. This can be seen from the photo of $CdTiO_3$ shown in figure 2 (f); if y were zero, as assumed in table 2, line 8 would be a (visually) symmetrical triplet, and the actual displacement of the middle line towards the low-angle side indicated a small positive value of y. In $CaSnO_3$, the displacement was towards the high-angle side, indicating a negative value. In $CaTiO_3$ and $CaZrO_3$, the displacement was too small to be observed at these angles, but a small negative value of y was required to explain the high-angle lines.

---

* In this connection it may be noted that in Rooksby's photograph of $CaSnO_3$, of the four lines marked 111, only the two central ones belong to this complex, the outer pair being extra lines requiring a doubled cell, referred to which their indices are $13\bar{1} + 131$ and $320 + 230$.

(iv) *Rhombohedral structure*

A rhombohedral perovskite structure, not previously described, has been found with $BaTiO_3$. Here the distortion is produced by a compression along a triad axis of the ideal cubic cell. There are extra lines not yet fully interpreted, and the true cell is almost certainly larger than the pseudo-cell. The photograph is reproduced in figure 2 (*g*).

For the rhombohedral structure, we may use a simplified expression for the spacing, since the observed departure from cubic symmetry is so small.

If α is the internal angle between the rhombohedral axes, we may neglect terms in $\cos^2\alpha$ and $\cos^3\alpha$ and write

$$d_{hkl}=\left(\frac{h^2+k^2+l^2}{a^2}-2\frac{hk+kl+lh}{a^2}\cos\alpha\right)^{-\frac{1}{2}}$$

$$=\frac{a}{\sqrt{N}}\left(1+\frac{hk+kl+lh}{N}\cos\alpha\right). \qquad \ldots\ldots(9)$$

Hence

$$\frac{d_{hkl}-d_{h\bar{k}l}}{d}=\frac{2}{N}(h+k)\,l\cos\alpha, \qquad \ldots\ldots(10)$$

whence α can be found.

Experimental results

Complete tables of spacings, observed and calculated, will not be published, but lists have been sent for inclusion in the A.S.T.M. index. Certain spacings used in determining cell dimensions are shown in tables 3 to 9. The values so obtained are given in tables 10 to 13.

Table 3. Barium titanium oxide

N	Indices	Intensity	θ (Cu Kα_1 or α_2)	log d	a (kX.) ($c/a=1\cdot0100\pm0\cdot0001$)
22	323 α_1	s	64·309	$\bar{1}$·93096	3·9849
	332 α_1	s	64·620	$\bar{1}$·92884	3·9835
	332 α_2	ms	64·931	$\bar{1}$·92981	3·9832
24	224 α_1	ms	69·838	$\bar{1}$·91322	3·9853
	224 α_2	m	70·228	$\bar{1}$·91323	3·9853
	422 α_1	s	70·636	$\bar{1}$·91105	3·9851
	422 α_2	ms	71·074	$\bar{1}$·91098	3·9844
25	304 α_1	w	73·430	$\bar{1}$·90418	3·9847
	403 α_1	w	73·928	$\bar{1}$·90305	3·9855
	430 500 α_1	w	74·612	$\bar{1}$·90161	3·9864
	,, α_2	vw	75·203	$\bar{1}$·90148	3·9852
26	105 α_1	ms	76·956	$\bar{1}$·89714	3·9854
	314 α_1	s	77·805	$\bar{1}$·89567	3·9857
	413 α_1	s	78·565	$\bar{1}$·89446	3·9854
	431 501 α_1	vs	79·441	$\bar{1}$·89317	3·9856
	431 501 α_2	s	80·276	$\bar{1}$·89312	3·9852

Extrapolated, $a=3\cdot9860\pm0\cdot0500$

Table 4. Lead titanium oxide

N	Indices	Intensity	θ (Cu Kα_1)	log d	a (kx.) ($c/a=1\cdot064\pm0\cdot001$)
24	$42\bar{2}$	s	73·38	$\bar{1}$·90463	3·8947
25	403	mw	75·18	$\bar{1}$·90079	3·8944
27	115	w	75·83	$\bar{1}$·90001	3·8982
26	314	m	76·04	$\bar{1}$·89913	3·8944
26	413	s	80·56	$\bar{1}$·89201	3·8953
25	430 500	w	80·74	$\bar{1}$·89181	3·8974

Extrapolated, $a=3\cdot896_6\pm0\cdot001$

Table 5. Lead zirconium oxide

N	Indices	Intensity	θ (Cu Kα_1)	log d	a (kx.) ($c/a=0\cdot988\pm0\cdot001$)
24	422	m	65·53	$\bar{1}$·92662	4·1458
26	501 431	ms	70·97	$\bar{1}$·91017	4·1482
	413	m	71·68	$\bar{1}$·90835	4·1463
	314	ms	72·18	$\bar{1}$·90711	4·1480

Extrapolated, $a=4\cdot150_2\pm0\cdot001$

Table 6. Calcium titanium oxide

N	Indices (using pseudo-cell)	Intensity	θ (Cu Kα_1)	log d	$a \sin\beta$ (kx.) $\beta=90°\ 40'$ $y=-0\cdot0012$
20	$40\bar{2}+20\bar{4}$	mw	63·77	$\bar{1}$·93297	3·8149
	$420+024$ $240+042$	s	64·46	$\bar{1}$·93039	3·8132
	$402+204$	ms	64·81	$\bar{1}$·92913	3·8156
22	$32\bar{3}$	w	70·16	$\bar{1}$·91232	3·8149
	$33\bar{2}+23\bar{3}$	m	70·44	$\bar{1}$·91159	3·8162
	$332+233$	ms	71·45	$\bar{1}$·90893	3·8165
	323	mw	71·65	$\bar{1}$·90842	3·8173
24	$42\bar{2}+22\bar{4}$	ms	79·33	$\bar{1}$·89331	3·8181
	$24\bar{2}$	s	80·14	$\bar{1}$·89221	3·8174
	242	mw	81·54	$\bar{1}$·89052	3·8173
	$422+224$	m	82·01	$\bar{1}$·89001	3·8180

Extrapolated, $a \sin\beta=3\cdot8188\pm0\cdot0008$

Table 7. Calcium zirconium oxide

N	Indices (using pseudo-cell)	Intensity	θ (Cu Kα_1)	log d	$a \sin \beta$ (kx.) $\beta = 91° 43'$ $y = -0{\cdot}0010$
24	$42\bar{2}+22\bar{4}$	m	68·88	$\bar{1}$·91595	3·9974
	$24\bar{2}$	m	69·71	$\bar{1}$·93156	3·9976
	242 $40\bar{3}+30\bar{4}$	ms	71·32	$\bar{1}$·90927	3·9981 3·9989
	$422+224$	ms	72·04	$\bar{1}$·90743	3·9990
25	$430+034$ $340+043$	s	74·05	$\bar{1}$·90281	3·9990 4·0000
26	$41\bar{3}+31\bar{4}$	m	75·13	$\bar{1}$·90055	3·9995
	$50\bar{1}+10\bar{5}$ $403+304$	w	77·02	$\bar{1}$·89701	3·9992 4·0010
	$43\bar{1}+13\bar{4}$	m	77·36	$\bar{1}$·89643	3·9999
	$34\bar{1}+14\bar{3}$	ms	77·73	$\bar{1}$·89579	3·9992
	$510+015$	ms	78·48	$\bar{1}$·89459	4·0002
	$150+051$	ms	78·77	$\bar{1}$·89416	4·0002
	$341+143$	ms	79·64	$\bar{1}$·89291	4·0011
	$431+134$	ms	79·93	$\bar{1}$·89250	4·0005
	$413+314$	s	83·28	$\bar{1}$·88875	4·0017

Extrapolated, $a \sin \beta = 4{\cdot}0015 \pm 0{\cdot}0015$

Table 8. Calcium tin oxide

N	Indices (using pseudo-cell)	Intensity	θ (Cu Kα_1)	log d	$a \sin \beta$ (kx.) $\beta = 91° 30'$ $y = -0{\cdot}0024$
20	$40\bar{2}+20\bar{4}$	w	59·74	$\bar{1}$·94937	3·9382
	$420+024$	ms	60·84	$\bar{1}$·94451	3·9377
	$240+042$	ms	60·97	$\bar{1}$·94408	3·9392
	$402+204$	mw	61·90	$\bar{1}$·94023	3·9380
22	$32\bar{3}$	m	64·93	$\bar{1}$·92872	3·9394
	$33\bar{2}+23\bar{3}$	ms	65·42	$\bar{1}$·92703	3·9405
	$332+233$	s	67·30	$\bar{1}$·92078	3·9405
	323	s	67·71	$\bar{1}$·91949	3·9399
24	$42\bar{2}+22\bar{4}$	m	71·32	$\bar{1}$·90927	3·9423
	$24\bar{2}$	m	72·36	$\bar{1}$·90668	3·9406
	242	mw	74·02	$\bar{1}$·90288	3·9408
25	$30\bar{4}+40\bar{3}$	ms	74·30	$\bar{1}$·90227	3·9421
24	$422+224$	ms	74·63	$\bar{1}$·90157	3·9409
25	$034+430$ $043+340$	s	77·45	$\bar{1}$·89626	3·9411 3·9435
26	$31\bar{4}+41\bar{3}$	ms	79·10	$\bar{1}$·89367	3·9438
25	$304+403$	m	80·84	$\bar{1}$·89133	3·9422
26	$10\bar{5}+50\bar{1}$	m	81·63	$\bar{1}$·89041	3·9420
	$13\bar{4}+43\bar{1}$	ms	82·35	$\bar{1}$·88964	3·9422
	$14\bar{3}+\bar{3}4\bar{1}$	ms	83·09	$\bar{1}$·88893	3·9425

Extrapolated, $a \sin \beta = 3{\cdot}9427 \pm 0{\cdot}001$

Table 9. Cadmium titanium oxide

N	Indices (using pseudo-cell)	Intensity	θ (Cu $K\alpha_1$)	log d	$a \sin \beta$ (kx.) $\beta=91°\ 10'$ $y=+0{\cdot}0044$
18	$41\bar{1}+11\bar{4}$ $14\bar{1}$	m	59·15	$\bar{1}{\cdot}95201$	3·7809 3·7797
	141 330+033	ms	59·39	$\bar{1}{\cdot}95096$	3·7789 3·7812
	411+114	m	60·06	$\bar{1}{\cdot}94794$	3·7795
20	240+042	s	64·97	$\bar{1}{\cdot}92860$	3·7809
	420+024	s	65·24	$\bar{1}{\cdot}92766$	3·7825
	402+204	m	66·48	$\bar{1}{\cdot}92342$	3·7799
22	$33\bar{2}+23\bar{3}$	m	71·15	$\bar{1}{\cdot}90790$	3·7809
	332+233	m	73·11	$\bar{1}{\cdot}90489$	3·7815
	323	ms	73·81	$\bar{1}{\cdot}90332$	3·7825
24	$42\bar{2}+22\bar{4}$ $24\bar{2}$	m	81·35	$\bar{1}{\cdot}89073$	3·7806 3·7856
	242	m	84·72	$\bar{1}{\cdot}88761$	3·7838

Extrapolated, $a \sin \beta = 3{\cdot}7833 \pm 0{\cdot}001$

Table 10. Cubic structures

Compound	Firing temperature (°c.)	Cell-edge a_0 (kx.)
$SrTiO_3$	1250	$3{\cdot}897_0 \pm 0{\cdot}001$
$SrZrO_3$	1250	$4{\cdot}093 \pm 0{\cdot}001$
$SrSnO_3$	1380	$4{\cdot}0254 \pm 0{\cdot}0005$
$BaZrO_3$	1280	$4{\cdot}181_5 \pm 0{\cdot}001$
$BaSnO_3$	1300	$4{\cdot}108_5 \pm 0{\cdot}001_5$

Table 11. Tetragonal structures

Compound	Firing temp. °c.	Cell-dimensions a (kx.)	c (kx.)	c/a	(Vol.)$^{1/3}$ (kx.)
Barium titanium oxide	1300	3·9860	4·0259	$1{\cdot}0100 \pm 0{\cdot}0001$	$3{\cdot}9993 \pm 0{\cdot}0005$
Lead titanium oxide	1180	$3{\cdot}896_6$	$4{\cdot}144_0$	$1{\cdot}063_5 \pm 0{\cdot}001$	$3{\cdot}998 \pm 0{\cdot}001$
Lead zirconium oxide	1250	$4{\cdot}150_3$	4·100	$0{\cdot}988 \pm 0{\cdot}001$	$4{\cdot}133 \pm 0{\cdot}001$

Table 12. Orthorhombic structures

Compound		Calcium titanium oxide	Calcium zirconium oxide	Calcium tin oxide	Cadmium titanium oxide
Firing temp. (°c.)		1500	1500	1400	1200
Monoclinic pseudo-cell	Cos β	$-0{\cdot}0115 \pm 0{\cdot}0003$	$-0{\cdot}0300 \pm 0{\cdot}0010$	$-0{\cdot}0262 \pm 0{\cdot}0005$	$-0{\cdot}0204 \pm 0{\cdot}0006$
	y	$-0{\cdot}0012 \pm 0{\cdot}0003$	$-0{\cdot}0010 \pm 0{\cdot}0005$	$-0{\cdot}0024 \pm 0{\cdot}0004$	$+0{\cdot}0044 \pm 0{\cdot}0006$
	$a \sin \beta$	$3{\cdot}818_8 \pm 0{\cdot}001$	$4{\cdot}001_5 \pm 0{\cdot}001_5$	$3{\cdot}942_7 \pm 0{\cdot}001$	$3{\cdot}783_3 \pm 0{\cdot}001$
	$a=c$	3·819	4·003	3·944	3·784
	b	3·815	3·997	3·933	3·800
	β	90° 40′ ± 1′	91° 43′ ± 4′	91° 30′ ± 2′	91° 10′ ± 2′
	$a/b=c/b$	1·0011	1·0015	1·0028	0·9958
	(vol.)$^{1/3}$	3·818	4·001	3·940	3·789
Orthorhombic large cell	A	10·740	11·152	11·034	10·594
	B	7·630	7·994	7·866	7·600
	C	10·864	11·492	11·302	10·812
	A/B	1·4076	1·3951	1·4028	1·3939
	C/B	1·4239	1·4376	1·4367	1·4226

Table 13. Rhombohedral structure

Barium titanium oxide II

$a=b=c=4{\cdot}035 \pm 0{\cdot}005$ kx.

$\alpha=90°\ 19' \pm 3'$

(vol.)$^{1/3}=4{\cdot}035$ kx.

§ 6. DISCUSSION OF RESULTS

Cubic

These need no further comment.

Tetragonal

There are considerable discrepancies between the accounts in the literature of the three substances.

$BaTiO_3$ was said by Naray-Szabo to be strictly cubic, though Goldschmidt classed it as only pseudo-cubic, but without further detail. It has been found in the present work that while it is normally tetragonal, polymorphous forms (such as the rhombohedral one, of which a preliminary account is given here) do occur under exceptional conditions, and these are at present being investigated. Only structures which exist at room temperature are considered here; it is hoped to deal with temperature changes in a subsequent paper.

The table gives cell-dimensions of typical material, but these are not necessarily the same for all conditions of preparation. In most of the material investigated, however, only small variations of axial ratio occur, leaving the cell-volume constant.

This leaves unexplained the discrepancy between Rooksby's values of the cell-dimensions and those found here, but it may perhaps be due to the polymorphism of the substance.

$PbTiO_3$ was originally said by Naray-Szabo (1943 a) to belong to the same sub-type as $CaTiO_3$ (see below); but in a later paper (1943 b) he showed it to be tetragonal, with cell-dimensions substantially in agreement with those found here, and space-group $D^1_{4h} - P4/mm$. Cole and Espenschied found it orthorhombic, with $a = 4{\cdot}000, b = 4{\cdot}211, c = 3{\cdot}875, a:b:c = 0{\cdot}95:1:0{\cdot}92$, and moreover, found that it was the only intermediate compound occurring in the system $PbO-TiO_2$. $PbZrO_3$ was classed by Naray-Szabo with $CaTiO_3$. The material investigated in the present work gives weak lines besides those due to the tetragonal structure; these have not been interpreted, and may be due to other compounds formed, to a second structure simultaneously present, or to a doubling of one or more of the cell-edges (in which case the dimensions given refer to the pseudo-cell).

Rhombohedral structure

This was found in a preparation of $BaTiO_3$ fired at a high temperature. Further work is in progress, and the report here is only a preliminary note, which seems desirable in view of the novelty among double oxides of the geometrical type illustrated. A rhombohedral perovskite-type structure has been described by Naray-Szabo (1943 b) for ScF_3, with $a = 4{\cdot}022$ kx. and $\alpha = 89^\circ\ 34\frac{1}{2}'$, and comparison should also be made with NiO, found by Rooksby (1943) to be rhombohedral with a very slight departure from cubic symmetry. The amount of departure from cubic symmetry in rhombohedral $BaTiO_3$, as in the tetragonal form, seems to vary with conditions of preparation, and here takes the form of a variation in the interaxial angle α. The value quoted in the table is the largest observed; against this, another preparation gave a strictly cubic structure with about the same cell-volume, which is appreciably larger than that of the tetragonal form.

Monoclinic and orthorhombic structures

Of the structures tabulated, $CaTiO_3$ has been investigated by Naray-Szabo (1943 a), and $CaZrO_3$ by Ruff, Ebert and Stephan (1929). Their results agree with those in the present work within the limits of accuracy claimed. It is possible that small variations in the cell-dimensions of different samples may exist, as in barium titanate; such a variation is stated by Goldschmidt and Rait (1943) to occur when $CaTiO_3$ takes up CaO in solid solution.

Naray-Szabo, using single-crystal methods, determined the atomic parameters of $CaTiO_3$. He found that the intensities are consistent with the assumption that the cations are not displaced, while the oxygens are displaced in such a way as to retain approximately regular octahedra round the Ti's, though leaving them tilted relative to one another and making a puckered network. His structure is shown in figure 5.

The displacement of the atoms from their special positions must be consistent with their true symmetry. Naray-Szabo's set of oxygen parameters has monoclinic symmetry only; however, very slight changes in some of them would give orthorhombic symmetry with the new axes postulated above, and it is probable that such changes are within his limits of accuracy.

It is noteworthy that in all the compounds of this type that have been examined, the *a* and *c* edges of the pseudo-cell remain equal. No difference is recorded by any author, and none was found in the present work, though special attention was paid to the point and the technique was such that very small differences could have been detected. While the evidence is not final, an orthorhombic structure thus seems much more probable, the new [001] and [100] axes being the [101] and [10$\bar{1}$] directions of the monoclinic lattice.

It was mentioned earlier that the true cell required the doubling of some of the edges of the pseudo-cell, but not necessarily all. It is simplest, however, to make the provisional assumption that all are doubled, transfer to the orthorhombic axes, and then look for special absences among the indices of reflexions. This has not been carried out in detail; enough lines have been indexed to confirm the fact that all can be indexed on this large cell, but the overlaps are too numerous for completely unambiguous indexing. The available evidence suggests that the doubled value of *b* is necessary, and also that of either *a* or *c*, possibly both. The volume of the true cell is then either $8a^3$ or $16a^3$ approximately.

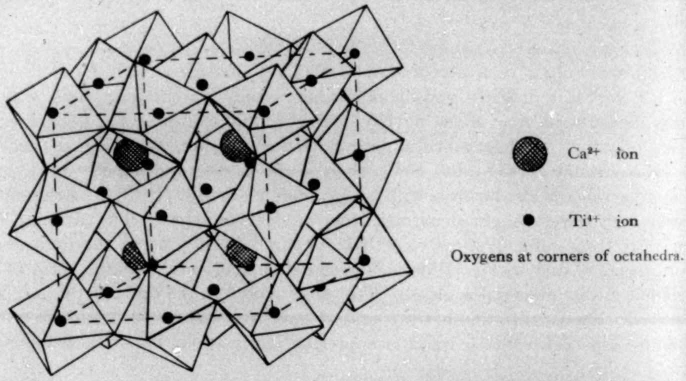

Figure 5. Structure of $CaTiO_3$ (according to Naray-Szabo).

While the extra lines, needing the doubled cell, are numerous and of moderate intensity for $CaTiO_3$, they are very few and weak for $CaZrO_3$ (as can be seen by comparison of figures 2(*d*) and (*e*), $CaSnO_3$ occupying an intermediate position. This strongly suggests that they are due to displacements either of the oxygens alone or of oxygens and Ca ions, leaving the 4-valent cation, whose contribution to the intensity increases rapidly in the order Ti^{4+}, Sn^{4+}, Zr^{4+}, undisplaced from the special position it occupied in the simple cell. This agrees with the conclusion reached by Naray-Szabo, from detailed work on the atomic parameters in $CaTiO_3$, that both cations remain in special positions and only the oxygens are displaced.

By contrast, there are certain striking intensity relationships in $CdTiO_3$. Firstly, the lines needing the doubled cell are prominent at high angles, where they are of the same order of intensity as the main lines (see figure 2(*f*)). This implies displacement of the cations from their special positions, as the oxygen contribution could not by itself effect this. Both from the intensity, and because the Cd ion is held by weaker electrostatic bond strengths in the structure (2/12 for the Cd-O bond as compared with 4/6 for Ti-O), it seems likely that it is the Cd ions that are displaced. Secondly, the reduction in intensity of "main" lines with high values of orthorhombic l index, (that is, with monoclinic h–l large), and the preponderance with appreciable intensity of "doubled-cell" lines also with high orthorhombic l, independently suggest that the atomic displacement is along the orthorhombic z-axis, that is, along the long diagonal of the monoclinic pseudo-cell. Even without any displacement of the oxygens, this brings the Cd ion closer to six of its neighbouring oxygens and further away from the other six, thus making a first step towards the attainment of 6-coordination which is appropriate to the radius of the Cd ions. Displacements of the oxygens are likely to reinforce this tendency.

§7. CRITERION FOR FORMATION OF DIFFERENT STRUCTURES.

Goldschmidt (1937) showed empirically that structures having the generalized perovskite type occur when the tolerance factor t, defined as

$$t=\frac{R_A+R_O}{\sqrt{2}(R_B+R_O)}$$

(where R_A, R_B, R_O are the ionic radii of the ions A, B, O respectively), lies between 0·80 and 1·00. Lower values of t are associated with the corundum-ilmenite type (a rhombohedral structure). Later authors showed that for values of t at the lower end of the perovskite range "deformed" (i.e. monoclinic or orthorhombic) structures occur.

Table 14. Values of tolerance factor t

			Ti^{4+}	Sn^{4+}	Zr^{4+}	Th^{4+}
	R_B (kx.) R_A (kx.)		0·64	0·74	0·77	1·10
	6-coord.	12-coord.				
Ca^{2+}	1·06	1·16	0·89	0·85	0·84	0·72
Sr^{2+}	1·27	1·37	0·97	0·92	0·91	0·78
Ba^{2+}	1·43	1·52	1·02	0·97	0·96	0·83
Pb^{2+}	1·32	1·40	0·98	0·92	0·93	0·79
Cd^{2+}	1·03	1·11	0·88	0·83	0·82	0·71

Table 14 shows the values of t for the compounds under discussion. They are calculated from Goldschmidt's ionic radii except that Naray-Szabo's corrected value of 0·77 kx. has been accepted for Zr^{4+}; this value has been confirmed by the present work, as appears in table 15. A correction for 12-fold coordination has been applied to the R_A, as Goldschmidt's radii are quoted for 6-coordination; the correcting factor was taken from Pauling's *Nature of the Chemical Bond* (p. 368).

It should be noted that the Goldschmidt radii are valid only to an accuracy of 1 or 2%; they depend on the assumption that ions can be treated as rigid spheres, which is only true to this degree of accuracy, even when the appropriate corrections for coordination number have been made.

Comparison of table 14 with table 15 shows general agreement with the empirical rule; all the compounds observed to have the perovskite structure have t-values not less than 0·80, and those with the orthorhombic modification lie between 0·80 and 0·89. The t value of $BaThO_3$ seems rather low for its cubic structure, but this is probable due to an incorrect Th^{4+} radius (as explained later). The lead compounds are slightly anomalous. $BaTiO_3$ is unique in having a value of t above unity.

The explanation of these relationships may be better seen by consideration of the interionic distances A-O and B-O actually observed. These are given in table 16, with the sum of the Goldschmidt radii quoted for comparison. The figures in brackets for the orthorhombic structures are approximations, based on the cubic oxygen parameters. For $BaTiO_3$, figures are also given calculated from Naray-Szabo's parameters (which are probably partly derived from the assumption of Goldschmidt's distance). Owing to the low symmetry there are sets of A-O and B-O distances for each substance, and the figures give an idea of the range included.

Table 15. Different structures observed

	Titanium	Tin	Zirconium	Thorium
Calcium	Orthorhombic * (referred to monoclinic axes, $\beta=90°\ 40'$)	Orthorhombic * (referred to monoclinic axes, $\beta=91°\ 30'$)	Orthorhombic * (pseudo-monoclinic with $\beta=91°\ 34'$)	—
Strontium	Cubic	Cubic	Cubic	—
Barium	Tetragonal $c/a=1{\cdot}01$	Cubic	Cubic	Cubic
Lead	Tetragonal $c/a=1{\cdot}06$	—	Tetragonal $c/a=0{\cdot}99$	—
Cadmium	Orthorhombic * (referred to monoclinic axes, $\beta=91°\ 10'$)	—	—	—

* For relation of orthorhombic and monoclinic axes, see text.

To realize the significance of these figures, it must be understood that the dimensions of the structure are primarily determined by the B-O octahedra, where the strong valence bonds of value 2/3 keep the octahedra as nearly rigid units (though they may be tilted relative to each other). The network is only stable if the holes are occupied by A cations to restore electrical neutrality. Since the valence bonds to these are weak, of value 1/6, the size of A has much less effect on the structure, but it must be small enough to fit in the hole and large enough to occupy it nearly completely. From table 16, the reasons for the occurrence of the different structures can now be explained in a very general way:—

(*a*) In all the cubic structures, the B-O distance is very little *less* than the sum of the radii, the difference not exceeding 2%. (An apparent exception is $BaThO_3$,

Table 16. Interionic distances (in kx.)

(*a*) A-O distances. Values for the same ion A derived from different compounds are read horizontally.

	Titanium	Tin	Zirconium	Thorium	Goldschmidt's R_A+R_O (R_A corrected for 12-coordination)
Calcium	(2·70) (2·3–3·0)	(2·79)	(2·83)	—	2·48
Strontium	2·755	2·845	2·894	—	2·69
Barium	2·818 2·832	2·907	2·957	3·17	2·84
Lead	2·755 2·844	—	2·917 2·934	—	2·72
Cadmium	(2·69)	—	—	—	2·45

(*b*) B-O distances. Values for the same ion B derived from different compounds are read vertically.

	Titanium	Tin	Zirconium	Thorium
Calcium	(1·91) 1·94–1·96	(1·97)	(2·00)	—
Strontium	1·949	2·012	2·047	—
Barium	1·992 2·013	2·054	2·091	2·243
Lead	1·948 2·072	—	2·050 2·075	—
Cadmium	(1·90)	—	—	—
Goldschmidt's R_B+R_O	1·96	2·06	2·09	2·42

but the discrepancy may be taken as evidence against the accepted value of the Th^{4+} radius.) In the same structures, the A-O distance is *greater* than the sum of the radii by amounts up to 10%. These facts fit the above conditions postulated for the ideal structure.

(*b*) In the orthorhombic structures, if the oxygens remained in their positions of cubic symmetry and the actual cell dimensions were retained, the B-O distances would be too small; a uniform expansion, to give the correct B-O distances, would leave the A-O distances unduly large. The actual structure retains the normal B-O distances, but decreases the average A-O distance (and the cell dimensions) by tilting the octahedra, thus abandoning cubic symmetry. In $CdTiO_3$ the displacement of the Cd ions achieves the same effect.

(*c*) Barium titanate deviates from the normal in the opposite direction. The A-O distance is *less* than the sum of the radii, the B-O distance *greater*. In other words, the Ba ion is too big for the space available in the normal Ti-O network, and a compromise is achieved with some extension of the Ti-O network and some compression of the Ba ion. Why the deformation should be tetragonal is not immediately clear, but it seems possible that the abnormal volume available to the Ti ion may result in the formation of directed bonds.* It is known that the interactions of atoms and ions are very sensitive to volume changes.

(*d*) The lead compounds are anomalous. The A-O distances are less than the sum of the radii; hence one would expect that the B-O distances should be equal to or slightly less than the sum of the radii, and that the symmetry should be cubic. In fact one Ti-O distance is greater than the sum of the radii, and both structures are tetragonal. The explanation may lie in the character of the Pb^{2+} ion, in which the inner shells affect the valency; such an ion cannot be treated, except very roughly, as an undeformable sphere, and formation of directed bonds is very probable, predominating over the purely size effects which determine the other structures.

These explanations of the structure differences are very general, but they and the experimental results on which they are based may suggest the lines along which further theoretical work could be pursued.

ACKNOWLEDGMENTS

I wish to thank Mr. M. A. Strivens for preparing the compounds investigated here. I am indebted to Mr. J. A. M. van Moll and the directors of Philips Lamps, Ltd., for permission to publish this work, which was carried out in the Material Research Laboratory (Philips Lamps, Ltd.), Mitcham.

REFERENCES

Barth, T., 1925. *Norsk. Geol. Tidsskr.* **8,** 201.
Bradley, A. J. and Jay, A. H., 1932. *Proc. Phys. Soc.* **44,** 563.
Cole, S. S. and Espenschied, H., 1937. *J. Phys. Chem.* **41,** 445.
Evans, R. C., 1939. *Crystal Chemistry* (Cambridge: Univ. Press), p. 166.
Goldschmidt, H. J. and Rait, J. R., 1943. *Nature, Lond.*, **152,** 356.
Goldschmidt, V. M., 1927. *Geochem. Vert. d. Elem.* VII, VIII.
Hoffmann, A., 1935. *Z. phys. Chem.* B, **28,** 65.
Lonsdale, K. and Smith, H., 1941. *J. Sci. Instrum.* **18,** 133.
Megaw, H. D., 1945. *Nature, Lond.*, **155,** 484.
Naray-Szabo, S., 1943a. *Naturwissenschaften,* **31,** 203; 1943b. *Ibid.* 466.
Rooksby, H. P., 1943. *Nature, Lond.*, **152,** 304; 1945. *Ibid.* **155,** 484.
Ruff, O., Ebert, F. and Stephan, E., 1929. *Z. anorg. Chem.* **180,** 215.

---

* It is hoped shortly to publish further work on this point.

THE MAGNETO-RESISTANCE OF HIGH COERCIVITY ALLOYS

By L. F. BATES,
University College, Nottingham

MS. received 19 *November* 1945

ABSTRACT. Measurements have been made of the change of resistance of ferromagnetic alloys of high coercivity when exposed to longitudinal and transverse magnetic fields. The changes in the cases of the permanent magnet materials alni, alnico (cast and sintered) and alcomax II are in marked contrast to those of pure ferromagnetic metals. The results are discussed on the basis of the domain concept in ferromagnetism.

§ 1. INTRODUCTION

SEVERAL new alloys of high coercivity and high $(BH)_{\max}$ have become available for the manufacture of permanent magnets within recent years, but data on their magneto-resistance, i.e., the change of resistivity as a function of the magnitude and direction of an applied magnetic field, are not to hand. In the present communication an account is given of the measurement of the magneto-resistance of some representative materials, together with a discussion of the theoretical aspects of the data so obtained.

It is convenient to take a thin rod of the material whose resistance in the unmagnetized state is R_0, and measure the changes $\Delta R_{\parallel}$ and $\Delta R_{\perp}$ which respectively occur when a magnetic field H is applied parallel to and perpendicular to the long axis of the rod, and to plot the values of $\Delta R_{\parallel}/R_0$ and $\Delta R_{\perp}/R_0$ against H. This requires a definition of the unmagnetized state; for present purposes this is taken to be the state of the rod when, by means of a magnetic potentiometer, no difference of magnetic potential can be found over its length. Unfortunately, there is some ambiguity in the matter, since, for example, this result is obtained when the magnetic vectors are either all aligned parallel and antiparallel to the long axis of the rod, or are all aligned perpendicular thereto, in such a way that there is no resultant magnetization.

Important data for polycrystalline specimens of the ferromagnetic metals have hitherto been obtained by Bittel (1938), Englert (1932), Gerlach (1932), McKeehan (1930), Obata (1925), and Scharff (1935). A special study of the relation between the phenomena and the change of spontaneous magnetization as shown by the magnetocaloric effect at high temperatures was made by Potter (1931–32). In the case of permanent magnet materials, initial investigations must, of course, be confined to room-temperature measurements.

The former workers have shown that, for a pure specimen of a ferromagnetic metal, $\Delta R_{\parallel}/R_0$ normally shows a marked initial increase with the applied field; it rises to a maximum and eventually decreases linearly with the field, so that in very high fields it may become zero and, indeed, change sign. In the present work, a specimen of pure cobalt was used for comparison measurements, and the upper curve of figure 1 shows the typical variation of $\Delta R_{\|}/R_0$. When the direction of H is perpendicular to the direction of the current in the specimen, the values of $\Delta R_{\perp}/R_0$ are at first subject to complications due to the high value of the demagnetization field, D.I., but when the demagnetization field is overcome, the value $\Delta R_{\perp}/R_0$ falls rapidly with increase in H and finally decreases with the applied field at the same rate as $\Delta R_{\|}/R_0$, as shown by the lower curve in figure 1. The two points nearest the origin on the lower curve lie above the H axis, but this is merely because the specimen is of finite cross-section and its long axis cannot be placed absolutely at right angles to the applied field; consequently, a small longitudinal component is always present.

The main features of the curves of figure 1 may be explained on the Weiss domain theory of ferromagnetism, if we suppose that magneto-resistance changes occur only when domain vectors turn through angles between 0 and 90° or when boundary displacements take place between neighbouring domains whose vectors are perpendicular to one another, and that they do not occur to any marked extent when vectors as, for example, those parallel to a direction of easy magnetization in a single crystal, turn through 180°. In order that Ohm's law may be satisfied, the resistance of a polycrystalline specimen of a ferromagnetic metal must be a function of $\overline{\cos^2\theta}$, where θ is the angle between the direction of the current in a portion of the specimen and that of the field when saturation conditions set in; the bar denotes the average taken over all portions of the specimen. Hence the resistivity of the material may in general be written as

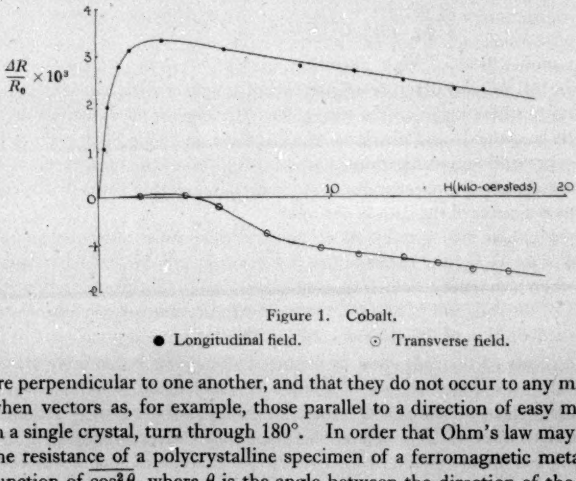

Figure 1. Cobalt.

● Longitudinal field. ⊙ Transverse field.

$$\rho = A + B\overline{\cos^2\theta}, \qquad \ldots\ldots(1)$$

where A and B are constants. In an isotropic demagnetized state $\overline{\cos^2\theta}$ would have the value $\frac{1}{3}$, giving $\rho = \rho_0 = A + \frac{1}{3}B$. Under saturation conditions, with current and field parallel, we have

$$(\rho_{\|})_{\text{sat}} = A + B, \qquad \ldots\ldots(2)$$

and, with current perpendicular to the field,

$$(\rho_{\perp})_{\text{sat}} = A. \qquad \ldots\ldots(3)$$

Since, in practice, we measure relative changes of resistance only, it is more convenient to write for the general case of non-isotropic material, starting from $\rho_0 = A + B\overline{\cos^2\theta_0}$,

$$\left(\frac{\Delta R_\parallel}{R_0}\right)_{\text{sat}} = \frac{B(1-\overline{\cos^2\theta})}{A+B\overline{\cos^2\theta_0}}, \qquad \ldots\ldots(4)$$

$$\left(\frac{\Delta R_\perp}{R_0}\right)_{\text{sat}} = \frac{-B\overline{\cos^2\theta_0}}{A+B\overline{\cos^2\theta_0}} = a, \qquad \ldots\ldots(5)$$

and

$$\left(\frac{\Delta R_\parallel}{R_0}\right)_{\text{sat}} - \left(\frac{\Delta R_\perp}{R_0}\right)_{\text{sat}} = \frac{B}{A+B\overline{\cos^2\theta}} = b, \qquad \ldots\ldots(6)$$

whence

$$\overline{\cos^2\theta_0} = 1\Big/\left[1-\left(\frac{\Delta R_\parallel}{\Delta R_\perp}\right)_{\text{sat}}\right]. \qquad \ldots\ldots(7)$$

In the case of isotropic material, it follows that $(\Delta R_\parallel)_{\text{sat}}$ should be equal to $-2(\Delta R_\perp)_{\text{sat}}$, as found by Thiessen (1940) for annealed nickel, and, moreover, equation (7) means that $(\Delta R_\parallel)_{\text{sat}}$ and $(\Delta R_\perp)_{\text{sat}}$ must have opposite signs or $(\Delta R_\parallel)_{\text{sat}}$ be zero. The value of *b*, which is the relative change in resistance when the magnetic state of the specimen is changed from transverse to longitudinal saturation, is clearly independent of the initial state of the specimen and, practically, of the value assumed for ρ_0. It should also be the same for polycrystalline as for single-crystal specimens. Positive values of *b* have been found for all materials previously investigated to date.

It is generally agreed that the intensity of magnetization of each Weiss domain may be increased slightly by the application of a strong field, and this provides the reason for the linear rates of change of $\Delta R_\parallel/R_0$ and $\Delta R_\perp/R_0$ at high values of the field, as depicted in figure 1. Theoretically, the two rates should be equal, and this is obviously the case for the cobalt specimen within the limits of experimental error. The values $(\Delta R_\parallel/R_0)_{\text{sat}}$ and $(\Delta R_\perp/R_0)_{\text{sat}}$ refer to saturation conditions extrapolated to zero external field. Consequently, to find the required value of $(R_\parallel/R_0)_{\text{sat}}$ from figure 1, the linear portion of the upper graph must be produced to cut the axis of ordinates, since we may neglect longitudinal demagnetization effects. The linear portion of the lower graph must be produced to cut the ordinate at $\mathrm{H} = 2\pi I_s$, where I_s is the value of the intensity of magnetization, obtained by producing back the (I, H) curve at high field values to cut the I axis, and 2π is the demagnetization factor for a long narrow cylinder or rod magnetized at right angles to its long axis.

§ 2. EXPERIMENTAL PROCEDURE

Modern permanent magnet materials cannot, in general, be forged or machined. They are roughly cast to shape and ground to size. All specimens used in the present work were approximately 2·2 cm. long and 1 mm. square in cross-section. A potentiometer method was used to measure relative changes of resistance. The specimen was mounted for $\Delta R_\parallel$ measurements as follows. Copper end plates 0·8 mm. thick were screwed flush to the end faces of an ebonite block 1·9 cm. long and about 1·25 cm. by 1·0 cm. in cross-section. Current leads were soldered to the plates. The specimen was sunk into a saw-cut made in the common upper surfaces of ebonite and copper plates, so that one side surface of the specimen was flush with the ebonite. Electrical connection between specimen and copper was made with a minimum quantity of soft solder and designed to give easily if the specimen suffered appreciable magnetostrictive change of dimensions. The potential leads consisted of thin tinned-copper wires inserted through fine holes drilled in the ebonite to lie with their axes slightly to one side of the specimen and some 1·8 cm. apart. The wires were pressed into contact with one side of the specimen by fine screws which ran parallel and close to the upper surface of the ebonite and at right angles to the axis of the specimen. The whole mounting was supported between the pole-faces of an electro-magnet, paper packing being used to prevent lateral motion and to allow for dimensional changes in the magnet, thermal expansion, etc.

The same ebonite and copper arrangement was used for measurements of $\Delta R_{\perp}$, but experience showed the specimen to be severely strained unless special precautions were taken. Accordingly, the ebonite block was placed horizontally inside a frame consisting of two thick vertical iron plates, 2·5 cm. by 2·5 cm. and 6 mm. thick, separated above and below the ebonite by brass distance pieces. The axis of the specimen was parallel to the steel plates, and the ebonite was fixed to one of them only, a small air gap existing between the ebonite and the other plate.

A constant current was maintained in the specimen, by balancing the p.d. across a standard 1 ohm, in series with the specimen, against a Weston cell. The p.d. between the potential leads on the specimen could then be balanced by means of a sensitive galvanometer against the p.d. in an adjustable resistance P forming part of a potentiometer circuit. The latter consisted of an accumulator in series with a fixed resistance of 20,000 ohms and the resistance P, which was made up from the following: a dial box resistance, reading to 0·1 ohm, a standard 1 ohm with shorting plug, two small home-made rheostats of thick copper wire, each of about 0·1 ohm resistance, and the necessary leads. The value of P was usually between 50 and 120 ohms, and, of course, provided a measure of the resistance of the specimen between the potential leads.

In the absence of a magnetic field, the p.d. between the potential leads on the specimen was first fairly accurately balanced against the p.d. in P by adjusting the resistances in the dial box, and then more exactly balanced by adjusting the copper wire rheostats. The magnetic field was thereupon switched on and the resulting galvanometer deflection δ was noted; its direction gave the sign of ΔR. The arrangement was calibrated by observing the galvanometer deflection D when the standard 1-ohm resistance in P was shorted, whence the value of $\Delta R/R$ was given by δ/PD. Checks on this calibration were obtained by shunting the standard 1 ohm in the main current circuit with a 50-ohm resistance and noting the corresponding galvanometer deflection D' when 50 D' should be equal to PD. At least four values of ΔR were taken with the main current in the two directions for each chosen value of H.

The field acting on the specimen when mounted for longitudinal measurement was found by means of a small semi-circular magnetic potentiometer of 542 turns, each of approximately 10 mm. × 3 mm. in area, with a distance of 1·3 cm. between the mid-points of its feet. It was joined in series with the galvanometer used in the ΔR measurements, together with resistances necessary to permit the range of fields to be measured. It was calibrated in the usual way (Bates 1939, 1945), the necessary factors required when additional resistances were used being found by means of a mutual inductance. In the case of the transverse measurements, a small contact search-coil of 17 turns, wound in one layer on a rectangular former 2·0 cm. long and 2mm. wide, was joined in series with the galvanometer and calibrated with the aid of a mutual inductance against a standard search-coil used in known magnetic fields.

Reference has been made to the lack of precise knowledge of the actual distribution of domain vectors in a demagnetized specimen. After each individual ΔR measurement, the specimen was demagnetized by reversals and the residual field acting upon it was measured by search-coil or magnetic potentiometer. This field was caused by residual magnetism in the electromagnet and in the specimen itself. It was brought to zero by applying momentarily a neutralizing field whose value was found by trial. The first measurements of the residual field usually gave a reliable indication of the magnitude and direction of the required neutralizing field; and greater and greater field currents were switched on momentarily in the electromagnet until, finally, no residual field could be detected. Yet, however carefully a specimen was initially demagnetized from a given state of magnetic saturation, there sometimes occured extraordinary variations in the magnitude and direction of the residual field. These were on occasion so large that the specimens had to be remagnetized and demagnetized *de novo*; accidental surges may have played a part here. Other points of interest are described under the several headings in the following section.

§ 3. EXPERIMENTAL RESULTS

Cobalt

The specimens were ground from a sample of No. 12 S.W.G. wire (hard-drawn) kindly supplied by Messrs. Brandhurst & Co., Ltd., The sample was 98·4% pure, the chief impurities being Ni 0·45, Fe 0·13, CaO 0·23, Mn 0·08, C 0·19, Zn 0·01, MgO 0·11, SiO_2 0·14 and S 0·02 per cent; the loss in hydrogen was 0·24 per cent. As mentioned above, the main reason for using cobalt was to test the accuracy and suitability of the method for magnetically hard materials. The results of figure 1 give $b = 4{\cdot}5 \times 10^{-3}$.

Cobalt steels

Results for a 15% cobalt steel, used in the manufacture of ships' compasses and made according to the original Kelvin recipe, are given in figure 2; the material was kindly supplied by Messrs. Swift, Levick & Sons, Ltd. The material gives values of $\Delta R_{\parallel}/R_0$ and $\Delta R_{\perp}/R_0$ on opposite sides of the H axis, in accordance with theory, with a value of $b = 2{\cdot}7 \times 10^{-3}$.

Two specimens, I and II, of 35% cobalt steel, kindly supplied by Messrs. Jessop & Sons, Ltd., gave the results shown in figure 3. This material has a remanent induction of 9350 gauss, a coercivity of 240 oersteds and a $(BH)_{\max}$ of $0{\cdot}96 \times 10^6$ gauss-oersteds. Both specimens showed very strange demagnetization characteristics. Following a set of $\Delta R_{\parallel}$ measurements, a specimen demagnetized by reversals in the routine manner showed only weak residual magnetism. Yet on trying to reduce the latter by the momentary application of demagnetizing fields of gradually increasing intensity, the magnetization actually increased to a maximum and then fell to zero. Again, in the case of $\Delta R_\perp$ measurements with specimen I, sudden large deflections were often observed when the galvanometer was placed in circuit immediately after the field had been excited. These might be explained on the assumption that the resistance changes showed a time lag, probably connected with the strange demagnetization behaviour. The values of b for the two specimens are respectively $0{\cdot}75$ and $0{\cdot}70 \times 10^{-3}$. It would be interesting to know whether a steel with, say, 40 per cent of cobalt give a value of b equal to zero.

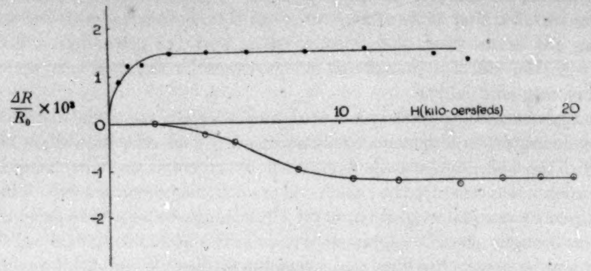

Figure 2. Kelvin magnet steel (15% cobalt steel).

● Longitudinal field. ⊙ Transverse field.

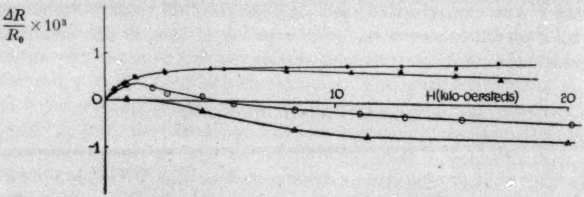

Figure 3. 35% cobalt steel.

● Longitudinal field
⊙ Transverse field
} Specimen I.

▲ Longitudinal field
△ Transverse field
} Specimen II.

Alni

The approximate composition of this alloy is iron 59, nickel 24, aluminium 13 and copper 4 per cent. Specimens were kindly supplied by Messrs. Jessop & Sons, Ltd. They gave a remanent induction of 6170 gauss, a coercivity of 515 oersteds and a $(BH)_{\max}$ value of $1{\cdot}38 \times 10^6$ gauss-oersteds. Results of ΔR measurements are given in figure 4. It will be noted that the graphs of $\Delta R_\parallel/R_0$ and $\Delta R'_\perp/R_0$ both lie below the axis. The value of b is $1{\cdot}15 \times 10^{-3}$.

Little significance is here attached to any difference in slope between the high-field portions of the two graphs, particularly as the specimen showed marked directional effects with respect to the field, especially in the case of the transverse measurements, where the values of $\Delta R_\perp$ for a field of given intensity (low) were about twice as great with the field in one direction as in the other. The mean values of $\Delta R_\perp/R_0$ are plotted in figure 4. The directional effect was much less pronounced in the longitudinal measurements, but before commencing a set of readings it was necessary to magnetize the specimen in a strong field, say 15,000 oersteds, and then demagnetize it by reversals, in order to obtain results which could be reproduced. This was also a feature common to steels containing much cobalt, and may perhaps be put forward in support of a suggestion by Brown (1945) that very low values of the coercivity of the single crystals of ferromagnetic metals, which have so far been investigated, have been obtained simply because these crystals have not been placed in a field, say 100,000 oersteds, sufficiently strong to break down the domains completely. Throughout the whole of the work the importance of demagnetization from high fields was constantly coming to the fore.

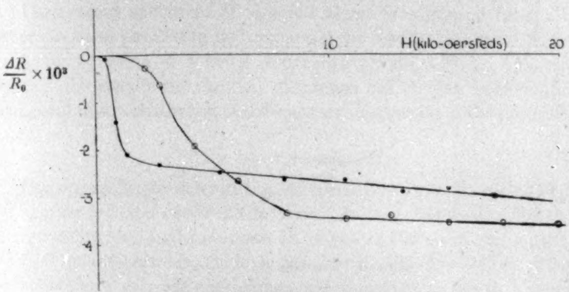

Figure 4. Nial or alni.

● Longitudinal field. ⊙ Transverse field.

Alnico

The approximate constitution of alnico is iron 54, nickel 17 to 18, aluminium 11 to 10, copper 6 and cobalt 12 per cent. It has a remanent induction of 8200 gauss, a coercivity of slightly over 500 oersteds and a $(BH)_{\max}$ value of $1{\cdot}7 \times 10^6$ gauss-oersteds. In figure 5 are given the results for a rod of cast alnico, kindly supplied by Messrs. Jessop & Sons, Ltd. The graphs make clear the difficulty caused in some cases by lack of precise knowledge of the demagnetization field appropriate to the transverse measurements. One cannot be much in error in taking $2\pi I_s$ in figure 5 to be the applied field at the point of inflection, i.e. 5000 oersteds. This gives the value of b equal to zero, but if we take a lower value of $2\pi I_s$ we obtain a negative value of b. At high values of the longitudinal field, some uncertainity in the measurements was experienced, suggestive of the specimen being unduly strained.

Two specimens of sintered alnico, kindly supplied by Messrs. Murex Ltd., were also used. Powdered alnico cannot be sintered, of course, and the specimens were made by sintering a mixture of the constituent metals under pressure.

Sintered alnico is supposed (cf. Wulff, *Powder Metallurgy*, Cleveland, 1942) to be fine-grained and therefore stronger than the relatively coarse-grained cast product. Since it is consolidated by inter-diffusion, it is reported to have no cracks, " cold shuts ", or segregation of impurities at grain boundaries, so that there are no consequent poles produced by physical imperfections and a more uniform flux distribution can be obtained in the material.

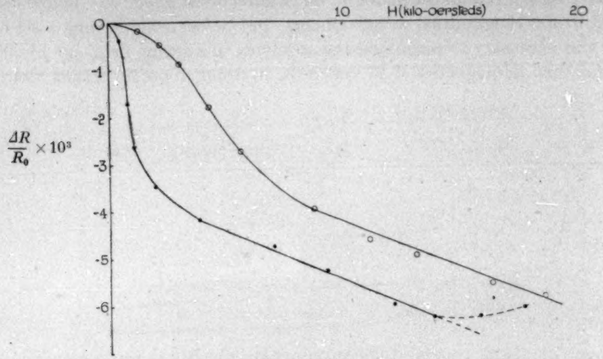

Figure 5. Cast alnico.

● Longitudinal field. ⊙ Transverse field.

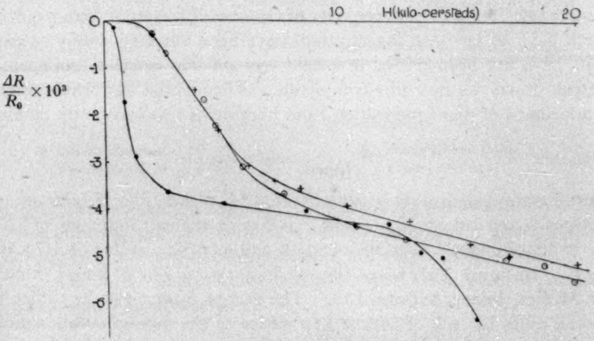

Figure 6. Sintered alnico cut from disc.

● Longitudinal field parallel to face of disc.

⊙ Transverse field perpendicular to face of disc.

+ Transverse field perpendicular to side of disc.

The first specimen of sintered alnico, for which the results are given in figure 6, was a rod of square cross-section ground from a disc 2·1 cm. in diameter and 0·15 cm. thick, sintered under pressure perpendicular to the disc face. It was not magnetically tempered during cooling. In figure 6 the encircled points refer to measurements made with the applied field perpendicular to the axis of the rod and to a surface of the rod which had previously formed part of the disc surface, and the crosses refer to measurements with the field perpendicular to the axis of the rod and parallel to this surface. The two sets of measurements coincide within the limits of experimental error, so that no marked difference existed due to directional effects associated with the application of pressure during manufacture. The most striking feature of the results is, again, the smallness of the value of b; indeed, the results represented by the crosses give a small negative value for b.

The second specimen of sintered alnico was ground from a rod prepared under pressure parallel to its long axis; the results are similar to those shown in figure 6, the value of b being approximately $0{\cdot}7 \times 10^{-3}$. The main difference between the results for the two specimens lies in their behaviour in the higher fields, and this is attributed to different states of strain in the two cases.

Alcomax II

The approximate constitution of this alloy is iron 50, nickel 11·5, aluminium 8·0, copper 5·5 and cobalt 25 per cent. It has a coercivity of 500 to 650 oersteds, corresponding residual induction 13,500 to 12,000 gauss and a $(BH)_{\max}$ value of $4{\cdot}3 \times 10^6$ gauss-oersteds, (vide *J. Sci. Instrum.* **22**, 56 (1945)). Its exceptionally high coercivity, etc., are obtained as directional properties by a special heat treatment in a strong magnetic field, after casting. The above values of coercivity, etc., are measured for fields applied in the same direction as that in which the specimen was placed during this heat treatment. The magnetic properties in the favoured direction are obtained, to some extent, at the expense of those in directions perpendicular thereto, which are less good. It is reasonable *a priori* to suppose that in the unmagnetized state the large majority of the magnetic vectors are aligned either parallel or antiparallel to the favoured direction.

Resistance measurements were made with four specimens kindly supplied by Messrs. Jessop & Sons, Ltd. The results of figures 7 and 8 were obtained with specimens III and IV respectively. In the latter case measurements of $\Delta R_{\parallel}/R_0$ in low fields showed marked peculiarities, the sign and the magnitude of the deflection δ depending on the direction of the applied field; these are very clear in figure 8. It is possible that these peculiarities were due to the existence of (small) regions of exceptionally high coercivity. If one such region had its magnetic axis coincident with the specimen, the application of a longitudinal field would cause an increase or a decrease in resistance according as the magnetization of the region was decreased or increased respectively. This would account for the observed changes in δ. It should be remembered that a weak external field would give rise to a big induction inside the specimen. If the magnetic axis of the region is not coincident with that of the specimen, then we have a ready explanation of the large increase in $\Delta R/_{\perp}R_0$ in low fields as depicted in figure 8.

The suggestion finds support from the difficulties experienced in demagnetizing the specimen by reducing its residual field to zero. Usually, the necessary opposing field current to be supplied momentarily to the electromagnet could be found in a straightforward manner, because with increasing values of the demagnetizing field the potentiometer gave smaller and smaller galvanometer deflections, which finally became zero when the correct state was reached. With specimens III and IV, however, a strange, rapid motion was superimposed upon the ordinary galvanometer deflection as the residual field became small, and it was difficult to decide when the ordinary deflection was zero. In fact, it was often found necessary to leave a very small residual field unneutralized. The concept of a small region of high coercivity is well supported by recent experiments made in this laboratory on alcomax magnets (Bates, 1945).

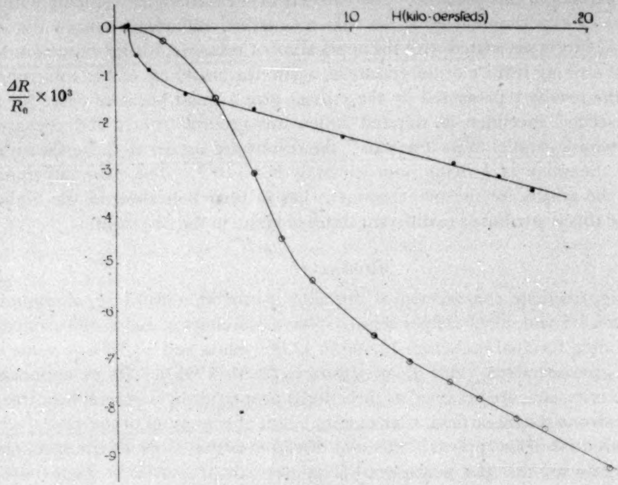

Figure 7. Alcomax II: specimen III.

● Longitudinal field. ⊙ Transverse field.

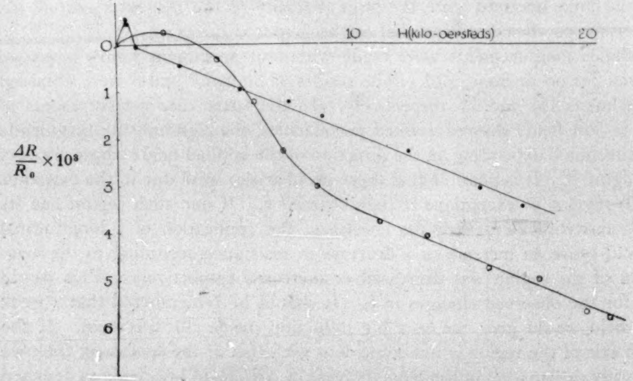

Figure 8. Alcomax II: specimen IV.

● Longitudinal field. ⊙ Transverse field.

The values of b from figures 7 and 8 are respectively $4{\cdot}4$ and $3{\cdot}7 \times 10^{-8}$. There are differences in the final slopes of the curves of longitudinal and transverse changes, but, in view of the uncertainty concerning the initial states of demagnetization, it is not profitable to discuss them at this stage. Resistance and corresponding magnetization and magnetostriction data for a large number of specimens of alcomax II would be necessary, for anyone with experience of high-coercivity alloys knows how wide is the variation in properties from specimen to specimen. Moreover, a special technique for measuring the slopes alone would have to be instituted to give the necessary accuracy.

It is reasonable to picture a rod formed from an ideal specimen of alcomax II as consisting of domains set with their magnetic vectors parallel to the axis of the rod, with domain sides likewise parallel to this axis. There should therefore be no abrupt change of resistance when a longitudinal field is applied, i.e., the linear portions of the upper graphs in figures 7 and 8 would, in these circumstances, pass through the origin. In ordinary specimens it is extremely unlikely that the magnetic vectors will lie exactly parallel to the geometrical axis of the rod, and that the walls of the domains will be perfectly straight and parallel. It is much more likely that there will be pockets and protuberances along the walls, which will be subject to strong lateral forces when large fields are applied. In other words, the slope of the linear portion of the $\Delta R_{\parallel}/R_0$ graph may be affected thereby, and the coarse-grained structure of alcomax is particularly liable to give rise to such phenomena. So far, no measurements have been made of magnetostriction effects, and these may play a very important part during the initial stages of magnetization.

§ 4. DISCUSSION

The interesting fact emerges from these experiments that the resistance of every modern high-coercivity alloy here investigated is always decreased by the application of a magnetic field, whether parallel or perpendicular to the direction of the current, apart from one or two small exceptions to this rule, when very small fields are used, which are readily understood. A similar behaviour had previously been noted only in the cases of Heusler alloy (Potter, 1932) and copper-rich alloys like constantan (Obata, 1925). Now, according to equation (7) above, the theory of domain magnetization requires that $\Delta R_{\parallel}/R_0$ and $\Delta R_{\perp}/R_0$ extrapolated to zero effective field from measurements made in strong fields should have opposite signs, which is in flat contradiction with the experimental data. An obvious suggestion to overcome this difficulty is that the magnetostriction deformations of the domain boundaries or, possibly, of the boundaries between the metal grains, play an important part. Nothing is known about the magnetostriction properties of high coercivity alloys, and it may be that their determination, now contemplated in this laboratory, will throw light on the problem.

It is also interesting that in all cases the value of b is positive or zero within the limits of experimental error; the one case, alnico, in which there are indications that b has a small negative value cannot be regarded as a proven exception to the rule. Measurements on cast and sintered alnico show no marked distinguishing features, possibly because cobalt is acting as a solvent metal in both types of material. It has been pointed out that b, which denotes the relative change in resistance when the magnetic state of the specimen is changed from longitudinal to transverse saturation in the same effective field, should be the same for polycrystalline as for single crystal-specimens. But we now have experimental proof that b can be zero within the limits of experimental error, and we are forced once again to the conclusion that the main resistance changes measured may be due to changes in the boundaries between the metal grains. This raises the interesting question of the reason for the marked directional properties of alcomax. Are they to be attributed to the boundaries between the grains?

Following Jones (1945), we may suppose that the boundaries in cast metals are likely to be peculiar to the alloy under consideration and likely to consist of an arrangement of atoms which is to some extent ordered. The suggestion sometimes made that there is a fundamental difference between the nature of the boundary in cast and sintered metals finds little or no support from the present experiments.

§ 5. ACKNOWLEDGMENTS

I am much indebted to the Government Grant Committee of the Royal Society for the electromagnet used in this work and also to Imperial Chemical Industries, Ltd., for much other apparatus. I am also indebted to the several firms and their research staffs who so kindly provided me with suitable specimens.

REFERENCES

Bates, L. F., 1939. *Modern Magnetism* (Cambridge: The University Press), p. 64; 1945. *Phil. Mag.* **36**, 297.

Bittel, H., 1937. *Ann. Phys., Lpz.*, **29**, 219.

Brown, W. F., 1945. *Rev. Mod. Phys.* **17**, 15.

Englert, E., 1932. *Ann. Phys., Lpz.*, **14**, 589.

Gerlach, W., 1932. *Ann. Phys., Lpz.*, **12**, 849.

Jones, W. D., 1945. *Principles of Powder Metallurgy* (London: Ed. Arnold & Co.), p. 74.

McKeehan, L. W., 1930. *Phys. Rev.* **36**, 948.

Obata, J., 1925. *Sci. Rep. Tôhoku Univ.*, Nagaoka Anniv. Vol., p. 219.

Potter, H. H., 1931. *Proc. Roy. Soc.* A, **132**, 560; 1932. *Phil. Mag.* **13**, 233.

Scharff, Gertrud, 1935. *Z. Phys.* **97**, 73.

Thiessen, G., 1940. *Ann. Phys., Lpz.*, **38**, 167.

THE ABSORPTION OF SOUND IN A HOMOGENEOUS POROUS MEDIUM

By R. A. SCOTT,
Manchester

MS. received 15 *October* 1945

ABSTRACT. Recent theories relating to the wave-propagation of acoustic disturbances in homogeneous, isotropic porous media are discussed, and expressions are given of the wave-equation and for the oscillatory pressure in the material in terms of a " velocity potential of average flow ". In their most general form these expressions are closely analogous to those which correspond to the propagation of sound in free air. The general theory is expressed in terms of two complex parameters which respectively take the place of the wave-length constant and the mean density of the air, which figure prominently in elementary acoustic theory. Expressions for the complex parameters are also given in terms of the " effective " inertia, compressibility and flow-resistance of the material.

Theory shows that numerical values of the components of the complex parameters can be obtained experimentally for practical absorbing materials at a given frequency by measurement of the attenuation constant and of the velocity of propagation of sound in the medium, together with measurement of the normal acoustic impedance at the surface of a sample of the material of effectively unlimited depth. Experimental methods suitable for these measurements are described and results of such measurements are given for a typical sample of porous material. Validity of the general theory as applied to this material is suggested by the good experimental agreement obtained on applying the theory to measurements of the normal acoustic impedance of specimens of various finite depths of the material.

From the measured values of the complex parameters referred to above, calculations of effective inertia, compressibility and porous resistance are made for the material used in the experimental work and the manner of variation of these quantities with frequency is deduced. The results throw interesting light on the mechanism of the propagation of sound in the material.

---

§ 1. INTRODUCTION

The bulk of the materials used in acoustics for the absorption of sound depend for their operation on the viscous dissipation of energy in the air contained in pores in the material. From the macroscopic point of view these porous materials may be either homogeneous, as in the case of cotton-waste, felt or rock-wool, or composite, as in the case of " acoustic tiles ", which have perforated coverings of semi-rigid material. In either case the performance of the whole material depends on the manner in which acoustic disturbances are propagated in the homogeneous porous medium. In this paper a treatment is given, following the lines of those of Wintergerst, Monna, Morse, and others, of the propagation of an acoustic disturbance in three dimensions in a homogeneous, isotropic porous medium. Experiments made to check the theory are described and their results discussed in the light of the theory.

§ 2. GENERAL THEORY

Rayleigh (1929) has investigated the performance of an idealized absorber of sound, consisting of a bundle of small tubes (see also Crandall, 1927). He extended the theories of Helmholtz and Kirchhoff that relate to the transmission of sound along tubes and was able to deduce a value for the absorption coefficient at the surface of such a material in terms of the proportion of the surface area occupied by open pores, the radius of the tubes and the physical constants of the air. This analysis has provided a qualitative basis on which to found more general theories and has led to a number of attempts to give a detailed description of the mode of action of materials such as are used in practice.

Rayleigh's theory is important in that it shows that a sound wave falling on the absorber continues, in part, to be propagated as a wave in the air in the material and that the phase velocity of the latter wave is determined by the viscosity as well as by the density and the elasticity of the air. Most porous materials used in acoustics are composed of an almost random entanglement of fine fibres in three dimensions, rather than of a collection of similar parallel tubes, and it is clear that detailed conclusions drawn from Rayleigh's theory would be inappropriate to such materials. It remains probable, however, that an acoustic disturbance is propagated as a highly attenuated wave of definite velocity through any type of homogeneous porous material, and it is demonstrated later in this paper that this surmise is correct. Wintergerst (1931), Monna (1938), and others (see Morse and Bolt, 1944) have shown that it is possible to remove the restriction of a cylindrical shape for the pore whilst still retaining wave propagation in the material. These investigators show that the attenuation and phase velocity of the wave can be expressed in terms of an effective density and elasticity of the air and of a coefficient representing the resistance offered by the material to alternating flow. In terms of these parameters, expressions can be readily deduced for the absorption coefficient and for the acoustic impedance of the material when sound falls normally on the surface. Monna has extended the theory to wave propagation in three dimensions for the case of an homogeneous, isotropic material and has deduced a wave equation to represent the disturbance. In the present paper the results of this three-dimensional type of theory are compared with the practical performance of a typical porous material (rock-wool).

It is necessary that the parameters used to express the performance of the material be clearly defined at once, since it is intended later to make deductions about the mechanism of propagation of the sound in a typical material from experimentally determined values of these parameters. For this reason the theory is briefly outlined below.

The analysis will be confined, for brevity, to the case of a medium which from the point of view of transmission of sound is homogeneous and isotropic.

The porous type of sound-absorbing material commonly consists of very many small fibres or particles which are packed together so as to leave between them interconnected air-spaces or pores of irregular shape. A sound wave falling on the bounding surface of such a material must necessarily set up disturbances, not only of the air in the pores but also of the fibres or particles themselves. The exact analysis of the performance of such a system would require a knowledge of the forces of restraint of the fibres and simultaneous solutions would then be required of the two problems:

(i) the motion of the fibres under the action of the forces exerted upon them by the moving air;

(ii) the motion of the air in the irregular pore space under the combined influences of the pressure in the initial sound wave, the movement of the fibres, and the inertial, compressive and viscous forces associated with the confined air.

When framed in this general form, the mathematics are intractable, and simplifying assumptions must be made in order to obtain a practically useful mathematical description of the progress of an acoustic disturbance in the material.

It is reasonable to suppose that the transmission of motion along the fibres by solid conduction is inappreciable, for the rigidity of a fibre is small and the motion of a portion of the fibre is localized by the restraint imposed by contact with adjacent fibres. In considering the average motion of the air in the pore space, it will be assumed that the effect of the forces due to the presence and the movements of the fibres is to modify the effective inertia of the air and to introduce into the equations of the motion of the air a dissipation term proportional to the oscillatory velocity of the air.

Let $\mathbf{v}$ be the instantaneous velocity of the air in the pore space averaged over an area normal to $\mathbf{v}$ which cuts many fibres. $\mathbf{v}$ may be called the average velocity of flow. Let the volume of the air in the pores be P times the total volume, where P is a factor less than unity and may be called the *geometrical porosity*. In unit area of any plane in the material, the cross-section of the pore space will tend to a constant value A by virtue of the random distribution in space of the many fibres. This quantity A is numerically equal to the porosity P, for a slice of thickness $\delta\mathbf{n}$ contains a volume $A\delta\mathbf{n}$ of pore space, and by summing this volume through unit distance in the direction $\mathbf{n}$ we have $P = A\Sigma_0^1\delta\mathbf{n} = A$.

The equation of motion of the air in a small volume $\delta\mathbf{v}$ of the porous medium is, if we ignore second-order effects:

$$-\operatorname{grad} p\,.\,P\,\delta V = m\rho_0 P\delta V\frac{\partial}{\partial t}\left(\frac{\mathbf{v}}{A}\right) + r\mathbf{v}P\delta V,$$

and since $P = A$, this may be rewritten

$$-\operatorname{grad} p = m\rho_0\frac{\partial}{\partial t}\left(\frac{\mathbf{v}}{P}\right) + r\mathbf{v}, \qquad \ldots\ldots(1)$$

in which m is the ratio of the effective density of the air in the pore space to the actual density ρ_0 of the air, p is the oscillatory pressure in the volume δV and r is a resistance coefficient analogous to the flow resistance r' in Darcy's empirical law for steady non-turbulent flow in porous media, viz.:

$$-\operatorname{grad} p = r'\mathbf{v}. \qquad \ldots\ldots(2)$$

Equation (2) becomes equivalent to (1) when acceleration forces are negligible.

If we express $\mathbf{v}$ in terms of a velocity potential of average flow ψ, we have $\mathbf{v} = -\operatorname{grad}\psi$, $\dot{\mathbf{v}} = -\operatorname{grad}\dot{\psi}$. For small changes of p and therefore of ρ_0, equation (1) gives on integration

$$p = \frac{m\rho_0}{P}\dot{\psi} + r\psi. \qquad \ldots\ldots(3)$$

Let the condensation $\delta\rho_0/\rho_0$ be represented by s and let κ be the effective compressibility of the air in the pore space; by definition $p = \kappa s$ and (3) may therefore be rewritten

$$\kappa s = \frac{m\rho_0}{P}\dot{\psi} + r\psi. \qquad \ldots\ldots(4)$$

The equation of continuity is

$$P\frac{\partial \rho_0}{\partial t}+\rho_0 \operatorname{div} \mathbf{v}=0,$$

i.e.

$$P\frac{\partial s}{\partial t}-\nabla^2\psi=0. \qquad \ldots\ldots(5)$$

Substituting for s in (5) from (4),

$$\nabla^2\psi-\left(\frac{m\rho_0}{\kappa}\ddot{\psi}+\frac{rP}{\kappa}\dot{\psi}\right)=0. \qquad \ldots\ldots(6)$$

If ψ varies periodically with pulsatance ω, (6) may be rewritten

$$\nabla^2\psi+h^2\psi=0, \qquad \ldots\ldots(7)$$

where

$$h^2=\frac{m\rho_0\omega^2}{\kappa}-j\frac{rP\omega}{\kappa}.$$

The expression for oscillatory pressure in the pore space is given in terms of ψ by (3), which becomes for periodic motion

$$p=\left(\frac{m\rho_0}{P}-j\frac{r}{\omega}\right)\dot{\psi}$$

$$=\frac{h^2\kappa}{P\omega^2}\dot{\psi},$$

and if we write

$$\frac{h^2\kappa}{P\omega^2}\equiv\rho' \qquad \ldots\ldots(8)$$

we have

$$p=\rho'\dot{\psi}. \qquad \ldots\ldots(9)$$

Equations (7) and (9) suffice to describe any periodic acoustic disturbance in the porous medium and are analogous to the well-known equations for the propagation of unattenuated waves in a gas

$$\nabla^2\phi+k^2\phi=0 \qquad \ldots\ldots(10)$$

and

$$p=\rho_0\dot{\phi}, \qquad \ldots\ldots(11)$$

in which ϕ is the velocity potential and k is the wavelength constant.

§ 3. DETERMINATION OF THE MAGNITUDES OF h AND ρ' FOR A TYPICAL POROUS MEDIUM

The equations (7) and (9), which with the requisite boundary conditions define the sound field in the medium at any one frequency, involve the values of h and ρ' for the medium. These parameters are in general complex, and the magnitudes of their components depend on the working frequency. A primary concern in the experimental work described below has been to determine the magnitude of these parameters and the manner of their dependence on frequency for a typical homogeneous porous material. The material used for the tests is a variety of rock-wool known commercially by the trade name of Stillite (bulk density 0·080 gm./cm.^{3}) The material possesses good homogeneity and proves to be reasonably isotropic in its acoustic properties.

From the experimental point of view the work divides into two parts. The first part involves the determination of the propagation constant associated with the passage of a uniform plane progressive wave in the porous material. The second part involves the measurement of the acoustic impedance at the face of a substantially unlimited depth of the material. From the former measurements h is obtained and from the latter ρ'/h. The two types of measurement are quite different in nature and the description of the experimental work must therefore be divided into two parts.

Experimental determination of the propagation constant in rock-wool

The parameter h describes the spatial variation of the acoustic disturbance in the medium. Thus for a uniform, progressive, plane wave in rock-wool, the velocity potential ψ of the average motion in the pores can be written

$$\psi=\psi_0 \exp(-jhx).\exp(j\omega t), \qquad \ldots\ldots(12)$$

where x represents distance in the direction of propagation of the wave. In current terminology the quantity jh is called the *propagation constant* of the wave.

If we write $jh=\alpha+j\beta$ i.e. $h=\beta-j\alpha$ and rearrange (12) we have

$$\psi=\psi_0 \exp(-\alpha x).(j[\omega t-\beta x]),$$

and it becomes apparent that the real part of jh is the attenuation constant of the wave and the imaginary part of jh is the *wavelength constant*, $2\pi/\lambda$, of the wave in the rock-wool. The experimental determination of h therefore reduces to the determination of the attenuation and of the wavelength of a plane progressive wave in the rock-wool.

The measurements were made by setting up a progressive sound wave in a tube filled with rock-wool and exploring the sound field by means of a " probe-microphone ". The decay of intensity with distance provides a measurement of the attenuation constant α. The change of phase of the oscillatory pressure with distance provides a measurement of the wavelength, and therefore of β. The combination $\beta-j\alpha$ then constitutes the quantity h.

A diagram of the apparatus is shown in figure 1. The specimen (R) of Stillite was in the form of a prism of 5·08 cm. square cross-section and 30·5 cm. long which was mounted at one end of a square tube of metal of length 91·5 cm. Sound from a moving-coil horn-type loudspeaker unit (Vitavox type: N) (L) was led to the specimen through a rubber pipe and an initial short flared horn (P), made by moulding Plasticene into the first 5 cm. of the square tube. The remaining 55·9 cm. length of the tube was filled with an additional, similar specimen of Stillite. The absence of discontinuity in the long length of Stillite in the tube allows a sound wave from the source to pass without backward reflection, well past the measurement specimen. The length of the terminating specimen was chosen so as to ensure that a reflected sound wave from the far end of the tube is sufficiently attenuated for its amplitude at the measurement specimen to be negligible compared with that of the forward wave. The sound wave, which has a substantially plane wave-front because of the smallness of the transverse dimensions of the tube in relation to the wavelength, is therefore effectively a single progressive wave travelling away from the loudspeaker. The exploring microphone (M) consists of a heavily encased piezo-electric microphone (rochelle-salt, with conical diaphragm) to which sound is led through a metal " probe-tube ". The electrical output from the microphone, which is proportional to the acoustic pressure at the mouth of the probe, is amplified, filtered by means of an electrical analyser (B) (Churcher and King (1934)) so as to remove such unwanted higher harmonics and any interference as may exist, and measured by means of a rectifier-type, moving-coil voltmeter (C). The voltage measuring equipment was calibrated by means of a known voltage supplied from the oscillator via a potentiometer to the input terminals of the amplifier.

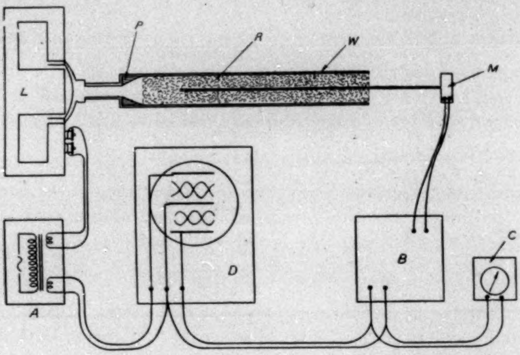

Figure 1. Apparatus for measurement of propagation constant.

The probe microphone was mounted on a trolley so as to allow the exploring end of the microphone tube to travel freely through the Stillite in the direction of the axis of the tube. The position of the orifice could be measured to within 1/10 mm. at the trolley by means of a reference scale. A view of the orifice end of the probe-tube is shown in figure 2; A is a bullet-shaped plug fitted into the end of the tube and S is one of two symmetrically placed slit orifices which were made by sawing part way through the wall of the probe-tube P. The bullet-nose pushes aside the porous material as the probe enters the medium and the porous material falls back substantially to its initial position on withdrawal of the probe. In the initial stages of the work the probe was used as an open-ended tube, without the bullet-nose, and gave sets of readings which could be continually repeated by retraversing the length of the specimen. The bullet-nose was found, however,

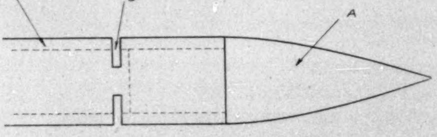

Figure 2. Orifice of probe-tube microphone.

to damage the specimen less and was therefore used in the main work. Preliminary tests with open-ended probes of different external diameters (stainless steel tubes) respectively as follows: (*a*) external diameter 0·318 cm., internal 0·214 cm.; (*b*) external 0·241 cm., internal 0·165 cm., gave results for the attenuation constant at a given frequency which were in close agreement (e.g. within 1 per cent at 200 c/s.) and this agreement is alone sufficient reason for assuming that the presence of the exploring tube has negligible effect on the field and that the microphone pressure is a correct indication of the pressure of the wave in the porous medium.

The vertical walls of the main experimental tube (W in figure 1) are made of brass of section 5·08 cm. by 1·27 cm. and the tube is completed by removable top and bottom covers of steel 0·63 cm. thick which are clamped with intermediary thin cork gaskets to the brass walls. Suitable holes, which can be tightly closed with screws, are provided at appropriate intervals in the walls and the cover plates so as to allow a probe microphone to be used to explore the transverse sound field in the duct. When in use the tube and loudspeaker were carefully inspected so as to ensure no appreciable leakage of sound through crevices in the apparatus either out of or into the apparatus.

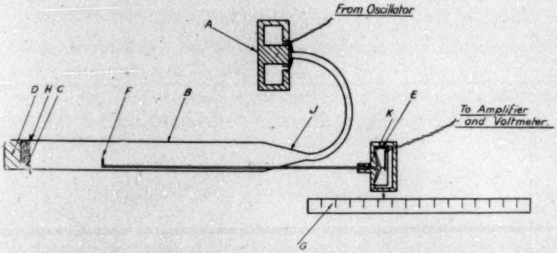

Figure 3. Apparatus for measurement of acoustic impedance.

Determinations of the attenuation constant were made from the slope of a graph of the pressure, on a decibel scale, plotted against distance; thus an attenuation of Y db./cm. corresponds to an attenuation constant α given by $\alpha = 2{\cdot}303Y/20$ cm.$^{-1}$ The wavelength of the sound in the porous medium was determined from the rate of change with distance of phase of the pressure at the probe mouth. The phase changes were determined with the aid of a Cossor double-beam cathode-ray oscilloscope (D) which was connected so that one pair of vertical deflection plates was operated by a voltage fed direct from the oscillator (A) and the other pair operated by the amplified voltage from the microphone. The former voltage was used to control the time base in such a fashion that each screen trace contained three half-cycles—as shown in figure 1. The voltage from the oscillator provides, of course, a reference trace of fixed phase, and this trace remains in position on the screen throughout each set of measurements. The trace due to the microphone pressure therefore moves across the screen as the microphone moves along the axis of the main tube. This particular kind of pattern was chosen because the doubling-back of the trace on itself provides in general for each trace three sharp intersections whose lateral positions on the screen are quite independent of the intensity of the deflecting voltage. Any one of these intersections therefore provides, for each of the two voltages, a convenient reference point in the pattern by means of which the relative movement of one pattern past the other can be measured. The interval between successive intersections on the screen represents 180° of phase change of the corresponding voltage. A movement of one-half wavelength of the probe orifice causes one screen pattern to move until one intersection of the trace is replaced by an adjacent intersection.

The form in which the theory has been cast earlier in this paper is appropriate only to materials which are isotropic in their acoustic properties. Many commercial porous materials, and this includes Stillite, are normally provided in sheet form and some degree of anisotropy is introduced in the manufacturing process. The measurements described below of the propagation constant in Stillite were therefore made for waves propagated in each of two directions: (**a**) parallel to a line in the surface of the sheet, (**b**) normal to the surface of the sheet.

Results of measurements of propagation constant in rock-wool

The specimens of Stillite were prepared as follows. Ten blocks of the material, each in the form of a cube of 5·08 cm. side, were cut with the appropriate common orientation from the centre of a 7·62 cm. thick sheet of Stillite. The cubes were weighed separately and their bulk densities determined, and of the ten, six were chosen, of closely similar density (range: 0·079 to 0·088 gm./cm^3), to form the measurement specimen. The 5·08 cm. cubes were first arranged in the main tube to form a specimen of type **a**; that is, the axis of the tube corresponded to a direction parallel to a line in the surface of the original sheet. Typical curves are shown in figure 4, for a frequency of 1500 c/s., of the variation of intensity

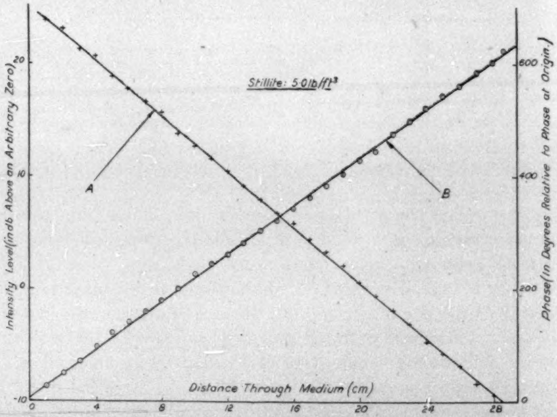

Figure 4. Variation of intensity and phase with distance for a wave propagated in a typical porous medium.

on a decibel scale (curve A) and of phase (curve B) with distance through the sample. In each case the curve is a straight line, whence it follows that the sound is propagated with a constant phase velocity and with a constant attenuation constant. Table 1 and figure 5 show the results for the attenuation, expressed in db. per cm., and for the phase velocity for frequencies from 200 to 4000 c/s.

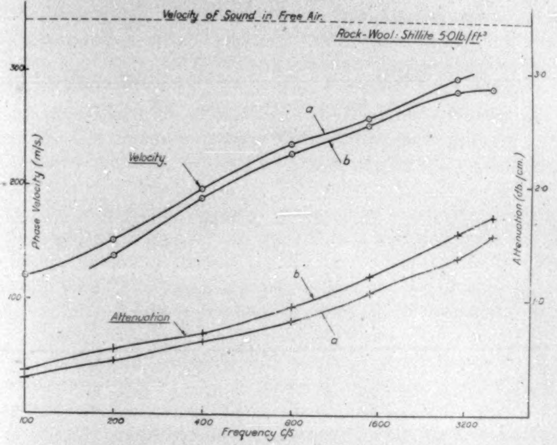

Figure 5. Attenuation and phase velocity of sound in a typical porous medium.

The values of α and of β calculated from these measurements for this direction are shown in table 2, columns 2 and 4 respectively. Each separate cube was then turned in the tube through a right angle so as to form a specimen of type **b**; that is, the axis of the tube then corresponded to a direction normal to the surface of the original sheet. The corresponding measurements of α and of β are shown

Table 1. Attenuation and phase velocity of sound waves in rock-wool

Stillite 0·080 gm./cm³

Frequency (c/s.)	Attenuation (db./cm.)			Velocity of propagation (m/s.)	
	a	**b**	Mean	**a**	**b**
100	0·301	0·368	0·344	—	120·0
200	0·452	0·546	0·499	151·6	137·9
400	0·623	0·693	0·658	196·0	188·2
800	0·800	0·937	0·868	236·5	228·0
1500	1·067	1·217	1·142	259·5	253·5
3000	1·376	1·583	1·479	295·0	283·5
4000	1·568	1·736	1·652	—	286·0

a denotes a direction parallel to surface of original sheet of material.
b denotes a direction normal to surface of original sheet of material.

in columns 3 and 5 in table 2. The combination $\alpha+j\beta$ of the above data gives the propagation constant in the appropriate direction on the Stillite. The combination $\beta-j\alpha$ of the data gives the appropriate value of the quantity h of the theoretical analysis.

The measurements of frequency were made by comparison of the working frequency with a standard frequency of 1000·0 c/s. from a Sullivan valve-maintained tuning fork, with the aid of the Cossor double-beam cathode-ray tube.

Table 2. Attenuation constant and wavelength constant for sound waves in rock-wool

Stillite 0·080 gm./cm^3

Frequency (c/s.)	Attenuation constant (cm.$^{-1}$)			Wavelength constant (radians/cm.)		
	10^{-2} **a**	10^{-2} **b**	Mean	10^{-2} **a**	10^{-2} **b**	Mean
100	3·46	4·24	3·85	—	5·24	—
200	5·21	6·29	5·75	8·29	9·11	8·70
400	7·17	7·98	7·57	12·82	13·35	13·09
800	9·21	10·78	10·00	21·25	22·05	21·65
1500	12·28	14·00	13·14	36·32	37·18	36·75
3000	15·84	18·22	17·03	63·89	66·49	65·19
4000	18·05	19·98	19·01	—	87·87	—

a denotes a direction parallel to surface of original sheet of material.
b denotes a direction normal to surface of original sheet of material.

The velocities of phase propagation in the Stillite shown in columns 4 and 5 of table 1 are obtained by dividing the pulsatance ω by β. The results show that the velocity of sound in the medium is substantially less than the velocity of sound (345 m./sec. at 22° c.) in free air and at 200 c/s. is indeed less than one-half of the free-air velocity. The measurements show some degree of acoustic anisotropy of the bulk material.

Experimental determination of the characteristic impedance in rock-wool

The characteristic acoustic impedance of a medium is the ratio of oscillatory pressure to oscillatory velocity in a progressive plane wave in the medium. Since the velocity potential for such a wave is given by an expression of the type

$$\psi=\psi_0\exp(-jhx)\exp(j\omega t)$$

for a wave in the direction x, the expression for the characteristic impedance Z_c can be obtained with the help of (9) above. Thus

$$Z_c=p\Big/-\frac{\partial\psi}{\partial x}=-\rho'\frac{\partial\psi}{\partial t}\Big/\frac{\partial\psi}{\partial x}$$
$$=\rho'\omega/h. \qquad \ldots\ldots(13)$$

The acoustic impedance at the surface of a block of the porous medium of substantially unlimited depth is clearly identical with the characteristic impedance of the medium: the experimental methods available for the measurement of acoustic impedance therefore lead to the determination of ρ'/h and thus to ρ'.

The apparatus used for this measurement of impedance has been described elsewhere (Scott, 1946). It is a form of the apparatus devised in 1913 by H.O. Taylor for the measurement of absorption coefficients of acoustic materials and developed by Paris for the measurement of acoustic impedance. The method involves the investigation of the stationary-wave pattern set up in a tube, driven by a source of sound at one end and terminated by the flat surface of the sample at the other end. The sound field along the axis of the tube is explored by means of a probe microphone which receives sound from the field through a tube of small diameter. The ratio of maximum to minimum pressure and of the position of the first minimum relative to the face of the sample are determined and the resistive (R) and reactive (X) components of the acoustic impedance are obtained from the results.

The apparatus has been designed in particular to provide sound waves of high uniformity in the tube and to allow precise measurements, i.e. to within 0·1 mm., of the position of the minima. In interpreting the results, the effect of attenuation in the tube in modifying the positions and magnitudes of the minima has been considered and corrections applied where necessary. Experience with the apparatus has shown it to be convenient and reliable in use. Measurements made on different occasions on a particular sample show a consistency of 1 to 2 per cent for both resistive and reactive components. Specimens for use in the apparatus must be cut in the form of cylinders 4·45 cm. in diameter so as to fit the tube. The material was cut carefully with a flat terminating surface normal to the axis of the cylinder and was positioned carefully in the tube.

A diagram of the apparatus is shown in figure 3. A is the source of sound, B the tube in which the stationary wave is formed, C is the sample of material backed by a heavy brass piston D, E is the microphone and F the orifice of the probe-tube. The position of the orifice of the probe-tube is determined by means of the scale G located near the microphone.

For the measurements of the characteristic impedance of rock-wool, the six specially chosen cubes of Stillite used in the measurement of propagation constant were divided into two sets of three. From the specimens of the first set, cylinders 4·45 cm. in diameter and 5·08 cm. long were cut, with the axes of the cylinders along the direction **a** referred to in the earlier experimental work. From the specimens of the other set, similar cylinders were cut with axes along the direction **b**. The three specimens with the **a** axis were then fitted in one end of the cylindrical specimen tube (27·4 cm. long) of the impedance-measuring apparatus so as to present a total depth of material of 15·24 cm. The results of the measurements of α already quoted, show that even at 200 c/s. a wave passing into the specimen and reflected completely at the far end would be diminished in amplitude to one-sixth on rearrival at the beginning of the specimen. The 15·24 cm. depth of Stillite was backed by a long (25 cm.) cylinder of similar material cut from the original block, though not as carefully selected; this continuation therefore largely suppresses any tendency for a reflected wave in the specimen to affect the sound field in the measurement tube of the impedance-measuring apparatus. This 15·24 cm. length of Stillite with the Stillite backing therefore behaves to a sound wave incident on an end surface, substantially as an infinitely deep specimen. The real and imaginary components of the acoustic impedance at the surface of the composite specimen were measured at frequencies in the range 200 to 4000 c/s. and the results are shown in columns 2 and 5 in table 3. The three component specimens which had been cut with axes in the **a** direction were replaced by the cylinders cut with axes in the **b** direction. The real and imaginary components of the impedance were measured for this sample and the results are shown in columns 3 and 6 of table 3.

Table 3. Characteristic acoustic impedance for sound waves in rock-wool

Stillite 0·080 gm./cm^3

Frequency (c/s.)	Resistive component *R*			Reactive component *X*		
	a	**b**	Mean	**a**	**b**	Mean
100	95·9	97·1	96·5	77·9	83·9	80·9
200	74·9	71·3	73·1	51·1	50·7	50·9
400	62·2	61·7	62·0	32·1	31·6	31·8
800	59·2	53·8	56·5	19·4	18·5	19·0
1500	52·8	49·5	51·2	12·5	11·3	11·9
3000	50·8	48·3	49·6	5·4	4·1	4·7
4000	51·2	48·2	49·7	4·8	5·0	4·9
5000	49·2	47·6	48·4	2·0	1·4	1·7

a denotes direction of propagation parallel to surface of sheet.
b denotes direction of propagation normal to surface of sheet.

Comparison of the measured values of acoustic impedance of the bulk material for the two directions **a** and **b** in the original sheet again shows acoustic anisotropy of the Stillite. Since the anisotropy is small, both in the measurements of the propagation constant and of the characteristic impedance, mean values have been used in the comparison, which follows, of the experimental results with the theoretical analysis.

§4. GENERAL DISCUSSION OF EXPERIMENTAL RESULTS

The measurements of attenuation and of velocity of propagation of sound in the Stillite allow us to calculate h at the appropriate working frequency, and the measurements of the characteristic impedance of the Stillite allow us to deduce the corresponding value of ρ'. The values of the parameters h and ρ', determined in this manner, are shown in table 4; these values are calculated from the mean of the measurements in directions **a** and **b** of α and of β. It should be remembered that for the propagation of sound in free air, h becomes the wavelength constant usually denoted by k ($=2\pi$/wavelength in free-air), and that ρ' becomes ρ_0 ($=0{\cdot}001205$ gm./cm^3, for these measurements). These quantities have been entered in table 4, columns 6 and 7, for purposes of comparison with h and ρ'.

In the work described above, it has been assumed that acoustic disturbances in porous materials can be represented completely by two parameters h and ρ', and it has then been shown experimentally, for the particular case of a variety of rock-wool, how measurements of these quantities may be obtained for frequencies in the range 200 to 4000 c/s. If the initial assumptions are true, it should now be possible to calculate, for example, the acoustic impedance Z_l of a layer of known thickness (l) of this material—Stillite—when backed by a substantially rigid backing. Thus it is easy to show (Scott, 1946 a) with these assumptions that

$$Z_l = Z_c \coth(jhl) = \frac{\rho'\omega}{h} \coth(jhl).$$

Using the values of ρ' and h of table 4, Z_l has been calculated for thicknesses of 2·54, 5·08 and 10·16 cm. from this formula, and the calculated values are shown in figure 6, plotted against frequency. Corresponding measurements of Z_l were made with the impedance-measuring apparatus, on the samples used earlier for the determination of ρ' and h, and these are plotted in figure 6.

At frequencies of 400 c/s. and above, the agreement between measured and deduced values of Z_l is excellent. At 200 c/s. the agreement, particularly in regard to the resistance, is not so good. It is probable that this discrepancy is due to experimental error in the measurement of h, since accuracy of measurement of the wavelength constant β was limited by the shortness, in terms of wavelength, of the specimen used.

Table 4. Experimental values of parameters h and ρ' for rock-wool

Stillite 0·080 gm./cm.^{3}

Frequency (c/s.)	h		ρ'		k	ρ_0
	Real	Imag.	Real	Imag.		
200	0·0870	−0·0575	0·002734	0·006870	0·03642	0·001205
400	0·1309	−0·0757	0·002669	0·003527	0·07284	0·001205
800	0·2165	−0·0100	0·002057	0·001941	0·1457	0·001205
1500	0·3675	−0·1314	0·001831	0·001178	0·2732	0·001205
3000	0·6519	−0·1703	0·001672	0·000611	0·5463	0·001205
4000	0·8504	−0·1901	0·001645	0·000542	0·7284	0·001205

The magnitudes of the attenuation and of the velocity of propagation of sound in the rock-wool are of interest in themselves to all who use such acoustic materials. Porous materials are most commonly used in acoustics for the production of wall linings which possess a low coefficient of reflection, and this property of the lining depends at least as much upon the characteristic impedance of the medium, which together with that of the air determines the amplitude of the wave immediately reflected from the lining surface, as upon the capacity of the medium itself to absorb energy. A secondary, and at the moment much less common, use of porous materials is for the purpose of sound insulation. For this latter purpose, the important factor is the ratio of the sound pressures on two sides of a given layer of the material and this is primarily dependent on the attenuation of sound energy in the material. The measurements of attenuation recorded in table 1 show rates of attenuation which, when converted to the appropriate units, correspond to 30 db. per foot thickness of the layer at 1000 c/s.

Rock-wool of the density (0·080 gm./cm.^{3}) used in these tests is not particularly useful as an insulating partition, except at high frequencies in the acoustic range. Similar tests which have been made during the present investigation of more tightly compressed material of the same type, show much higher attenuation, e.g. for Stillite of density 0·384 gm./cm.^{3} the attenuation is 75 db./ft. at 200 c/s. and 120 db./ft. at 1000 c/s.

The measurements of the velocity of propagation of sound in the porous material are particularly interesting. At frequencies of 100 c/s. the velocity is about one-third of that for free air (345 m/s. under corresponding conditions), whereas at frequencies in the region above 4000 c/s., the velocity in the Stillite approaches that in free air. This considerable dispersion of velocity with frequency is closely analogous to anomalous dispersion of light and is, indeed, commonly found in cases of wave-propagation in dissipative media. It is of interest to compare the directly measured values of the velocity of sound in this sample of rock-wool with the rough estimates of the velocity of propagation of sound in felt as made by Crandall many years ago from an analysis of W. C. Sabine's measurements of the absorption coefficient of layers of wool-felt (Crandall, 1927). Crandall obtained values ranging from 91 m/s. at 480 c/s. to 127 m/s. at 2048 c/s. These results show the same upward trend of velocity with rising frequency as has been measured in the present work.

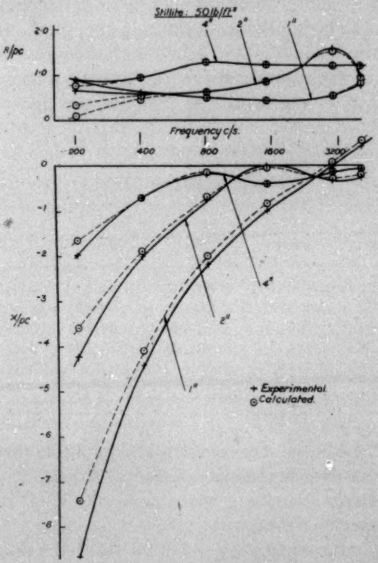

Figure 6. Comparison of measured and calculated values of acoustic impedance of rock-wool samples of various thicknesses.

§ 5. INTERPRETATION OF THE MEASURED VALUES OF h AND OF ρ' IN TERMS OF THE GENERAL THEORY

In the theory of Monna, Wintergerst and others which has been outlined earlier in this paper, it has been shown that with certain simplifying assumptions it is possible to construct a wave equation for the propagation of sound in a homogeneous, isotropic porous material in terms of parameters P, m, κ and r which represent respectively the geometrical porosity factor, the effective mass of the contained air, the effective compressibility of the contained air and the porous resistance for alternating flow of the material.

The geometrical porosity factor P can be determined by direct methods. For example, if ρ_B is the bulk density of the material, measured in terms of the weight of a specimen of known volume, and if ρ_s is the density of the material of the solid fibres determined on a crushed specimen with the aid of a specific-gravity bottle, the porosity P which is defined as the proportion of the voids to the total volume is given by

Table 5. Calculated values of parameters m, r, $|\kappa|$, amp κ and $|\gamma'|$ for rock-wool

Stillite 0·080 gm./cm.^{3}

Frequency (c/s.)	m	r (gm.cm.$^{-3}$ sec.$^{-1}$)	$\lvert\kappa\rvert$	amp. κ (degrees)	$\lvert\gamma'\rvert$
200	2·20	8·63	1·041	−1·4	1·03
400	1·83	8·86	1·131	+2·8	1·12
800	1·66	9·76	1·218	+6·3	1·20
1500	1·47	11·06	1·232	+6·6	1·22
3000	1·35	11·52	1·352	+9·2	1·33
4000	1·32	13·62	1·397	+7·0	1·38

$$P=(\rho_s-\rho_B)/\rho_s=1-\rho_B/\rho_s.$$

The mean bulk density of the samples of Stillite used in the experimental work is 0·080 gm./cm.^{3} and the density of the fibres 2·65 gm./cm.^{3}, whence $P=0{\cdot}970$.

The experimental determinations of h and of ρ' for the porous material, allow the calculation of the values of the parameters m, κ and r. Thus

$$h^2=\frac{m\omega^2\rho_0}{\kappa}-j\frac{\omega rP}{\kappa},$$

$$\rho'=\frac{\kappa}{P\omega^2}\left(\frac{m\omega^2\rho_0}{\kappa}-j\frac{\omega rP}{\kappa}\right)=\frac{m\rho_0}{P}-j\frac{r}{\omega}.$$

Hence

$$\kappa=P\omega^2\rho'/h^2,$$

$$m=\text{Real part of } P\rho'/\rho_0,$$

$$r=\text{Imaginary part of } \rho'\omega.$$

These quantities have been calculated from the data of table 4 and are shown plotted against frequency in figure 7. None of these quantities remains constant as the frequency is varied. At low frequencies (200 c/s.) the effective mass of the air in the pores of the material is roughly double that of a similar quantity of unrestricted air. At higher frequencies (3000 c/s.) the effective mass decreases and, indeed, approaches the value appropriate to unrestricted air. The value of r, the effective porous resistance coefficient of the material, increases with frequency. At 200 c/s. r has a value (8·63 gm. cm.$^{-3}$ sec.$^{-1}$) which is closely the same as the steady flow porous resistance coefficient (8·6 gm. cm.$^{-3}$ sec.$^{-1}$) of Darcy's law. The latter coefficient was determined by measuring the pressure differences across samples used in the earlier tests, for known rates of flow of air through the sample. The velocity of flow was never allowed to exceed 1·1 cm./sec. which is a velocity of about the same order as the oscillatory velocities in the sound wave during the acoustic measurements. The relation between pressure difference across sample and velocity of flow through sample was shown to be linear for the velocities used and the value quoted above is the mean of measurements (8·0 and 9·2 respectively) for flow parallel to and normal to the original surface of the Stillite sheet.

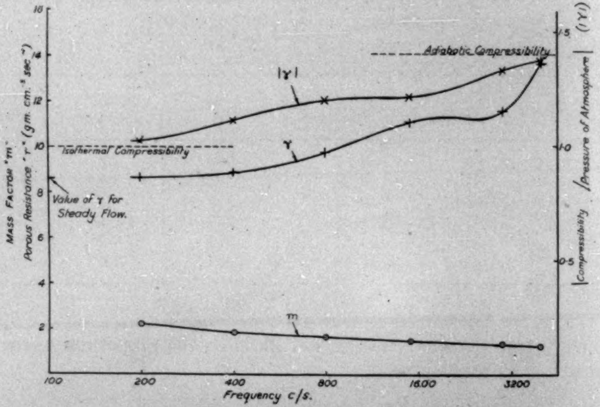

Figure 7. Variation wtih frequency of parameters m, r and $|r|$.

The compressibility of the air in a sound wave propagated in air is ordinarily the adiabatic elasticity $\gamma\Pi$, in which γ is the ratio of the specific heats of the air (1·403) and Π is the atmospheric pressure. For a condensation which takes place under isothermal conditions, the elasticity of the air is numerically equal to the atmospheric pressure Π. The effective compressibility κ determined from h and ρ' for the sample of rock-wool is in general a complex quantity, but at all frequencies the phase angle is small. The values of $|\gamma'|(=|\kappa'|/\Pi)$ are plotted against frequency in figure 7. At the low-frequency end of the range, the compressibility $|\kappa|$ tends to Π and at the high-frequency end it tends to 1·4 Π.

The construction of a theory relating to the propagation of an acoustic disturbance in terms of effective values of inertia, compressibility and resistance, involves only a partial view of the behaviour of the air in the pores. The effective values of these various quantities depend for their magnitude on the detailed movements of the air and of the fibres. Reference has already been made to the difficulties of an exact mathematical analysis of the individual motions; nevertheless, qualitative deductions are possible about the values to be expected for the parameters.

The effective values of inertia, resistance (and, to some extent, compressibility), will depend on the distribution of velocity across the air space between the fibres. At the surface of a fibre there will be no relative motion between the air and the fibre. For positions well away from the fibre surface, the velocity will tend to a uniform value. The velocity over the intervening sections will depend on the frequency, on the kinematic viscosity of the air, and on the geometrical arrangement of the fibres (vide: the classical analyses by Helmholtz and Kirchhoff of the propagation of waves in tubes, given in Rayleigh's *Theory of Sound*, vol. 2). At high frequency the velocity gradient will tend to be concentrated near the surface of the fibres, whereas at lower frequencies this phenomenon will be less pronounced and the flow become much as in the case of steady flow.

At frequencies high in the acoustic range, the bulk of the air in the pores will tend to move as a core in which the motions are all in common phase. It may therefore be expected that the effective inertia will depend on the mass of the bulk of the air present in the pores and correspond with the normal density of the air (i.e. $m=1$). At frequencies lower in the range, the proportion of the total mass of air that moves with phase different from that of the core will become larger and the inertia due to the motion of the air alone will correspond in consequence to an effective density of air less than the true density.

In the considerations advanced so far, the fibres have been assumed stationary. The viscous and accelerative forces which are imposed on the fibres by the motion of the air lead to movements of the fibres themselves, and these movements imply an increase in the effective inertia of the air. At frequencies of the order of 4000 c/s. it appears to be legitimate to assume that the inertia of the fibres is so high that their motion may be neglected; at frequencies of 200 c/s., the fibres take up an appreciable proportion of the velocity of the air as has been shown by an auxiliary experiment. Thus observations have been made of (*a*) the amplitude of fibres and (*b*) the amplitude of the air as traced out by MgO smoke particles, for a wave set up in a small wad of rock-wool of the type used in the earlier experiments. The results show that at 200 to 400 c/s. motions of the fibres are of the order of 1% of the mean motion of the air. In view of the high ratio of the mass of the fibres to the mass of the air (about 60: 1 in the present case) the comparatively small motion of the fibres can contribute to the total inertia an amount about equal to that due to the air alone. This increase in the effective inertia more than outweighs the decrease due to lack of uniformity in phase of the motion of the air and accounts for the high experimental values of the corresponding parameter m (approximately 2 at 200 c/s.).

The tendency of the gradient of velocity to steepen at the fibres as the frequency is increased leads to a viscous force on the fibres, and therefore to a porous resistance coefficient, which increases with frequency. Apart from such dissipation as may occur due to the motion of the fibres themselves, the observed rise of porous resistance with frequency can be explained by the change of velocity distribution of the air that accompanies increase of frequency.

The effective compressibility of the air depends jointly on the elasticity of the air itself and upon the bulk elasticity of the fibres. Since the latter elasticity must be very high, the effective compressibility may be considered as that of the air alone. The presence of the fibres will, however, affect the temperature of the air during the cycle of compression and rarefaction and it is therefore necessary to consider whether the compressibility corresponds to isothermal or to adiabatic conditions. The heat capacity of the fibres is approximately fifty times that of the included air and hence the fibres form a heat reservoir easily sufficient to retain the air at substantially constant temperature. The thermal conditions during the cycle therefore depend upon whether the air is in sufficiently intimate contact with the surrounding fibres for equalization of temperature to be complete in a small fraction of a cycle. The experimental values found for κ may therefore be interpreted as indicating that at 200 c/s. equalization is almost complete and the compression tends to be isothermal, whilst at high frequencies (4000 c/s.) the cycle occupies such a short time that the compression tends to be adiabatic. At frequencies intermediate between the two extremes it is to be expected that the maximum pressure of the cycle will be in advance of the phase of the condensation, on account of the thermal loss to the walls. The experimental values of κ show just such a lead to middle and high frequencies, but show a lag (which is physically impossible from energy considerations) at the lowest frequency used (200 c/s.). It has already been indicated in another context that the measurements of phase velocity are a little in doubt at this frequency and it is probable that such an experimental error is responsible for the discrepant sign of amp κ.

§6. CONCLUSIONS

A theoretical analysis based on the assumption that the effect of the fibres can be regarded as modifying the inertia and compressibility of the air and as introducing a dissipative force into the equation of motion, shows that an acoustic disturbance of fixed frequency is propagated in a porous medium as an attenuated wave. Explorations of the sound field in a typical porous material (rock-wool) have shown that such wave-propagation is characteristic of the material, and have led to direct determination of the propagation constant of the waves in this material. The measured values of the propagation constant, together with those of the characteristic impedance, have been used to calculate the acoustic impedance of layers of the material of thickness 2·54 cm., 5·08 cm. and 10·16 cm. when backed by a substantially rigid wall. The calculated values of the impedance agree sufficiently well with the corresponding measured values to leave little doubt that description of the performance of sound in the material in terms of a simple, attenuated sound wave is adequate.

The experimentally determined values of the propagation constant, and of the characteristic impedance have been used further to find the effective magnitudes of the inertia, compressibility and porous resistance, characteristic of the sample of rock-wool. The results show that each of these quantities changes with frequency and the reason for this variation is discussed. Thus the effective inertia of the air at low frequencies corresponds to a density of the air of about twice its ordinary value, and the increase is attributable to movements of the fibres; at higher frequencies such movement is small, and the effective inertia of the air has a lower value. The compressibility of the air, that is, the ratio of the oscillatory pressure to the condensation, proves in general to be a complex quantity with a small phase angle. The reason for the phase factor is discussed. The modulus of the compressibility has a value which at low frequencies corresponds closely to the isothermal value and at high frequencies to the adiabatic value. The porous resistance factor associated with sound waves in the material is shown to approximate in value to the steady-flow resistance for frequencies of about 200 c/s., but thereafter to rise steadily with frequency.

The above conclusions about the variation with frequency of the parameters which are associated with sound propagation in rock-wool, qualify the conclusions arrived at by Morse from an interpretation of the results of the impedance measurements of Beranek: namely, that values of m, κ and r that are independent of frequency lead to a satisfactory description of the sound field in a porous material.*

ACKNOWLEDGMENTS

The author's thanks are due to various of his colleagues in the Research Department, and in particular to Mr. B. G. Churcher, M.Sc., Manager of the department, and to Dr. A. J. King for authorization of the work and for their interest in its progress. The author also expresses his thanks to Sir Arthur P. M. Fleming, C.B.E., Director of Metropolitan-Vickers Electrical Co., Ltd., for permission to publish this paper.

REFERENCES

CHURCHER and KING, 1934. *J. Inst. Elect. Engrs.* **75**, 411.

CRANDALL, 1927. *Vibrating Systems and Sound* (London: Macmillan), chapters 3 and 5, and p. 197.

MONNA, 1938. *Physica*, **5**, 129.

MORSE and BOLT, 1944 a. *Rev. Mod. Phys.* **16**, 89; 1944 b. *Ibid.* 99.

RAYLEIGH, Lord, 1929. *Theory of Sound* (London: Macmillan), vol. ii, 328.

TAYLOR, 1913. *Phys. Rev.* **2**, 170.

WINTERGERST, 1931. *Schalltechnik*, **4**, 85.

---

* In a recent publication by Morse and Bolt (1944 b) the author indicates that some variation of the parameters with frequency must be postulated for certain materials.

THE APPLICATION OF ULTRA-SHORT-WAVE DIRECTION FINDING TO RADIO SOUNDING BALLOONS

By R. L. SMITH-ROSE and H. G. HOPKINS,
Radio Division, National Physical Laboratory

MS. received 22 *October* 1945

ABSTRACT. The paper describes the early portion of an investigation into the possibilities of determining wind velocities at high levels by radio methods. It was prepared in the spring of 1939, but publication has been delayed owing to the important part which this technique has contributed to meteorology during the war. In the intervening six years considerable progress has been made in the application of the basic principles described in this paper. An account of this later work, leading to the practical techniques now used by the Meteorological Office, will be published later.

The position of a radio-sounding balloon transmitter can be determined by the aid of two direction-finders set at a suitable distance apart, together with a measurement of the altitude, which can be obtained from the barometric pressure and the thermometer units attached to the apparatus. The present paper is concerned with an investigation of the accuracy of the direction-finding technique used for the observation of bearings on the signals from radio sounding balloons during actual flight. From a knowledge of the precision of such radio bearings, the accuracy of position location of the balloon can be computed with the aid of curves given in the paper.

Preliminary experiments conducted with direction-finders of both the closed-loop and spaced-aerial types on wave-lengths between 8 and 10 metres (frequencies 30 to 38 Mc/s.) showed that a reasonably high instrumental accuracy was obtainable ; but that in order to utilize this to the best advantage it was necessary to install the direction-finders on very satisfactory sites. Accordingly, the experiments were continued with the aid of specially designed direction-finders of the rotating-loop type installed on two superior sites situated at the ends of a suitable base-line for balloon location work. As a result of the calibration of these direction-finding installations, it was found that the observational accuracy was of the order of 0°·1. The maximum error in bearing obtained in the course of the ground calibrations at a short distance was about 1°, but successive calibrations of the installations over a three-monthly period disclosed a variation in this site error of about 0°·5.

The results of tests carried out on some twenty balloon flights show that, by taking mean observed bearings over each minute period, 95% of the bearings are correct to within 2° and nearly 80% correct to within 1° ; the probable error of such mean observed bearings, after correction for the ground calibration, is about 0°·3.

Foreword

THIS paper was originally prepared in the spring of 1939, but publication has been delayed owing to the important part which this technique has contributed to meteorology during the war.

§1. INTRODUCTION

During several years prior to 1939, considerable progress had been made in the use of free sounding balloons with small radio transmitters attached for exploring the meteorological conditions of the atmosphere. The transmitters which formed the prototype of those used at the present time were designed to emit radio waves, with suitable superimposed characteristics dependent upon the pressure, temperature and humidity of the air in which the balloon is situated. At the ground receiving station, measurements made on the incoming signals led to a direct interpretation of these three meteorological quantities. A description of the type of transmitter developed in this country has been given elsewhere by H. A. Thomas (1938), and preliminary experiments have shown this to be suitable for exploring aerological conditions up to altitudes of some 45,000 feet. These experiments have indicated that the necessary radio transmissions can be carried out very effectively on a wave-length in the region of 10 metres (frequency 30 Mc/s.). While much of the early experimental work was carried out mainly on a wave-length of 8·5 metres (34 Mc/s.), the standardized type of balloon transmitter used in recent years by the Meteorological Office operates within the international wave-band for radio sonde work, viz., 10·7 to 10·9 metres (27·5 to 28·0 Mc/s.).

In the past, a further aerological condition—the speed and direction of the wind at various heights—had been determined by making visual observations on free sounding balloons with theodolites. The attachment of a radio transmitter to the balloon opened up the possibility of using a radio method of determining the wind velocity, this method having the great advantage of not being limited by conditions of visibility. This limitation implies that the theodolite method is useless for determining wind conditions above the prevailing cloud level. With a view to exploring the possibilities of such a method, an investigation was conducted during 1938–39 on the accuracy attainable in the use of radio direction-finders on the ultra-short-wave signals emitted by the balloon transmitters. A preliminary investigation of radio direction finding on wave-lengths between 6 and 10 metres (frequencies 30 to 50 Mc/s.) using signals emitted from ground transmitters has been published previously (Smith-Rose and Hopkins, 1938), and the present paper deals with the extension of this work to observations made on signals from balloon transmitters.

§ 2. THE LOCATION OF A FREE BALLOON EQUIPPED WITH A RADIO TRANSMITTER

There are two straightforward methods of determining the position of a radio transmitter, given its height above the earth's surface. The first method is to measure the azimuth and angle of elevation of the balloon transmitter by observations taken at a single ground station. In the second method two direction-finders located at a known distance apart are employed to determine the position of the projection of the balloon on the ground.

(a) *Method involving the measurement of elevation*

The first method has the obvious advantage of requiring only a single observing station; but, while the measurement of azimuth can be carried out with the existing pattern of radio direction-finder, the determination of the angle of elevation is much more difficult. This matter has been previously referred to briefly by H. Diamond, W. S. Hinman and F. W. Dunmore (1937), but no experiments on the subject appear so far to have been carried out. In a British Patent, H. A. Thomas (1937) has described one method of determining azimuth and elevation with a single instrument. This is of the Adcock direction-finder type, with a pair of vertical aerials spaced more than one wave-length apart. During the rotation of such an aerial system about a central vertical axis, the received signal passes through a series of minimum intensity positions, two of which indicate the azimuth and the others indicate the elevation of the transmitter. Practical considerations limit the application of such an instrument to wave-lengths of about 3 metres or below (frequencies of 100 Mc/s. or above), and the technique of the subject on these wave-lengths is accompanied by many difficulties and inaccuracies, the removal of which will require considerable investigation and development. It was therefore considered to be more expedient to devote attention in the first instance to the two-direction-finder method, since this made use of instruments and a technique which were already in an advanced stage of development and which were therefore expected to produce more rapid results.

(b) *Method involving two direction-finders*

At the time of the commencement of this investigation (1938) it was known that radio direction-finders were subject to various classes of error, some of which are directly associated with the instrument. As a result of various phenomena accompanying the propagation of electric waves either along the ground or through the atmosphere, the error of bearings observed on distant transmitting stations may at times be considerably greater than the instrumental error, and this frequently places a limit on the accuracy obtainable in the practical use of direction-finders. A considerable amount of modern research in direction finding has been devoted to the removal of errors resulting from the incidence of the waves at an appreciable angle of elevation above the ground. This is precisely the case in which direction-finders are employed to locate a transmitter attached to a free balloon, and it is a matter of experiment to ascertain exactly what accuracy in bearing is attainable under these conditions. From a knowledge of the accuracy in bearing obtainable with a single direction-finder, the consequent accuracy of position determination can be calculated.

When simultaneous bearings are taken on a fixed transmitter with two direction-finders having a known liability to error, the position of the transmitter lies within a quadrilateral which defines the maximum error in position under the conditions of the observations. The size and shape of this quadrilateral vary with the distance and direction of the transmitter from the direction-finders. The accuracy of position finding by this means has been studied by Corriez and Perlot with the same objective as that of the present investigation, and their results were given in a paper published in 1935. Based on the analysis outlined in this paper, the authors have calculated the curves drawn in figures 1 *a* and 1 *b*, which show the error in location of the transmitter as a function of its position for maximum bearing errors of $\pm 0^\circ{\cdot}5$ and 1° respectively. For clarity, each diagram is drawn in two halves with separate scales of distance. These graphs are curves of equal error expressed as the ratio of the error in position to the length of the base line between the two D.F. stations. It will be seen that the curve of optimum accuracy is a circle of diameter equal to the base-line. Thus when the balloon transmitter is on the perpendicular bisector of the base-line, the maximum accuracy is obtained at a distance from this line equal to half its length. Under these conditions the maximum possible error in position measurement is 0·9% and 1·8% of the base-line for the two D.F. bearing accuracies of ±0°·5, and 1°·0. In the first of these cases, the error in position increases to 7·5 and 28·5% for distances along the perpendicular bisector of twice and four times the base-line respectively. If the balloon transmitter remains at a constant distance from the centre of the base-line, but changes in azimuth, then the maximum error in position is a function of this position, as is shown by the graphs. On the other hand, if the path of the balloon should coincide with one of the curves in the figure, then the possible error in its location will be constant in value. It should be pointed out that these curves become unreliable when the transmitter is in such a position that the bearings from the two direction-finders are nearly equal, i.e., when the transmitter is approximately on the base-line or an extension of it, or when the balloon is distant from the base-line.

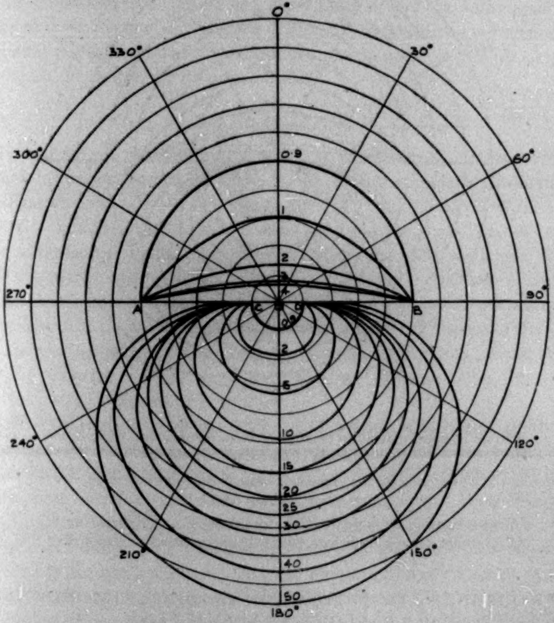

Figure 1 *a*. Curves of equal maximum possible error in determining the position of a transmitter from bearings of maximum error ±0·5°.

The figures on the curves indicate the maximum error in position expressed as a percentage of the length of the base line.

AOB = base line for upper half, i.e. for distances from O less than OA.
COD = base line for lower half, i.e. for distances from O greater than OC.

In the practical application of the method, observations are made continuously on the signal radiated from the balloon transmitter, and consequently the errors of individual readings can be smoothed out, to a large extent, by averaging the results over fixed time intervals. This is an important point to be borne in mind when this method of locating the free balloon is applied to the determination of wind velocity.

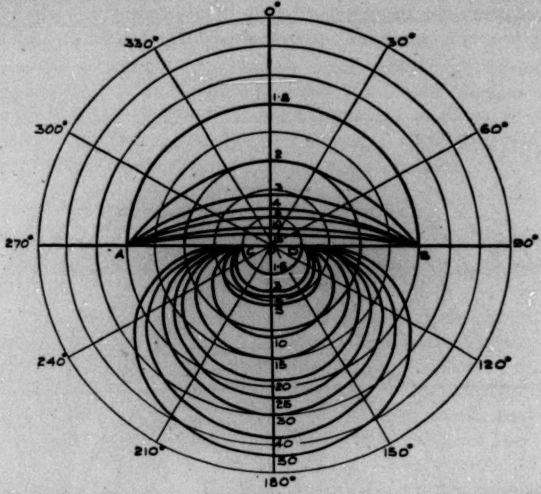

Figure 1 *b*. Curves of equal maximum possible error in determining the position of a transmitter from bearings of maximum error ±1°.

The figures on the curves indicate the maximum error in position expressed as a percentage of the length of the base line.

AOB = Base line for upper half, i.e. for distances from O less than OA.
COD = base line for lower half, i.e. for distances from O greater than OC.

§ 3. PRELIMINARY INVESTIGATION OF DIRECTION FINDING ON BALLOON TRANSMITTERS

As it appeared likely that the two-direction-finder method was the only practicable one available, experimental work was conducted with a view to determining the accuracy attainable with existing ultra-short-wave direction-finders. A previous paper (Smith-Rose and Hopkins, 1938) has outlined the results obtainable with transportable direction finders on signals emanating from a fixed ground-transmitting station, but it was now desired to ascertain the reliability of the bearings observed on the radiation from a transmitter attached to a free balloon. Some of the experiments were carried out with the transportable apparatus just referred to, while for later work use was made of fixed-station direction-finding apparatus, the rotating-loop type of which has already been described elsewhere (Hopkins, 1938).

The balloon transmitters used in these investigations were of the type developed at the National Physical Laboratory for meteorological sounding of the atmosphere, and a description of the transmitter and the experimental work conducted with it has been published by H. A. Thomas (1938). The experiments were made by releasing a balloon with transmitter attached, and then following the course of the balloon with a theodolite while bearings were being taken on the transmitter with the direction-finder. A comparison between the visual and radio bearings then gave the accuracy of the latter. The radio bearings were taken by the usual aural-null method, some ten to twenty observations being made per minute. The mean of such a group of bearings was then compared with the mean of the theodolite bearings for the same minute, and the summaries given below refer to these mean observations. The radio observations were sometimes continued after the balloon had passed out of sight, in order to provide data as to the range of usefulness of the direction-finder.

(a) *Measurements with field direction-finders.*

The first series of measurements were carried out with the experimental transportable direction-finders referred to above, and especially developed for field investigation work. These were of two types : one was fitted with a simple rotating loop, while the other used a rotating spaced aerial of the Adcock pattern. The great advantage of using these instruments in the early work was that the experiments could be conducted at open field sites where previous calibrations had indicated that errors due to the site itself were likely to be small. As the investigation progressed, it became increasingly evident that the influence of the site, or the radio interfering effect of any obstacles thereon, is likely to be the limiting factor in the accuracy of this method of locating elevated radio transmitters whether attached to balloons or aircraft.

Employing balloon transmitters designed to operate in the wave-length range 8 to 10 metres, the sensitivity of the loop direction-finder was found to be adequate to enable good bearings to be taken at ranges up to some 40 miles ; while, with some sacrifice of quality, radio observations have been obtained at ranges up to about 90 miles. The form of the Adcock direction-finder used in these early experiments had a maximum range of 20 miles. Later, a more sensitive Adcock set has been developed and a description of this is in course of publication. A direct comparison carried out between the loop and the Adcock direction-finders showed that the means of each group of bearings taken over a period of one minute were in fairly good agreement, although the oscillation of the individual bearings due to the swinging of the transmitter aerial was in general much greater with the loop set than with the Adcock receiver. The results obtained during balloon ascents in which theodolite observations were taken are given in table 1. These measurements were made with the direction-finders placed at several sites ; with the exception of those at which balloons Nos. 4 and 30 were released, these sites were carefully chosen so as to minimize any influence of the surroundings on the radio bearings.

Consideration of this table shows that in the case of the loop receiver the extreme error was 7°·5, while with the Adcock receiver the extreme error was 3°·0. It should be noted that the results above cover a range of elevation from 4° to 36°. The importance of the angle of elevation of the balloon is discussed later, but it should be pointed out that as the angle of elevation increases, the wanted pick-up, that is, the e.m.f. induced in the vertical portions of the aerial array, falls off very rapidly. Furthermore, the magnitude of the unwanted pick-up, that is, the e.m.f. induced in the direction-finding system by the swinging of the transmitter aerial from the vertical, increases. Thus at high angles of elevation the accuracy of D.F. observation falls off considerably. The principle of the Adcock direction-finder eliminates, to a large extent, the unwanted pick-up, and this type of direction-finder would therefore be expected to give better results than the loop at high angles of incidence. Unfortunately, the sensitivity of the early experimental Adcock was insufficient to make use of this advantage, and the satisfactory working range of the instrument even at low angles of elevation was limited to about ten miles. Later work with the more sensitive instruments has shown them to be free from this limitation, and it is not considered that the accuracy of the D.F. bearings will deteriorate appreciably for ranges of the balloon somewhat beyond that at which it was possible to make visual observation during these tests.

Table 1. Results of D.F. tests at field sites with balloons using wave-lengths between 8 and 10 metres

Balloon No.	Duration of visual observations (min.)	Range of elevation during test (deg.)	Estimated distance of balloon at last observation (miles)	Accuracy of D.F. bearings for each minute			
				Extreme error (deg.)	Mean error (deg.)	% within 2°	% within 1°
			Loop results				
4	15	16–21	5	6·0	3·2	50	12
5	7	17–26	3	1·1	0·4	100	86
17	57	12–26	15	2·0	0·9	100	49
18	31	4–12	4	1·7	0·6	100	90
30	12	24–36	5	5·0	1·9	67	42
32	9	28–32	3	7·5	2·9	45	44
Comprising all the six tests					1·3	88	58
			Adcock results				
17	57	12–26	15	2·0	0·8	100	67
18	31	4–12	4	1·4	0·5	100	96
27	7	21–28	2	1·3	0·7	100	71
28	11	8–16	4	1·0	0·4	100	100
30	12	24–36	5	1·1	0·4	100	92
32	9	28–32	3	3·0	1·2	78	44
38	21	8–17	16	1·6	0·5	100	86
Comprising all the seven tests					0·6	99	79

The results of this first series of experiments were very encouraging in showing that it was practicable to use an ultra-short-wave direction-finder to determine to a reasonable accuracy the bearing of a free balloon carrying a radio transmitter. The tests showed that with a rotating loop set, 88% of the bearings were correct to within 2°, while with the experimental Adcock sets the accuracy was appreciably higher.

It has naturally been impossible to check the accuracy of the direction-finders when the transmission path has been partly through clouds.* It is, however, reasonable to suppose that clouds will not materially affect these results, except possibly during thundery weather, when ionization in the clouds may be considerable.

It was next decided to ascertain to what extent this accuracy could be improved by using a fixed-station instrument of more rigid and robust design. At the period under consideration, certain technical difficulties were being experienced with the Adcock or spaced-aerial direction-finder, and while these were being investigated, the experimental work with balloon transmitters was continued with the improved form of rotating-loop instrument specially developed for the purpose (Hopkins, 1938).

(b) *Measurements with a direction-finder in a wooden hut*

Preliminary experiments carried out with the improved rotating-loop direction-finder installed in a hut at the Radio Research Station, Slough, indicated that a considerable improvement in instrumental performance was now obtainable. The results of two balloon ascents from Slough in which comparison observations were made with a theodolite are shown in table 2.

Table 2. Results of D.F. tests at Radio Research Station, Slough, with balloons using wave-lengths between 8 and 10 metres

Balloon No.	Duration of visual observations (min.)	Range of elevation during test (deg.)	Estimated distance of balloon at last observation (miles)	Accuracy of D.F. bearings for each minute			
				Extreme error (deg.)	Mean error (deg.)	% within 2°	% within 1°
36	7	20–25	8	3·7	1·1	86	57
37	26	16–26	20	2·9	1·0	89	65
Mean of the two tests					1·0	88	64

These results, which are rather better than those obtained with the field sets, confirmed the view that the effect of the hut on the bearing accuracy would be small. Experiments with a portable transmitter set up close to the hut had already shown that the latter was not effective in producing bearing errors in this wave-band when dry, uniformly wet, or even when one or more sides were dry and the remainder wet.

All these results were sufficiently encouraging to warrant the continuation of the work with loop direction-finders of the fixed-station type on better sites than had so far been available, and the details of this work are described in the following section.

---

* Modern radar methods are now available to assist in such investigations.

§ 4. DIRECTION FINDING ON BALLOON TRANSMITTERS AT FIXED GROUND STATIONS

(a) *Choice of sites for experimental work*

Through the co-operation of the Meteorological Office, Air Ministry, two direction-finding sites near Larkhill, on Salisbury Plain, were made available for experimental work. Each of these sites was selected by personal inspection and was quite evidently superior to those at present available at the Radio Research Station.

The first site, at Elston Hill, was situated in the centre of a flat expanse of arable land, which was about three-quarters of a mile square, and was reasonably level over the whole area. The hut containing the direction-finder was situated near a footpath at approximately 300 yards from a minor road, and the nearest obstacles of any magnitude were the trees surrounding a farm-house some 1000 yards distant. In the earlier experiments an area of radius 25 yards around the hut was kept free of crops, but this was found to be insufficient, and the radius was later increased.

The other site was at Lavington, about five miles away, and was a large stretch of pasture land reasonably flat, but with a gentle slope of about 1° in one direction and a somewhat steeper slope after a distance of 500 yards in the opposite direction. The nearest obstacles were trees more than 1000 yards away and a steel water tower, also at about 1000 yards.

At each site the direction-finder was housed in a large wooden hut containing no metal-work larger than six inches, and, apart from the instrument, no metal objects formed part of the equipment.

(b) *Calibration of sites*

In order to ascertain the inherent accuracy of each instrument as installed in its hut, each direction-finder was calibrated by observing the bearings on a small portable transmitter set in turn at various positions round the hut at a radius of about twenty yards. In all except the preliminary experiments, care was taken to ensure that the assistant placing the transmitter in position did not produce spurious readings on the direction-finder ; it was found that if he retired to a distance of about ten yards behind the transmitter on the line joining this to the receiver, no error was introduced. To facilitate the repetition of the calibrations at various times, it was found convenient to install a circle of wooden pegs marking the transmitter positions : in the earlier work these were provided at intervals of 30°, but as the work progressed it was found desirable to place additional pegs at 10° intervals. Also in the earlier tests, a landing-type magnetic compass was used to ascertain the true bearing of the various pegs, but various comparisons between this compass and theodolite indicated that the compass readings were limited to an accuracy of about $\pm 0^\circ{\cdot}3$. As the results soon showed that an accuracy of this order was attainable with the direction-finder, the peg positions were finally located to a high accuracy by a theodolite method. The majority of the balloon work at these sites was carried out on a wave-length of 8·5 metres (frequency 34 Mc/s.) arbitrarily chosen, but it was known that ultimately the technique would have to be transferred to the recently allocated international band of 10·7 to 10·9 metres (27·5 to 28·0 Mc/s.). In the calibration work, therefore, the observations were carried out for a range of frequencies, and it was usually found that the observed bearing was in error and the value of the latter varied with frequency.

Throughout the calibrations, the observed bearings on the local transmitter were sharp, with a swing of about ± 0°·2. As a result, the observational accuracy is considered to be of the order of 0°·1. In general, the maximum error obtained in the course of the calibrations was about 1°, although in certain circumstances errors of 2° have been noted.

Typical calibration curves obtained for the Elston and Lavington sites in September and December 1938 on a frequency of 34 Mc/s. are shown in figures 2 *a* and 2 *b*. It is seen that there is an appreciable change in the calibration with time, the change being more marked at Elston Hill (figure 2 *a*) than at Lavington (figure 2 *b*). A maximum of about 0°·2 of this change was subsequently traced to a possible change in the position of the flexible transmission line leading from the turn-table down to the receiver on the floor. This fault in the instrument has now been rectified.

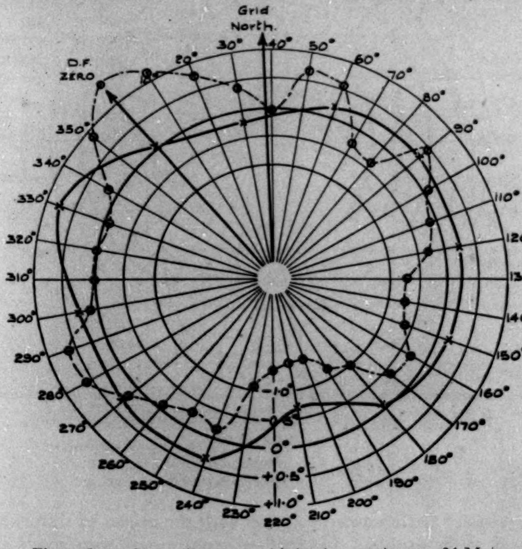

Figure 2 *a*. Site calibrations with local transmitter on 34 Mc/s. Elston Hill site.

Error { × September 1938.
⊙ December 1938.

On a few occasions, calibrations of a similar nature to the above have been conducted with the portable transmitter removed to distances up to 150 yards. It was found that the errors in the observed bearings varied within the range ± ·0°3, depending upon both the actual azimuth and the working frequency. It has not so far been practicable to extend this type of measurement to greater distances with a view to ascertaining the degree to which the short-radius calibration curves may be applied as corrections to bearings observed on distant transmitters. In view of this practical difficulty, the applicability of such ground calibrations to results obtained on balloon transmitters will depend upon the relative importance of errors having their cause only a few yards from the direction finder and those

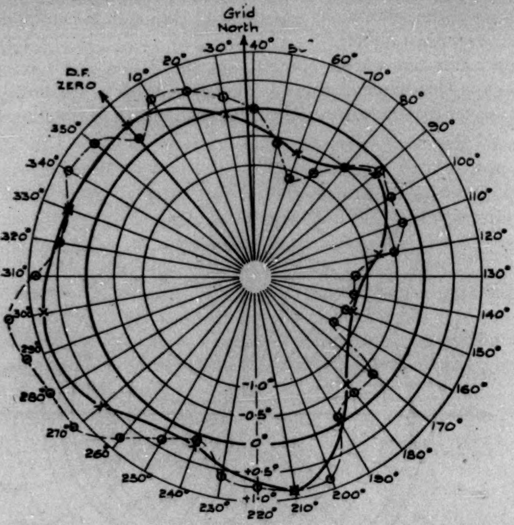

Figure 2 *b*. Site calibrations with local transmitter on 34 Mc/s. Lavington site.

Error { × September 1938.
⊙ December 1938.

caused by obstacles farther away. It was with the object of throwing more light on this aspect of the problem that further experiments were made at the Elston and Lavington sites, in which the radio bearings were directly compared with visual bearings obtained with theodolites.

(c) *Further results on balloon transmitters*

In these experiments a number of balloons equipped with transmitters were released from each of the two sites, and the course of each of these was followed visually with a theodolite set up near the direction-finder. A second theodolite was used to determine the position of the balloon during the early part of each ascent, so that the observations on the first theodolite could be corrected for the small error introduced by the distance which separated the direction-finder from the theodolite. During the ascent of a balloon, radio-bearing observations (on a wave-length of 8·5 metres) were taken continuously at the rate of some 10 to 20 per minute, and theodolite observations were taken at half-minute intervals. In this way it was possible to compare directly the mean bearing of the balloon transmitter during each minute as given by the direction-finder with the mean true bearing as given by the theodolite results. A summary of the results obtained during twelve ascents at Elston and nine at Lavington is given in table 3. These results refer to the actual readings on the instruments, before introducing any corrections derived from the ground calibrations, and they may therefore be compared directly with the earlier results summarized in table 1.

Table 3. Results of tests with radio-equipped balloons using direction-finders installed in wooden huts ($\lambda = 8{\cdot}5$m.)

Balloon No.	Duration of visual observations (min.)	Range of elevation during test (deg.)	Estimated distance of balloon at last observation (miles)	Accuracy of D.F. bearings for each minute				
				Extreme error (deg.)	Mean error (deg.)	% within 2°	% within 1°	% within 0°·5
	(a) *Direction-finder at Elston Hill*							
1	6	41–45	1	1·6	0·8	100	60	60
2	43	23–60	11	5·0	1·5	83	31	21
4	5	9–61	1	3·5	1·6	80	40	0
6	54	11–42	18	5·7	0·7	96	78	63
8	73	10–24	35	2·0	0·6	99	78	49
10	73	13–25	19	4·3	0·8	99	71	18
11	60	12–21	22	4·7	0·7	98	93	26
12	7	—	1	9·3	2·3	57	57	29
14	7	11–22	2	0·6	0·4	100	100	57
16	29	7–12	15	2·5	0·4	95	95	89
19	20	19–53	4	2·0	1·1	100	47	0
22	28	20–34	9	4·2	1·0	93	43	29
Comprising all the twelve tests					0·8	96	72	37
	(b) *Direction-finder at Lavington*							
3	28	7–18	6	5·0	0·9	89	68	64
5	35	8–24	11	1·1	1·7	100	86	23
7	34	17–27	8	5·2	0·5	94	94	79
9	8	28–45	2	2·1	1·0	86	57	14
13	8	6–23	1	9·6	2·1	62	62	50
15	17	7–13	8	1·7	0·6	100	88	47
17	16	8–23	3	1·1	0·4	100	94	56
20	35	9–21	10	4·4	0·5	94	94	77
59	68	6–29	9	4·9	0·6	97	82	50
Comprising all the nine tests					0·7	95	84	55

It will be seen that this improved form of loop direction-finder erected on a superior site gives a considerable increase in overall accuracy in this work. The maximum error in the radio bearings was about 5°, while about 95% are within 2° and nearly 80% within 1°. It was found that the largest errors in bearing generally occur in the first three minutes of flight. Factors contributing to this effect are the violent aerial swings in this period, the observer's initial "mental inertia" in following the consequent variations in bearing, his preoccupation with tuning adjustments, and the high rate of change of mean bearing in the first minute or so of flight. These large initial errors are, therefore, not truly representative of the capabilities of the direction-finders observing on a balloon transmitter during the major portion of a flight.

In order to ascertain to what extent the ground calibration may be usefully applied to these results, a direct comparison has been made of the errors in bearings before and after the appropriate correction derived from the site calibrations at twenty yards radius was applied to each D.F. observation (minute means). This comparison is shown in the following table, which refers to the whole of the results given in table 3, omitting the first three minutes of each ascent, and for both the Elston and Lavington sites.

This table clearly demonstrates that the ground calibration made at a short distance around each direction-finder is quite useful in improving the overall accuracy of the observed radio bearings on balloon transmitters. It is evident, therefore, that at least part of the error in bearings is associated with the immediate vicinity of the direction-finding installation: the instrument itself and the hut would appear to be exonerated by the irregular shape of the calibration curves on any one frequency. Reference may be made at this stage to the high overall accuracy which is now associated with these direction-finding arrangements. Bearing in mind that the results refer particularly to the mean observed radio bearings over one-minute intervals during the whole flight of a number of free balloons, it is to be noted that over 90% of these mean bearings are correct to within 1°, and that the probable error calculated from all the readings, after correction for ground calibration, is 0°·35 for Elston and 0°·25 for Lavington.

Table 4. Effect of correction for ground calibration on bearings taken on radio balloon transmitters

Site	Correction for ground calibration applied	Percentage of minute means of radio bearings differing from visual bearings by not more than			
		2°	1°	0°·6	0°·2
Elston	No	99	76	49	14
,,	Yes	99	91	73	33
Lavington	No	99	90	68	23
,,	Yes	100	95	82	44

One further aspect of the results is illustrated by table 5, in which the errors of the radio bearings are separated for various arcs of elevation covered by the balloons in flight. The first three minutes of each ascent have been neglected, for reasons explained above.

From this table it is seen that there is a definite tendency for the errors to increase with the angle of elevation. This is to be expected from the fact that with a swaying aerial the effect of the horizontally polarized component in the emitted radiation will be to produce errors on the loop direction-finder which increase with the angle of elevation. So long as this work is restricted to loop sets it will obviously be advantageous to arrange the balloon ascents to give as small angles of elevation as possible, but this is not always practicable when a rapid ascent to high altitudes is required. The conversion of the direction finders to the spaced-aerial or Adcock system should, therefore, give a considerable improvement in the radio-bearing accuracy from this point of view.* In addition, the use of the Adcock system brings about a greater steadiness of the individual observations, the variations of which are due to the swaying of the balloon transmitter aerial.

§ 5. DISCUSSION OF RESULTS AND CONCLUSIONS

Before summarizing the conclusions which may be drawn from the results of the experiments described above, it will be useful to review the various types of error to which the bearings observed on a radio direction finder are subject. It is essential to understand clearly these various errors and their relative importance and to investigate their causes before further progress can be made in the particular application of direction finding discussed in this paper, viz., the location of a radio transmitter attached to a free balloon. It will be evident that the conclusions may equally apply to the case of the location of aircraft transmitters within the limitations of distance, type of aerial, etc., imposed by the former application.

Table 5. Variation of mean error of radio bearings with elevation of transmitter, after correcting for local calibration

Site	Arc of elevation (degrees)	Mean arithmetic error (degrees)
Elston	5–10	0·2
	10–15	0·3
	15–20	0·4
	20–25	0·5
	25–30	0·7
	30–35	0·7
	35–40	0·9
	40–45	1·3
Lavington	5–10	0·3
	10–15	0·3
	15–20	0·4
	20–25	0·4
	25–30	0·6
	30–35	0·6

(a) *General discussion of errors in direction finding*

In general direction-finding work it is convenient to classify the various effects observed under the headings of *Instrumental* (including reciprocal effects and polarization errors), *Site*, *Ground path*, *Atmospheric path* and *Source* errors.

---

* With spaced-aerial systems the amplitude of the wanted voltage due to the vertically polarized component from the balloon is likely to fall off more rapidly with increase of elevation angle than that due to a similarly polarized reflection from an obstacle near the site. Even with an ideal Adcock system, therefore, we should expect site errors to be more troublesome at high angles of elevation.

Instrumental errors are inherently due to defects in the design or construction of the instrument, which introduce an error into the bearings indicated or observed. The reciprocal-error effect is made evident by the fact that the observed bearings in the two possible positions of the rotating system are not exactly 180° apart. Although the resulting error in bearing can be reduced by taking the mean of such readings, with the appropriate 180° correction, it is desirable that the reciprocal error should be reduced as much as possible. The effect arises from lack of symmetry of the receiving aerial circuit, and can be reduced or avoided by careful design and construction supplemented, if necessary, by a compensating device. It is not usually difficult to reduce such an effect to less than $0^\circ{\cdot}5$, and in the instruments used in the later portions of this investigation the error was reduced to less than $0^\circ{\cdot}1$.

The polarization errors are due to the reception of horizontally polarized electric waves on the aerial system, the magnitude of the effect decreasing as the angle of incidence of the arriving waves is increased, to a minimum for horizontally propagated waves. The loop direction-finder is very susceptible to such effects, but the magnitude of the error depends upon the relative intensities of the vertical and horizontal fields in the incoming waves. Using a balloon transmitter with a steady vertical aerial, no such polarization errors would be experienced on the loop direction-finder. In practice, however, the transmitting aerial performs a conical oscillation about an axis which, due to the horizontal motion of the balloon, may not be vertical; and it is therefore to be expected that variable polarization errors would be experienced with such a direction finder. The results already obtained and discussed in the previous sections show that by taking the mean of several bearings observed over one-minute periods the effect of such oscillation of the bearing can be kept reasonably small, providing the angle of elevation of the balloon itself is not excessive.

Site errors arise from the reception of re-radiated fields from currents induced by the incoming waves in obstacles such as trees, buildings and metal conductors on the site of the direction finder which may arbitrarily be taken as the area of terrain within about a quarter of a mile from the direction finder. From earlier general experience in direction finding on other wave-lengths, it is known how to avoid the larger errors due to bad site conditions, but with the general improvement in the accuracy of direction-finding technique, the matter has called for further investigation on a wide scale. The subject is found to be of a somewhat complex nature, and detailed discussion of the general problem is beyond the scope of the present paper. The results of experiments described above indicate the order of the effects observed in relation to the particular application dealt with in this investigation.

Ground and *atmospheric path* errors are due to any deviation or reflection effects introduced in the propagation of the waves and caused either by topographical features, such as hills, masses of trees or the ground, or by atmospheric conditions such as clouds or temperature gradients in the path between transmitter and receiver. The experiments described in this paper tend to confirm the view that the error due to these effects of topography—although small—are likely to be a factor limiting the accuracy of bearings taken on signals from balloon-borne transmitters. On the wave-lengths and at the distances used for this work it is considered that the field at the direction finder is free from radiation returned from the ionosphere.

Source error arises from any peculiarities in the distribution of radiation from the immediate vicinity of the transmitter, due either to the aerial system employed or to re-radiation effects from obstacles close to the transmitter. In the case of free balloons of the type used in this investigation, such source effects are quite negligible.

(b) *Conclusions*

The above general discussion makes it clear that in order to obtain a high degree of accuracy in locating free balloons by radio direction-finding methods, it is necessary to pay special attention to the instrument itself and the site on which it is placed.

The greater part of the investigation described in this paper has been carried out with direction-finders which have been specially developed to have a high instrumental accuracy of bearing indication, which is of the order of 0°·1 under the best conditions, using a working wave-length of about 10 metres. Some difficulty has been experienced in utilizing this accuracy, however, due first to effects introduced by the site on which the direction finder is placed, and secondly, by the departure during flight of the balloon aerial from a vertical position. By a careful choice of the site on which the direction-finder is placed, the former error has been restricted to within a range of about ±1°, but variations of about half this magnitude have been experienced in the course of successive calibrations with a three-monthly interval. The cause of this error and of its variation have not so far been ascertained, but the results of various experiments suggest that the bearings observed on a balloon transmitter can be improved in accuracy by applying a correction for this local site error. The effects of the swaying of the transmitting aerial while a balloon is in flight can be largely compensated for by taking the mean of a succession of radio-bearing observations over a period of a minute, and the results of tests carried out on some twenty balloon flights under these conditions show that 95% of the observed bearings are correct to within 2°, and nearly 80% correct to within 1°. These results can be still further improved with the use of a more fully developed Adcock or spaced-aerial direction-finder than was available for the experiments described in this paper.

It must be pointed out that since the assessment of the direction-finding accuracy is carried out by comparing the radio observations with visual bearings obtained by means of theodolites, all the tests described above were necessarily conducted under fair-weather conditions when visibility was reasonably good. In many cases, however, the radio observations were continued long after the balloon had passed out of sight above the clouds, and the general experience obtained under such conditions indicates that the above accuracies are likely to be maintained for the whole period during which the signals from the transmitter are of adequate strength at the direction-finding receiver. It thus appears that within the range of such balloon location work, which may cover distances up to the order of 50 miles and altitudes up to some 40,000 feet, no serious errors due to the propagation of waves through the atmosphere are likely to be encountered.

The work described above is limited to a study of the accuracies of individual radio direction-finders. The resulting accuracies in the location of a free balloon by means of two direction-finders operating simultaneously can be deduced from theoretical curves given in the paper. The extension of the experimental investigation to such simultaneous operation and the resulting application for meteorological purposes must remain outside the scope of the present paper.

ACKNOWLEDGMENTS

The investigations described above were carried out for the Director of the Meteorological Office, by whose permission the paper is now published. The authors are particularly indebted to Mr. L. G. Hemens, B.Sc., and the staff of the Meteorological Office at Larkhill, with whose co-operation the work at Larkhill was conducted. They also have to acknowledge the assistance rendered by Mr. W. Dougharty, B.Sc., throughout the experiments.

REFERENCES

Corriez and Perlot, 1935. "The radiogoniometric method of the National Bureau of Meteorology for measuring the direction and velocity of winds during overcast weather." *La Météorologie*, August, 368.

Diamond, H., Hinman, W. S. and Dunmore, F. W., 1937. "The development of a radio meteorograph system for the Navy Department." *Bull. Amer. Meteorological Soc.* **18,** 95.

Hopkins, H. G., 1938. "A loop direction finder for ultra-short waves—wave-range 6 to 11 metres." *Wireless Engr.* **15,** 651.

Smith-Rose, R. L. and Hopkins, H. G., 1938. "Radio direction finding on wavelengths between 6 and 10 metres (frequencies 50 to 30 Mc/s.)" *J. Inst. Elect. Engrs.* **83,** 87.

Thomas, H. A., 1938. "The determination of the meteorological conditions of the atmosphere by the use of radio-sounding balloons." *Proc. Roy. Soc.* A, **167,** 227.

Thomas, H. A. "A method of determining the position of an elevated radio transmitter." British Patent 28,921/37.

THE ACCURATE DETERMINATION OF CELL DIMENSIONS FROM SINGLE-CRYSTAL X-RAY PHOTOGRAPHS

By MARGARET C. M. FARQUHAR and H. LIPSON,
Cavendish Laboratory, Cambridge

MS. received 20 *October* 1945

ABSTRACT. The importance of improving the accuracy of the determination of cell dimensions determined from single-crystal photographs is pointed out and the general principles upon which such improvements can be obtained are outlined. These principles, which are based on those used for powder photographs, are illustrated by application to an orthorhombic crystal, thallium hydrogen tartrate, the cell dimensions being determined to an accuracy of the order of 0·005%. Extensions of the method to monoclinic and triclinic crystals are also discussed.

§ 1. INTRODUCTION

Rotation and oscillation photographs provide a ready means for finding the unit-cell dimensions of a crystal, since, if the crystal is rotating about a crystallographic axis, the distances apart of the layer lines provide a measure of one of the lattice spacings. The accuracy of this method is, however, not high;

it is great enough for unequivocal indexing of the spots on oscillation photographs, but few workers would claim an accuracy of more than about 1% for cell dimensions deduced in this way. This accuracy is probably sufficient for most crystal-structure work, since interatomic distances are not usually determined to this accuracy. But recent work with three-dimensional Fourier methods suggests that an accuracy of 1% in interatomic distances has been approached (Jeffrey, 1945) and even surpassed (Booth, 1945), and therefore it appears that for crystals studied by these methods a greater accuracy in the determination of cell dimensions would be desirable.

In certain other applications of x-ray diffraction an increased accuracy would also be desirable. For example, in the determination of molecular weights an accuracy of 0·03% is needed to match the 0·1% that can sometimes be obtained in the determination of densities. Buerger (1937) has described a special Weissenberg instrument by which this accuracy can be obtained. It is, however, unnecessary to have a special camera for the purpose; an accuracy of 0·01% can easily be obtained with an ordinary single-crystal goniometer, only small changes in design being necessary. The only qualification is that the crystal should be perfect enough to give sharp spots with Bragg angles θ near 90°.

§ 2. THEORY OF THE METHOD

The method to be described is based essentially on that already extensively used for powder photographs (Lipson and Wilson, 1941). The positions of resolved α doublets with θ near 90° are measured and the value of one of the cell dimensions is deduced from each; the values are plotted against $\sin^2\theta$ and the value at $\sin^2\theta = 1$ is taken as correct.

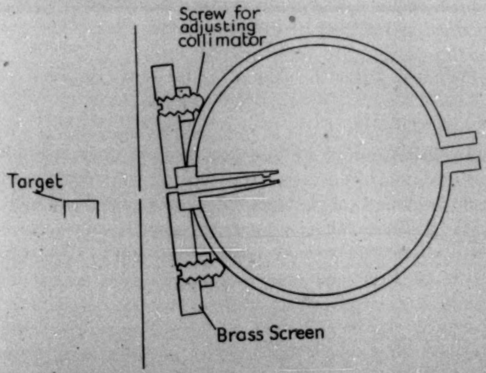

Figure 1 *a*. Section of camera with collimator attached.

A difficulty arises in the determination of the Bragg angles of the spots. Single-crystal cameras are not usually fitted with calibrated knife-edges, and to introduce these would require considerable redesign. This difficulty can be avoided by using the van Arkel method (Lipson and Wilson, 1941) of mounting the film; the x rays enter through a hole in the film and the reflections with θ near 90° are then recorded near the middle of the film, not near the edges. (This film mounting is not recommended for ordinary indexing, where it is important to know the position corresponding to $\theta=0°$). The angles can then be evaluated with a knowledge of the camera radius, and even though this may not be the effective radius of the film, because of film shrinkage, the error is eliminated by the method of extrapolation.

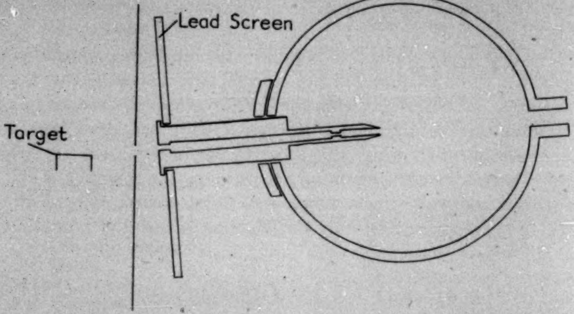

Figure 1 *b*. Section of 3-cm. radius Unicam camera.

The film can be most easily mounted in the camera if the collimator is rigidly attached to the camera, since then only a small hole is needed in the film, as shown in figure 1 *a*. This has an additional advantage over the more usual arrangement, shown in figure 1 *b*, in that the camera can be put closer to the x-ray tube. With a camera of 3-cm. radius it was found that this modification resulted in about a three-fold increase in intensity of the spots in the film. The presence of the collimator in the camera also facilitates the loading of the film, and renders unnecessary the movement of the goniometer between exposures.

§ 3. USE OF THE METHOD FOR AN ORTHORHOMBIC CRYSTAL

The spots which are used are those on the zero layer line of an oscillation photograph. If an axis of the crystal is oscillating symmetrically with respect to the x-ray beam a symmetrical photograph will be obtained and values of θ can be derived from the distances S between corresponding spots on the two sides of the film. If S is the distance between two such spots,

$$90° - \theta = \frac{S}{4R} \cdot \frac{180}{\pi}. \qquad \ldots\ldots(1)$$

For a camera of 3-cm. radius this reduces to

$$90° - \theta = 4{\cdot}77S. \qquad \ldots\ldots(2)$$

The symmetrical oscillation photograph provides another advantage. In figure 2 is shown the a^* b^* section of an orthorhombic reciprocal lattice with the reflecting circles (Bernal, 1926) symmetrically disposed with respect to the b axis. It will be seen that the spots with θ near 90° have a large k and small h index. These spots will be particularly well suited to the determination of the value of b, since a small error in *a* will not greatly affect the results. In order to find *a*, another photograph can be taken with the *a* axis oscillating symmetrically with

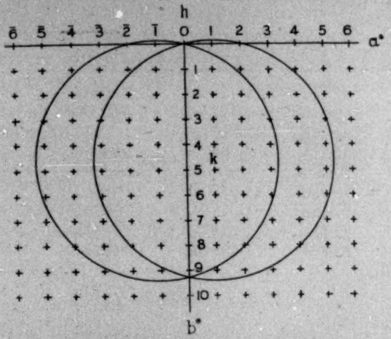

Figure 2. Section of orthorhombic reciprocal lattice and extreme limits of circles of reflection for a symmetrical oscillation photograph.

respect to the x-ray beam, the axis of rotation being the same as for the former photograph. To determine the value of *c*, however, either the *a* or *b* axis must be set as axis of rotation.

§4. A PRACTICAL EXAMPLE

The method has been used to determine the cell dimensions of thallium hydrogen tartrate. Groth (1910) gives the axial ratios as

$$a : b : c = 0{\cdot}6976 : 1 : 0{\cdot}7275,$$

and these values are supported by the measurements of Porter (1928), who gives

$$a : b : c = 0{\cdot}6950 : 1 : 0{\cdot}7234.$$

A crystal was mounted with its *a* axis as axis of rotation; this axis was parallel to the longest dimension of the crystal and, on the oscillation photographs taken with Cu Kα radiation, the x-ray reflections were sharp and accurately measurable. Measurements of the layer lines gave $a = 7{\cdot}63$ kx., from which, using the axial ratios given by Groth, we obtain $b = 10{\cdot}94$ kx. and $c = 7{\cdot}96$ kx. These values were used for the analysis of the photographs.

Two symmetrical 15° oscillation photographs were taken, as explained in §3. The positions of all the resolved α doublets on the zero layer line of each photograph were measured; the results for the determination of *c* are given in table 1. The points as plotted (figure 3 *a*) for extrapolation show a great deal of scatter, and it is impossible to deduce more than that the value of *c* is in the neighbourhood of 7·91 kx. The scatter is not, however, a random one; the points for reflections with larger *k* tend to lie above the others. This is an indication that the axial ratio is in error. This was confirmed by the measurement of *b*, which gave $b = 10{\cdot}99$ kx.; the axial ratio is thus about $0{\cdot}7197_5$, not 0·7275. A recalculation of *c* with this axial ratio (shown in the lower part of table) gave the points shown in figure 3 (*b*);

Table 1

The derivation of *c* from an oscillation photograph of a single crystal of thallium hydrogen tartrate taken with Cu Kα radiation in a camera of radius 3 cm.

$h\ k\ l$	Radn.	θ	cosec θ	$\frac{1}{2}\lambda\sqrt{\frac{c^2}{b^2}k^2+l^2}$	c	$\sin^2\theta$
0 6 8	α_1	62·267	1·129783	7·00548	7·9147	0·784
	α_2	62·496	1·127423	7·02296	7·9278	0·787
0 4 9	α_1	66·832	1·087720	7·27095	7·9088	0·845
	α_2	67·171	1·084991	7·28909	7·9086	0·850
0 5 9	α_1	70·529	1·060660	7·46201	7·9147	0·889
	α_2	70·930	1·058067	7·48063	7·9150	0·893
0 2 10	α_1	79·153	1·018192	7·76792	7·9092	0·965
	α_2	79·892	1·015767	7·78731	7·9101	0·969
0 3 10	α_1	83·894	1·005705	7·86793	7·9128	0·989
0 6 8	α_1			6·98834	7·8953	0·784
	α_2			7·00579	7·8985	0·787
0 4 9	α_1			7·26362	7·9008	0·845
	α_2			7·28175	7·9006	0·850
0 5 9	α_1			7·45085	7·9028	0·889
	α_2			7·46945	7·9032	0·893
0 2 10	α_1			7·76621	7·9075	0·965
	α_2			7·78560	7·9084	0·969
0 3 10	α_1			7·86413	7·9090	0·989

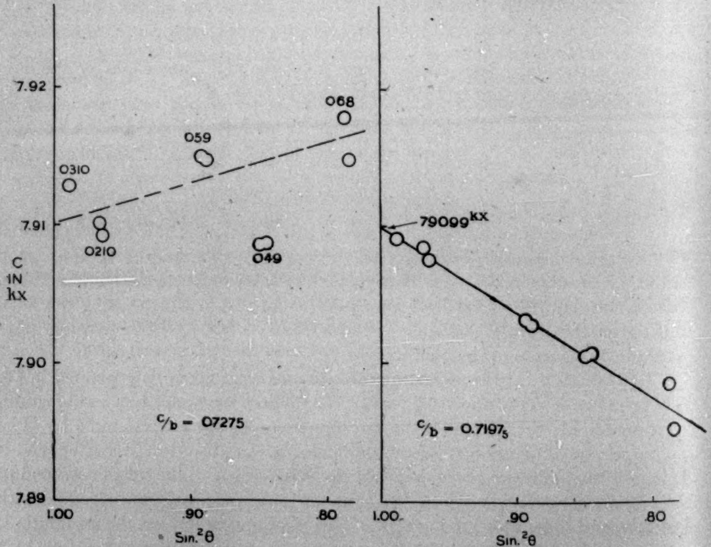

(*a*) (*b*)

Figure 3. Extrapolation curves for the determination of *c*: (*a*) with an inaccurate value of *c*/*b*; (*b*) with an accurate value of *c*/*b*.

these lie satisfactorily in a straight line and give the value of c as 7·9099 ± 0·0003 kx. A similar recalculation of b gave 10·9945 ± 0·0005 kx.

In order to find a, a photograph was taken with the crystal set with the b axis as axis of rotation. With 15° oscillation and Cu Kα radiation, however, no spots with θ greater than 70° appeared on the symmetrical photograph. The range of oscillation was therefore increased to 30° by taking two successive exposures on the same film, and two reflections with higher angles were recorded. The results were not so good as with the other photographs, in that the extrapolation curve was not straight, but nevertheless the value of a was found to be 7·6395 ± 0·0005 kx. As a check, the value of c was also deduced from a photograph taken with the same axis of rotation; the value, 7·9101 ± ·0004 kx., agreed with the previous value well within the limits of experimental error.

To summarize, the results for the crystal are

$$a=7{\cdot}6395\text{ kx.},\qquad b=10{\cdot}9945\text{ kx.},\qquad c=7{\cdot}9100\text{ kx.},$$
$$a:b:c=0{\cdot}69485:1:0{\cdot}71945.$$

The lattice parameters are probably correct to 0·0005 kx. and the axial ratios to 0·0001. (It is interesting to note that the value of a deduced from layer-line measurements was correct to 0·1%, but this agreement is probably fortuitous.) The density ρ, calculated by means of the formula

$$\rho=1{\cdot}65026\,\Sigma A/abc, \qquad \ldots\ldots(3)$$

where ΣA is the sum of the atomic weights of the atoms in the unit cell (Stockdale, 1940; Foote and Jette, 1940), is $3{\cdot}511_5 \pm 0{\cdot}001$ gm/cc., which is about 0·5% higher than the experimentally determined values of 3·491 and 3·496 gm./cc. (Porter, 1928).

§ 5. DEPENDENCE OF THE RESULTS UPON THE VALUE ASSUMED FOR THE RADIUS OF THE CAMERA

It might be thought that the assumption of a value of 3 cm. for the radius of the camera might lead to appreciable errors since film-shrinkage can introduce errors of the order of 0·3% (Lipson, 1942). The calculation of c, as shown in the lower part of table 1, was therefore repeated with constant 4·77 in equation (2) changed to 4·80; this value was chosen because it gave a much smaller drift in the results. The value of c so deduced was 7·9097 kx., which agrees with the previous value well within the limits of error. This source of error, although it is small, would be eliminated if a camera with calibrated knife-edges were used, but it will be seen that the accuracy obtainable even without such knife-edges is quite high.

§ 6. DEPENDENCE OF THE RESULTS ON THE METHOD OF MEASUREMENT

The films were measured in an instrument of the type described by Sears and Turner (1941), and the positions of strong spots could be read to an accuracy of about 0·03 mm. Since such an instrument may not be available in some laboratories, it was thought desirable to find out how much accuracy would be lost if much simpler methods of measurement were used. Accordingly the spots on the photograph that forms the subject of table 1 were measured by visual comparison with a steel scale graduated in $\frac{1}{2}$ mm. The result was 7·909 ± 0·002 kx. Thus even with this simple method of measurement an accuracy of about 0·02% can be obtained.

§7. EXTENSION TO THE MONOCLINIC AND TRICLINIC SYSTEMS

Similar methods can be used for the determination of $a \sin \beta$, b and $c \sin \beta$ for a monoclinic crystal, for both the a^* b^* and the b^* c^* sections of the reciprocal lattice are orthogonal. The determination of β, however, involves some difficulties, for it has to be obtained from the $h0l$ spectra, the relation being

$$\sin^2\theta = \tfrac{1}{4}\lambda^2(h^2a^{*2} - 2hla^*c^* \cos\beta - l^2c^{*2}). \qquad \ldots\ldots(4)$$

If a^* and c^* are known, then β can be derived from spectra for which neither h nor l is zero; for greatest accuracy the spots used to determine β should be those with h and l nearly equal. It is not possible, however, to arrange for a symmetrical photograph except by complete rotation, and it may not be possible to index unambiguously all the spots on a rotation photograph.

Two possibilities of overcoming these difficulties suggest themselves; first, a composite photograph may be taken with a series of small oscillations so that chosen spots appear on both sides of the film; secondly, the crystal may be coated with a fine powder of a crystalline material such as quartz so that the Bragg angles of the spots can be deduced by interpolation from the Bragg angles of the powder reflections. This latter method is less troublesome, although it would mean that the crystal could not be used for any other purpose.

For the triclinic system it is impossible to take symmetrical oscillation photographs, and, therefore, methods such as those described in the preceding paragraph would have to be used for all the lattice parameters.

REFERENCES

Bernal, J. D., 1926. *Proc. Roy. Soc.* A, **113**, 117.
Booth, A. D., 1945. *Nature, Lond.*, **156**, 51.
Buerger, M. J., 1937. *Z. Kristallogr.* **97**, 433.
Foote, F. and Jette, E. R., 1940. *Phys. Rev.* **58**, 81.
Groth, P., 1910. *Chemische Krystallogr.* **3**, 322.
Jeffrey, G. A., 1945. *Nature, Lond.*, **156**, 82.
Lipson, H., 1942. *J. Sci. Instrum.* **19**, 63.
Lipson, H. and Wilson, A. J. C., 1941. *J. Sci. Instrum.* **18**, 144.
Porter, M. W., 1928. *Z. Kristallogr.* **68**, 531.
Sears, J. E. and Turner, A., 1941. *J. Sci. Instrum.* **18**, 17.
Stockdale, D., 1940. *J. Inst. Metals,* **66**, 287.

THE RATIO OF THE NEW INTERNATIONAL LUMEN TO THE LIGHTWATT

By E. F. CALDIN,
Queen's College, Oxford; now at Leeds University

MS. received 4 *September* 1945

ABSTRACT. The ratio of the new international lumen to the lightwatt is expressed as a function of the radiation constants alone, to a close approximation. Its value is calculated for various recommended values of these constants. The corresponding values of the ratio of the present, or "old", international lumen to the lightwatt are also given.

---

§1. INTRODUCTION

The ratio of the practical unit of luminous flux (the lumen) to the lightwatt is often needed in calculations on the emission of light from total radiators and other sources. (It is numerically equal to the value, in lumens per watt, of the luminous efficiency of radiation of the wave-length for which the relative luminosity function has its maximum value unity.) It has long been a source of uncertainty, for three reasons. In the first place, the present, or "old", international candle, from which the lumen is derived, is not physically defined. This difficulty will be removed when the new international candle comes into use as the standard of intensity, for this unit is defined in terms of the brightness of a total radiator at the temperature of freezing platinum, and the new lumen will be derived from it. Secondly, the ratio of the new lumen to the lightwatt depends on the form of the relative luminosity function. This is settled if we accept the internationally-agreed table of values which has been in use since 1924. Thirdly, the ratio depends on the values of the radiation constants C_1 and C_2; these have undergone considerable changes in the last twenty-five years and are still somewhat a matter of choice and liable to revision. A direct computation of the ratio for each pair of values of C_1 and C_2 would be very laborious, and a rapid method of computation of sufficient accuracy is clearly desirable. In this paper a close approximation is developed which expresses the ratio of the new international lumen to the lightwatt as an explicit function of C_1 and C_2 alone; the value of the ratio corresponding to any pair of values of the radiation constants can thence be readily calculated. The limits of error are determined mainly by the experimental error in the determination of the melting-point of platinum.

A relation between the temperature and brightness of a total radiator has been given in a previous paper (Caldin, 1945). This relation assumes the C.I.E. values for the relative luminosity function (C.I.E., *Compte Rendu*, 1924; Judd, 1931), and it can be expressed as an explicit function of C_1 and C_2. For a perfect diffuser such as a total radiator, the total luminous flux per unit area of surface is equal to π times the brightness, and so a relation between temperature (°K.) and total luminous flux per unit area (lightwatts cm.$^{-2}$) is easily derived.

Using this relation, it is possible to relate the lightwatt directly to the new international lumen, since the brightness of a total radiator at the freezing point of platinum is by definition equal to 60 new candles per cm.^{2} of projected area (*International Lighting Vocabulary*, *C.I.E.*, 1938), and so the total luminous flux is 60π new lumens per cm.^{2} of the area of the source. The value on the international scale of the temperature of freezing platinum is itself dependent upon the value of C_2, since it is measured by finding the ratio of the energy flux at a fixed wave-length due to a total radiator at the temperature of freezing platinum to that at the temperature of freezing gold (Roeser, Caldwell and Wensel, 1931). Thus the total luminous flux per unit area in lightwatts cm.$^{-2}$ of a total radiator at the temperature of freezing platinum can be expressed (assuming the C.I.E. relative luminosity function) as an explicit function of C_1 and C_2 alone. For any pair of values of C_1 and C_2, the ratio of 60π to the value obtained gives the ratio of the new lumen to the lightwatt. The ratio of the present, or "old", international candle to the new candle has been experimentally determined (for references see Wensel, 1939, p. 393), and it appears that the brightness of a total radiator at the temperature of freezing platinum is 58·9 old candles per cm.^{2} The ratio of the old lumen to the lightwatt can thence be calculated for any given values of C_1 and C_2.

From the relation here obtained, the values of the two ratios are calculated for various values of C_1 and C_2 which have been recommended at various times.

§ 2. DERIVATION OF AN EXPRESSION FOR THE RATIO OF THE NEW LUMEN TO THE LIGHTWATT AS AN EXPLICIT FUNCTION OF C_1 AND C_2 ALONE

The total luminous flux per unit area of a total radiator, F, expressed in lightwatts cm.$^{-2}$, is given in terms of the temperature (°K.), the values of the radiation constants C_1 and C_2, and the relative luminosity function, by the equation

$$F = \pi B = \int_0^\infty V_\lambda J'_\lambda \, d\lambda, \qquad \ldots\ldots (1)$$

where

$$J_\lambda d\lambda = \frac{C_1 \lambda^{-5} d\lambda}{e^{C_2/\lambda T} - 1}. \qquad \ldots\ldots (2)$$

Here F = total luminous flux per unit area of surface (lightwatts cm.$^{-2}$);

B = brightness (in corresponding units);

$J_\lambda d\lambda$ = total energy flux per unit area from a total radiator, between the wave-lengths $\lambda \pm d\lambda/2$, as given by Planck's equation (watts cm.$^{-2}$);

V_λ = value of the relative luminosity factor at the wave-length λ;

T = temperature (° K).

Using these equations, and assuming the C.I.E. values for the relative luminosity function (*loc. cit*), values of B for various temperatures between 2000 °K. and 3120 °K. have been calculated and a relation between B and T derived (Caldin, 1945). It is concluded that F can be expressed as a function of T, C_1 and C_2 with considerable accuracy by an expression of the form

$$\log_{10} F = a + \log_{10}(C_1/3{\cdot}703) - (10860 C_2/14330 T), \qquad \ldots\ldots (3)$$

where a is a constant, C_2 is in micron degrees, and C_1 is in erg. sec.$^{-1}$ cm.$^{-2}\times 10^{-5}$. Near the freezing point of platinum, which lies between 2040 °K. and 2050 °K., the value of F is given within $\pm 0{\cdot}001$ log units (0·2%) by equation (3) with the value $a=4{\cdot}775$.

The freezing point of platinum is given on the international temperature scale by the formula (Roeser, Caldwell and Wensel, 1931)

$$\log_e R_1=\frac{C_2}{\lambda}\left(\frac{1}{T_0}-\frac{1}{T_1}\right), \qquad \ldots\ldots(4)$$

where $T_1=$ freezing point of platinum;

$T_0=$ freezing point of gold $=1336$ °K.;

$R_1=$ experimentally-determined ratio of the values of J for a given wave-length λ at temperatures T_1 and T_0.

With the value $C_2=14320$ micron degrees, the value found for T_1 was $2046{\cdot}7\pm 1$ °K. The estimated error corresponds to an error of $\pm 0{\cdot}6\%$ in F.

For a small change dC_2 in C_2, equation (4) gives the corresponding change in T_1:—

$$\frac{dT_1}{T_1}=-\frac{dC_2}{C_2}\left(\frac{T_1}{T_0}-1\right)=-0{\cdot}53\frac{dC_2}{C_2}. \qquad \ldots\ldots(5)$$

Thus we obtain the following expression for T_1 in terms of C_2:

$$T_1=2046{\cdot}7[1-0{\cdot}53(C_2-(14320/14320]. \qquad \ldots\ldots(6)$$

Substituting this value for T in equation (3), we obtain finally the following expression for F_1, the total luminous flux per unit area, in lightwatts per cm.^{2}, of a total radiator at the freezing point of platinum:—

$$\begin{aligned}\log_{10}F_1=&\,4{\cdot}775+\log_{10}(C_1/3{\cdot}703)\\&-[3{\cdot}7027\times 10^{-4}C_2]/[1-3{\cdot}7\times 10^{-5}(C_2-14320)]. \qquad \ldots\ldots(7)\end{aligned}$$

Since the value of F_1 at this temperature is 60π new lumens, the ratio M_1 of the new lumen to the lightwatt is given by

$$\begin{aligned}\log_{10}M_1&=\log_{10}60\pi-\log_{10}F_1\\&=-2{\cdot}500-\log_{10}(C_1/3{\cdot}703)\\&\quad+[3{\cdot}7027\times 10^{-4}C_2]/[1-3{\cdot}7\times 10^{-5}(C_2-14320)]. \qquad \ldots\ldots(8)\end{aligned}$$

From this equation, so long as the C.I.E. relative luminosity data are accepted, the ratio M_1 can be calculated for any given values of C_1 and C_2. The limits of error are obtained by summing the estimated errors in the use of equation (3) and in the experimental determination of T_1; the result is $\pm 0{\cdot}8\%$. Assuming in addition the experimental value 58·9 old candles = 60 new candles, the ratio M_2 of the old international lumen to the lightwatt is given by a similar equation in which the first term is not $(-2{\cdot}500)$ but $(-2{\cdot}508)$.

The ratio M_1 could of course be directly computed for each pair of values of C_1 and C_2, using equations (1), (2) and (4), but such a computation is laborious; the purpose of the present treatment is to show how the previous computations of B (Caldin, 1945) can be used to give a rapid method of computation of sufficient accuracy.

§ 3. RESULTS FOR CERTAIN VALUES OF C_1 AND C_2

The values of the two ratios, M_1 and M_2, have been calculated for three pairs of values of C_1 and C_2 which have been recommended at various times.

The results are given in the table below. The values of M_1 should be correct to about ± 5 units; this uncertainty is mainly due to the experimental errors in the determination of T_1, the freezing point of platinum. The values of T_1 corresponding to the various values of C_2 are also given in the table.

Authority	C_2 (micron deg.)	C_1 (erg. sec.$^{-1}$ cm.$^{-2}$) $\times 10^{-5}$	T_1 (° K.)	Ratio M_1 (new lumen/lightwatt)	Ratio M_2 (old lumen/lightwatt)
International Critical Tables	14330	3·703	2045·9 ± 1	643	631
Wensel (1939)	14360	3·732	2043·7 ± 1	664	652
Birge (1941)	14384·8	3·7403	2041·8 ± 1	683	671

§ 4. ACKNOWLEDGMENT

The author's thanks are due to Mr. J. S. Preston, of the National Physical Laboratory, for his suggestions.

REFERENCES

BIRGE, R. T., 1941. *Rev. Mod. Phys.* **13**, 233.
CALDIN, E. F., 1945. *Proc. Phys. Soc.* **57**, 440.
C.I.E., 1924. *Compte Rendu* (Geneva), p. 67.
JUDD, D. B., 1931. *Bur. Stand. J. Res., Wash.*, **6**, 465.
ROESER, W. F., CALDWELL, F. R. and WENSEL, H. T., 1931. *Bur. Stand. J. Res., Wash.*, **6**, 1119.
WENSEL, H. T., 1939. *Bur. Stand. J. Res., Wash.*, **22**, 375.

REVIEWS OF BOOKS

Radium Therapy. Its Physical Aspects, by C. W. WILSON. Pp. xi + 224. (London: Chapman and Hall, Ltd., 1945.) 18*s*.

Dr. Wilson has attempted with considerable success to fill a gap of long standing in the literature of radiation physics applied to medicine. The publication is also timely, as the author points out in his preface, in view of the expected implementation in the near future of the Cancer Act (1939), when the wider application of radiotherapy is likely to attract more workers, medical and otherwise, to this interesting field.

The book should amply meet the needs, as regards radium therapy physics, of the postgraduate student of radiology, particularly, of course, if he intends to specialize in radium therapy. It provides at the same time a handy reference volume and data book for the practising radium therapist and the hospital physicist, however familiar they may be with much of its contents. It is written with the clarity of style and the close attention to detail which has characterized all Wilson's many publications on the subject. Little work of importance in the last decade or so has been overlooked, and the book abounds in references to the literature.

The scope of the book is clear from the chapter headings : (1) Radium : its properties and application to medicine ; (2) The interaction of high-voltage radiation and matter ; (3) Gamma-ray dosimetry : methods and theory ; (4) Gamma-ray dosimetry : apparatus for dosage measurement ; (5) Radium therapy with surface applicators (plaques) ; (6) Cavity and interstitial radium therapy ; (7) Radium teletherapy ; (8) Protection. There are four appendices, valuable as aids to practical dosage calculation.

While the general treatment is on very practical lines, theoretical aspects are by no means neglected. Thus, while details of the construction and design of " air-wall " ionization chambers are fully described, recent work on " air-wall " materials and chamber wall-thickness is clearly presented from the theoretical standpoint. The chapter on radium teletherapy is particularly good, and here the author has drawn considerably on his wide and intimate association with the many physical problems involved in the technique.

It is not surprising to find, in the chapters dealing with surface radium applicators and interstitial gamma-ray therapy, that the well-known dosage systems of Paterson and Parker receive much attention and are described in detail. The dosage graphs are given, but, as in the original published work, they are too small for practical use. In this connection a useful addition, in appendix form, would be the table published by Oddie in 1941, relating radium-skin distance, area and milligramme-hour dose for surface applicators, preferably recalculated to 0·5 mm. Pt screenage (instead of 0·8) and adjusted to 8·3 r. per hour (instead of 8·0) for the value of the dosage rate at 1 cm. from a point source of 1 mg. Ra element with this screenage.

The layout of the book is excellent and the line diagrams are numerous and clear. The production would be considered satisfactory even on peace-time standards, and the price is very reasonable. In future editions, when the paper shortage is less acute, the addition of some blank pages for notes alternating with squared paper would be useful at the end of the book.

It is abundantly clear that the author, who is Physicist in the Department of X-ray and Radium Therapy at Westminster Hospital, fully appreciates the clinical problems which confront the radium therapist. The fruitful co-operation of physicists and others engaged in radiation therapy depends largely upon a mutual appreciation of each other's problems and difficulties. The author expresses the hope that his book will help to make the physicist's work appear as a more co-ordinated whole than hitherto. There is little doubt that it will do so. D. E. A. J.

Fluid Dynamics, by R. VON MISES and K. O. FRIEDRICHS, with supplementary notes by S. BERGMANN. (Rhode Island : Brown University.)

There is some doubt about the propriety of reviewing these papers, as copies can only be obtained by writing to Brown University. The papers consist of " Roneoed " notes of lectures given at courses of advanced instruction and research in mechanics at Brown University in 1941 and 1942. They are sufficiently comprehensive to be published as a book, but there is no indication that this is intended. This would be useful, as the notes provide a good exposition of the field covered and would help the student attending the lectures.

Fluid dynamics is treated from a strongly theoretical standpoint, as might be expected from the reputation of the authors. The first chapter gives a résumé of the standard theory of the motion of an ideal fluid ; vector methods are used throughout and the treatment is thorough yet concise. This chapter is followed by a chapter on motion in two dimensions, with special reference to the aerofoil ; this treatment follows the lines developed by von Mises in 1917 in stressing the geometric aspects of the conformal transformations and of the resulting aerofoil section. It is doubtful whether the student should be burdened with this kind of treatment, which is hardly ever used in modern developments of aerofoil theory. Chapter 3 gives the basic theory and elementary application for the wing of finite span, and includes a full account of the properties of vortex lines and sheets.

The first three chapters are written by von Mises, and the next two chapters, discussing viscous and compressible flow, are written by Friedrichs. The basic theory of viscous flow, in particular the validity of the boundary-layer equations, is fully discussed, while the applications of the theory are treated as examples. The treatment of the instability of laminar flow is more thorough than in any available book on aerodynamics and is clearly one of the subjects of special interest to the author. This subject has occupied the attention of mathematicians and physicists since the time of Osborne Reynolds ; due to the complicated equations, it has been difficult to deduce conclusive results, but it is gradually becoming accepted that Tollmien's 1929 investigation and those following from it are valid.

The discussion of compressible flow covers flow in channels, flow across and in shock waves, linearized theory of subsonic and supersonic flow, and the flow round corners.

The concluding section, by Bergmann, on the hodograph method in the theory of compressible fluid flow is more specialized than most of the rest of the " book ". The hodograph method enables the equations of motion to be linearized and solutions in terms of hypergeometric functions to be obtained. In the hands of Karman and Tsien it has yielded general approximate formulae relating the flow of a compressible fluid to the flow of an incompressible fluid round a body. Ringleb and Karman have shown that the limiting speed, above which solutions of the equations cannot be applied, is associated with the occurrence of infinite accelerations in the field ; this occurs only at speeds well above the local speed of sound. The question whether this phenomenon is the cause of the development of shock waves is unlikely to be answered by mathemetical analysis only, as some instability of the steady supersonic flow may be present at lower speeds.

The hodograph method is well adapted to deal with general problems, but its application to determining the flow round definite bodies is difficult, as the body shape tends to vary with the speed of flow unless troublesome corrections are made. The only practical alternative to the hodograph method is numerical analysis, but it is always difficult to deduce general conclusions from numerical data.

In conclusion it is to be hoped that the material contained in the lecture notes will be published in due course as a book.

H. B. SQUIRE.